Aus der Medizinischen Universitätsklinik

und Poliklinik Tübingen

Abteilung VIII, Klinische Tumorbiologie

Combined application of oncolytic vaccinia and measles vaccine viruses for the treatment of highly resistant human tumor cells

Inaugural-Dissertation
zur Erlangung des Doktorgrades
der Medizin

der Medizinischen Fakultät
der Eberhard Karls Universität
zu Tübingen

vorgelegt von

Meinhardt, Milena

2018

Dekan: Professor Dr. I. B. Autenrieth

1. Berichterstatter: Professor Dr. U. M. Lauer
2. Berichterstatter: Professor Dr. Dr. T. Iftner

Tag der Disputation: 06.12.2018

Widmung

Meiner Familie

Table of Contents

List of Figures

List of Tables

Abbreviations

5-FU	5-fluorouracil
Ad(5)	adenovirus
APS	ammonium persulfate
BF	bright-field
CD	cytosine deaminase
CEA	carcinoembryonic antigen
CEV	cell-associated virion
CMC	carboxymethyl cellulose
CPA	cyclophosphamide
CRC	colorectal cancer
dbi	days before infection
DMEM	Dulbecco's Modified Eagle Medium
DMSO	dimethyl sulfoxide
(ds)DNA	(double-stranded) deoxyribonucleic acid
ECL	enhanced chemiluminescence
EDTA	ethylendiamintetraacetate
EEV	extracellular enveloped virion
EGF	epidermal growth factor
EGFR	epidermal growth factor receptor
FBS	fetal bovine serum
F-protein	fusion protein
(e)GFP	(enhanced) green fluorescent protein
GM-CSF	granulocyte-macrophage colony-stimulating factor
HCV	hepatitis C virus
HDI	histone deacetylase inhibitor
hpi	hours post infection
H-protein	haemagglutinin protein
HRP	horseradish peroxidase
hrs	hours
IEV	intracellular enveloped virion
IFIT1	interferon-induced protein with tetratricopeptide repeats 1
IFN(-ß)	interferon (ß)
IMV	intracellular mature virion
ISG	interferon-stimulated gene
LDH	lactate dehydrogenase
LIVP	Lister strain from the Institute for Research on Viral Preparations
L-protein	large protein
MeV/MV	measles virus
MeV-/MV-CEA	measles virus expressing carcinoembryonic antigen
MeV-/MV-NIS	measles virus expressing sodium-iodide symporter
MeV-SCD	measles virus expressing super cytosine deaminase
MeV-GFP	measles virus expressing green fluorescent protein
MHC	major histocompatibility complex
MOI	multiplicity of infection
M-protein	matrix protein

mTOR	mechanistic Target of Rapamycin
NCI	National Cancer Institute
NDV	Newcastle disease virus
NIS	sodium-iodide symporter
N-protein	nucleoprotein
OD	optical density
OV	oncolytic virus
PBS	phosphate buffered saline
PDGFR	platelet-derived growth factor receptor
PD-L1	programmed cell death 1 ligand 1
Pen/Strep	penicillin/streptomycin
PFA	paraformaldehyde
pfu	plaque-forming unit
P-protein	phosphoprotein
PVDF	polyvinylidene difluoride
RAS	human rat sarcoma
RIG-I	retinoic acid-inducible gene I
RNA	ribonucleic acid
RNP	ribonucleoprotein
rpm	rounds per minute
RT	radiotherapy
SCD	super cytosine deaminase
SD	standard deviation
SDS	sodium-dodecyl-sulfate
SDS-PAGE	sodium-dodecyl-sulfate polyacrylamide gel electrophoresis
SLAM	signaling lymphocyte activation molecule
SRB	Sulforhodamine B
TAA	tumor-associated antigen
TBS	TRIS-buffered saline
TCA	trichloroacetic acid
TCR	T cell receptor
TEMED	tetramethylethylenediamine
TK	thymidine kinase
TRIS	tris(hydroxymethyl)aminomethane
T-VEC	talimogene laherparepvec, a herpes simplex virus
UV	ultraviolet
VACV/VV	vaccinia virus
VEGF	vascular endothelial growth-factor
VGF	vaccinia growth factor
VSV	vesicular stomatitis virus
VVDD	double-deleted vaccinia virus
VVLister	Lister vaccine strain of vaccinia virus

1 Introduction

1.1 Cancer statistics

Cancer is one of the major burdens of the 21st century, both in economically developed and less developed countries.

As estimated in the GLOBOCAN series of the International Agency for Research on Cancer, the worldwide incidence and mortality for all cancers increased to 14.1 million new-diagnosed cases and 8.2 million cancer-related deaths in 2012 (Ferlay *et al*, 2015).

When age-standardized rate as a weighted mean of the age-specific rates is taken as a basis, the most common types in men remain lung, prostate and colorectal cancer, respectively breast, colorectal and cervical carcinoma in women (Torre *et al*, 2015). Worldwide, most cancer patients die from lung, liver or stomach cancer (Ferlay *et al*, 2015).

In developed regions, however, colorectal cancer is the second leading cause of cancer-related death in men, respectively the third in women (Torre *et al*, 2015). Malignant neoplasia are number two following heart disease as cause of death in the United States (Siegel *et al*, 2016).

Looking worldwide, cancer is responsible for even more deaths than coronary heart disease or stroke (Ferlay *et al*, 2015).

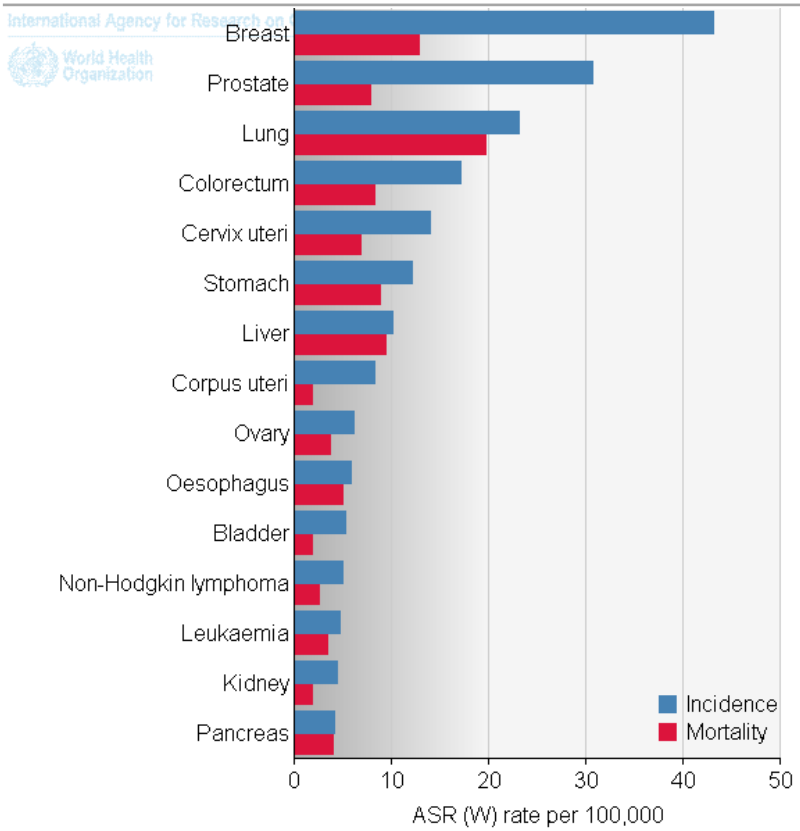

Figure 1. Worldwide estimated age-standardized incidence and mortality rates for both sexes in 2012, taken from Ferlay *et al.* (Ferlay *et al*, 2013)
The unrestricted use of this figure is granted by the publisher.

1.2 Selected tumor entities and therapeutic options so far

In this thesis, we focused on three tumor entities, i.e., colorectal carcinoma, renal cell carcinoma and soft tissue sarcoma. As specified in section 1.4, cell lines of these origins were selected because of their assured high-grade resistance towards oncolytic virotherapy. Moreover, it is of great importance to analyze these cancer types in detail because of their world frequency and quite limited treatment options.

1.2.1 Colorectal cancer

Colorectal cancer (CRC), as one of the most common types in both sexes, is diagnosed in localized stages only in 39 % of the cases (Siegel *et al*, 2017). Due to the use of CRC screening, however, precursor lesions and CRC are detected earlier and in some cases exclusive endoscopic resection is sufficient

(von Karsa *et al*, 2013). In localized stage, surgery is the favored treatment option for CRC, provided that resection with adequate margins and lymphadenectomy is feasible (Cunningham *et al*, 2010). For invasive rectal cancer, the total excision of the mesorectum is indispensable (Quirke *et al*, 2009). Combinatorial approaches with chemotherapy and radiation treatment are common practice in rectal cancer (Cunningham *et al*, 2010), since chemo-radiation provides a lower incidence of local recurrence (Bosset *et al*, 2006). For colon cancer, the recommendation of adjuvant chemotherapy depends on the lymph node status. The application of targeted drugs in early stage disease is also discussed with caution, since bevacizumab and cetuximab (monoclonal antibodies against vascular endothelial factor (VEGF), respectively against epidermal growth factor receptor (EGFR)) seem to have no or only small effect on survival rates for this subgroup, but do include severe side-effects (Cunningham *et al*, 2010).

Fortunately, CRC diagnosed as oligometastatic but resectable disease is no longer a death sentence (Cunningham *et al*, 2010; Jones *et al*, 2014). Even for patients suffering from unresectable metastatic disease, combinatorial treatment containing targeted therapy and multiple cytotoxic agents has increased overall survival to more than 30 months (Fakih, 2015; Kasi *et al*, 2015). Nevertheless, for most patients with stage IV disease, CRC remains incurable. Thus, the 5-year survival rate decelerates to 14 % when patients are diagnosed at distant stages (Siegel *et al*, 2017).

1.2.2 Kidney cancer

Kidney cancer is ranked the ninth most common cancer type in men, respectively the fourteenth in women (Ferlay *et al*, 2013). Although improved relative survival rates have been reported recently, the incidence of renal cell carcinoma has increased (Capitanio & Montorsi, 2016).

Moreover, masses are often diagnosed in advanced or metastatic stages (Siegel *et al*, 2016). Due to robot-assisted or laparoscopic nephron-sparing surgery and active surveillance, radical nephrectomy (the former standard of

care) can be prevented in most cases of local-stage disease (Sun *et al*, 2012). Renal cell carcinoma has been considered both chemo- and radioresistant for quite a long time. However, radiotherapy (RT) offers adjuvant treatment options in selected patients and palliative low-dose RT improves pain level and cancer-related symptoms in unresectable metastatic disease (Dengina *et al*, 2017). With limited success and severe side effects, those patients were formerly treated with immunomodulatory drugs like interferon α and interleukin-2. Today, targeted therapies affecting mainly VEGF, PDGFR and mTOR pathways reduce toxic effects and convince with sustainable response rates in this subgroup (Capitanio & Montorsi, 2016). Nevertheless, an ongoing, complete remission remains the great exception.

1.2.3 Sarcomas

Soft-tissue and bone sarcomas, which are tumors of mesenchymal cell origin, play a minor role in adults, but following leukemia and cancers of the brain and nervous system, sarcomas are the third most common cancer type in children (Siegel *et al*, 2016). In this age group, soft-tissue sarcomas occur more frequently with rhabdomyosarcoma as the most common histologic subtype (von Mehren *et al*, 2016).

Dependent on the affected region of the body, cancer stage and tumor histology treatment options diverge. Surgical resection as standard of care is usually accompanied by pre- or postoperative radiation and/or chemotherapy (von Mehren *et al*, 2016). In advanced metastatic stage and unresectable disease, the application of the chemotherapeutic agent doxorubicin alone or in combination with ifosfamide has been first-line therapy for more than three decades (Skafida *et al*, 2017). Nevertheless, other chemotherapeutic treatment regimen showed promising results (von Mehren *et al*, 2016). Recently, pazopanib, a receptor tyrosine kinase inhibitor, has been recommended for the application in palliative situations (von Mehren *et al*, 2016). However, with a median overall survival of 14–17 months, the outcome of patients with metastatic disease is unacceptable (Frezza *et al*, 2017).

Summing up, there are three major treatment options to defeat various types of cancer: Surgery, chemotherapy and radiation treatment. Additionally, a plentitude of innovative therapeutics is offered including, i.e., hormone-therapy, targeted therapy using small molecules or monoclonal antibodies and immunotherapy.

However, all of these treatment options offer limited success for any number of reasons. On the one hand, therapeutic options and response rates are dependent on cancer type, stage and subgroup analysis. On the other hand, cancerous cells behave heterogeneously: they evolve continuously and may have acquired drug resistance and additional features during the time of first-line treatment (Bell, 2007; Melcher *et al*, 2011). Furthermore, each therapy implies severe side-effects and may be therefore not appropriate for each patient to the same extent.

Especially in metastatic stage disease, a complete remission and cure of cancer is most rare (Melcher *et al*, 2011; Ottolino-Perry *et al*, 2010). Thus, novel therapeutic approaches, which are established with the knowledge of the need of individualized medicine, are desperately required.

1.3 Oncolytic virotherapy

Oncolytic viruses (OVs) have an inherent potential to destroy cancer cells without causing damage to normal tissue (Russell & Peng, 2007; Russell *et al*, 2012). OVs are live, self-replicating agents that can be attenuated for safety concerns and genetically armed to improve their anticancer efficacy (Bell, 2007). Until now, the molecular and cellular mechanisms of tumor cell killing are not completely elucidated, but selective, direct tumor cell lysis and the subsequent occurrence of systemic antitumor immunity seem to be of prime importance (Kaufman *et al*, 2015).

1.3.1 Historical overview

Described first in the early 20th century, oncolytic virotherapy has been extensively researched over the last century. The discovery of viruses as

cancer therapeutics, however, happened by accident. Cases of cancer patients, who experienced clinical remission after contagion with an infectious disease, were reported since the turn of the 19th century (DePace, 1912; Dock, 1904; Kelly & Russell, 2007). While the discovery of viruses and their function as triggers of infectious diseases was at its very beginning, occasional case reports of cancer patients in remission provided us with another perspective. In some cases the observed tumor regress was associated with a coincidental infection of known viral etiology, e.g., a contagion with wildtype measles virus (Bluming & Ziegler, 1971; Pasquinucci, 1971; Taqi *et al*, 1981; Zygiert, 1971). Even though remissions were short-lasting and incomplete, first clinical trials, promoting viruses as novel anticancer agents, were executed shortly after (Bierman *et al*, 1953; Hoster *et al*, 1949; Southam & Moore, 1952).

Although temporary cancer regress in patients suffering from immunosuppressive malignancies had been demonstrated, arising virus infection of normal tissue became an unacceptable side-effect (Cattaneo *et al*, 2008; Kelly & Russell, 2007). In the 1950s and 1960s, after enhanced cell culture techniques and rodent models had been established, oncolytic viruses were characterized enthusiastically (Alemany, 2013; Kelly & Russell, 2007). However, once these viruses were applied to immunocompetent animals and men, the previously observed regress was no longer convincingly reproducible (Moore, 1954; Southam & Moore, 1952). The host´s immune response against the virus was traded as prime suspect, and, as a consequence, virus oncotherapy was almost abandoned in the 1970s (Alemany, 2013).

Later on, the unintentional immune rejection turned out to be a “double-edged sword”: in preclinical (Boone *et al*, 1971; Kaji *et al*, 1969; Lindenmann & Klein, 1967) and clinical (Asada, 1974) trials researchers were able to detect a sustainable antitumor immunity after application of OVs (Alemany, 2013; Melcher *et al*, 2011). Subsequently, the concept of viruses as immunotherapeutic agents attracted interest. Although attempts had been made to induce specific tropism by successive passage of oncolytic viruses in cultured cancer cells (Moore, 1952), the third and enduring phase of research oncolytic virotherapy started only two decades ago, when genetically engineered OVs

have become available (Alemany, 2013; Cattaneo *et al*, 2008; Kelly & Russell, 2007).

Referring to the current state of research, clinical trials seem to overcome previous hurdles. In 2005, world´s first oncolytic agent, the modified adenovirus H101, was accredited for cancer treatment by the Chinese regulatory authorities (Garber, 2006; Jiang *et al*, 2006). Currently, talimogene laherparepvec (T-VEC), a modified herpes simplex virus encoding granulocyte-macrophage colony-stimulating factor, was approved by the US Food and Drug Administration and the European Commission as “first-of-its-kind” cancer treatment of melanoma (Andtbacka *et al*, 2015; Ledford, 2015; Zhang, 2015). By overcoming remaining obstacles, oncolytic virotherapy shall become the long-awaited cure of metastatic cancer.

1.3.2 Mechanisms of tumor cell destruction

Oncolytic viruses do selectively infect, replicate within and lyse tumor cells, while attack of normal tissue occurs only to a limited extent (Kaufman *et al*, 2015; Russell *et al*, 2012). Cancer cell specific cell entry followed by viral replication, initiation of cell death programs and cell lysis are indispensable components of direct tumor cell killing. Some OVs, like herpes simplex and measles virus, infiltrate cells by docking to specific receptors, which are fortunately overexpressed on cancer cells (Alemany, 2013; Kaufman *et al*, 2015). Others, like vaccinia virus, enter host cells by endocytic process (Kaufman *et al*, 2015).

Effective antiviral response mechanisms, based most frequently on the inhibition of protein translation, will be executed, if a normal cell experiences viral entry (Alemany, 2013; Kaufman *et al*, 2015). Thus, so called Toll-like-receptors, which are activated by local interferon (IFN) release or triggered by viral fragments, stimulate several downstream pathways for the induction of apoptosis and viral clearance (Elde *et al*, 2009; Kaufman *et al*, 2015).

In cancer cells, however, cell cycle regulating pathways are often defective (Alemany, 2013; Kaufman *et al*, 2015). Most commonly, this is due to mutations

of the antiviral IFN pathway, the EGFR cascade, the protein kinase B, protein kinase R or human rat sarcoma (RAS) family (Bell, 2007; Kaufman *et al*, 2015). Thereby, abnormal cells are enabled to avoid immune detection and to resist apoptosis (Bell, 2007; Kaufman *et al*, 2015; Russell *et al*, 2012). Fortunately, mutations in cell cycle regulating pathways offer specific tropisms to oncolytic viruses. Vaccinia virus, for example, is most reliant on RAS signaling, which is induced by the activation of EGFR (Parato *et al*, 2012). Accordingly, poxviruses show a natural selectivity for EGFR-overexpressing cancer cells (Kaufman *et al*, 2015).

Although being a “double-edged sword”, the emerging immune response after oncolytic virus treatment plays another leading role in oncolytic virotherapy - perhaps it is the more important one (Alemany, 2013; Russell *et al*, 2012). Coming along with direct tumor cell killing, oncolytic viruses are able to induce a strong and sustainable anticancer immunity by release of tumor-associated antigens (TAA), death signals (cellular proteins that stimulate the host immune system) and neo-antigens (new, cancer-specific antigens) (Kaufman *et al*, 2015). The host anticancer immune reaction consists of systemic innate and tumor-specific adaptive immune response. Antigen-presenting cells process TAA and neo-antigens, represent those fragments on their cell surface and, thereby, activate antigen-specific $CD4^+$ and $CD8^+$ T cells (Kaufman *et al*, 2015). $CD8^+$ T cells and natural killer cells, which are either stimulated by downregulated major histocompatibility complex (MHC) class I expression or by type I IFN, identify and subsequently eliminate the tumor cells (Zamarin *et al*, 2014). Thus, targeting the host immune response to cancer cells may lead to tumor regression even at distant, uninfected tumor sites (Kaufman *et al*, 2015; Russell *et al*, 2012).

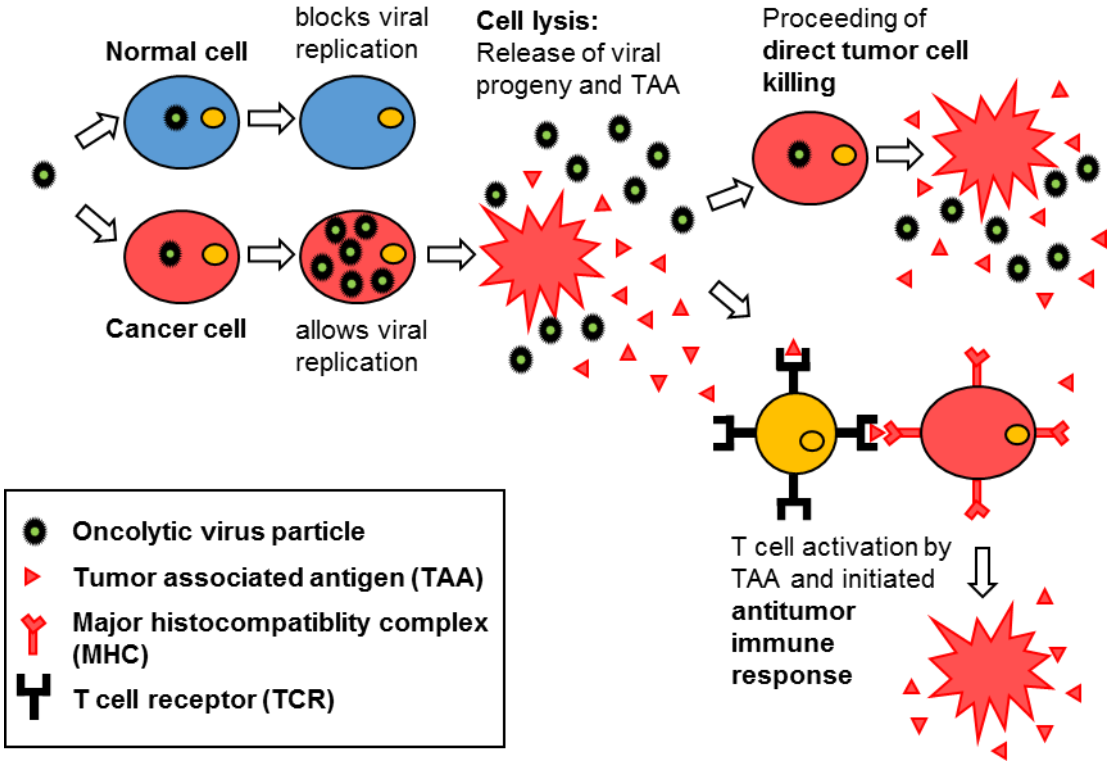

Figure 2. Mechanisms of tumor cell destruction

Summing up, oncolytic virotherapy is a promising new approach in cancer treatment due to two distinct mechanisms of action: direct tumor cell killing and the subsequent occurrence of anticancer immune response (Kaufman *et al*, 2015).

So far, numerous DNA and RNA viruses have demonstrated their ability to act as such anticancer agents. To name only a few, recombinant adenovirus (Ad) (Jiang *et al*, 2006), recombinant herpesvirus (Andtbacka *et al*, 2015), human reovirus (Norman & Lee, 2000), recombinant enteroviruses (Yla-Pelto *et al*, 2016), Newcastle disease virus (NDV) (Cassel & Murray, 1992), vesicular stomatitis virus (VSV) (Hastie & Grdzelishvili, 2012), recombinant vaccinia virus (VACV) (Kirn & Thorne, 2009) and attenuated measles virus (MeV) (Russell & Peng, 2009) have revealed convincing oncolytic potential in several preclinical and clinical trials (Alemany, 2013; Kaufman *et al*, 2015).

1.3.3 Obstacles and limitations

Despite all advantages of oncolytic virotherapy, obstacles to a successful application in immunocompetent men have come into focus in the last decades. Thus, premature viral clearance due to preexisting or quickly generated antibodies and activated T lymphocytes constitutes a problem (Chiocca & Rabkin, 2014; Kaufman *et al*, 2015). Secondly, evidence has grown that oncolytic viruses are also blocked by haemagglutination and components of the complement system (Kaufman *et al*, 2015; Magge *et al*, 2013; Tesfay *et al*, 2014). Additionally, tumors pursue intelligent strategies to evade immune detection: by recruiting tumor-promoting immune cells and expression of immune-inhibitory surface molecules, cancer cells create an immunosuppressive tumor microenvironment in order to protect the tumor and promote malignant degeneration (Hanahan & Weinberg, 2011; Kaufman *et al*, 2015). Furthermore, virus delivery is halted by sequestration of virions in liver and spleen, procured by the mononuclear phagocytic system, as well as by poor extravasation of viral agents from tumor blood vessels (Russell *et al*, 2012). In addition, physical barriers like hypoxia, acidosis, calcification and high interstitial pressure - conditions that characterize tumor microenvironments - limit oncolytic virus efficacy (Kaufman *et al*, 2015). Finally, extracellular matrix proteins and cancer-associated fibroblasts, although non-permissive to viral replication, reduce the delivery of viral progeny (Alemany, 2013; Kaufman *et al*, 2015; Lopez *et al*, 2009).

Besides the manifold challenges of virus delivery, the lack of selective cancer cell tropism is a hurdle that needs to be conquered both for improved anticancer efficacy and better safety of oncolytic agents (Rudin *et al*, 2011). However, the attenuation of oncolytic viruses for safety concerns includes quite often the limitation of their oncolytic potential (Kelly & Russell, 2007; Russell *et al*, 2012).

OVs, as self-replicating agents, are able to multiply independent of the applied dose. On the one hand, this constitutes a certain benefit, since small doses of viral particles can achieve a clinical effect (Kaufman *et al*, 2015). On the other

hand, tumor lysis syndrome and massive cytokine release in answer to a successful virus replication may represent the second side of the coin (Alemany, 2013). Another safety topic addresses the theoretical concern of virus evolution: Genetically attenuated oncolytic agents could regain their wild type pathogenicity, which would lead to a safety problem not only for patient but for contacts (Russell *et al*, 2012). In addition, the risk of virus integration into the host genome provides ground for discussion (Kaufman *et al*, 2015).

As detailed in section 1.3.2, the partial inhibition of antiviral mechanisms in most cancers make tumor cells an ideal breeding ground for oncolytic viruses. Nevertheless, maintained antiviral activity can lead to a limited sensitivity or even resistance to oncolytic viruses (Russell *et al*, 2012).

Accordingly, the ideal oncolytic virus needs to combine an outstanding safety profile with convincing antitumor mechanisms - mediated through direct tumor cell killing and subsequent induction of anticancer immune response. The viral agent needs to be successfully delivered by systemic application and should be able to reach all kinds and states of tumor cells.

1.3.4 Approaches to overcome limitations

Since the first promising attempt in 1991, the concept of an ideal oncolytic virus has been further promoted by the application of three principles of genetic engineering, referred to as shielding, targeting and arming (Martuza *et al*, 1991). Moreover, oncolytic viruses have been combined with well-established therapies like chemotherapy, radiation treatment and immunotherapy for quite a while (Cattaneo *et al*, 2008; Kaufman *et al*, 2015; Ottolino-Perry *et al*, 2010). A novel therapeutic approach, as executed in this thesis for oncolytic vaccinia and measles vaccine virus, is pursued by combinatorial treatment using two distinct oncolytic virus constructs.

1.3.4.1 Combination of oncolytic viruses

In order to overcome partial resistance of cancer cells towards oncolytic virotherapy, the application of two complementary oncolytic virus constructs

represents a sustainable approach. Although the idea of gaining a benefit from synergistic interactions has been pursued by combination therapies before, here, the innovative character is due to the fact that both viral agents can be genetically engineered to compensate each other´s malfunctions (Le Boeuf *et al*, 2010; Tysome *et al*, 2012). Furthermore, oncolytic viruses are able to destroy cancer cells in more than one way: they induce apoptosis as well as necrosis or pyroptosis in infected cells (Kaufman *et al*, 2015). These multitude forms of induced cell death may provide an advantage over the key-and-lock principle of a combination of oncolytic viruses with highly acclaimed targeted therapy (Le Boeuf *et al*, 2010).

In 1991, Japanese researchers demonstrated a first coinfection of swine testicular cells by Hog Cholera Virus and NDV (Kumagai *et al*, 1961). Some years later, Tsuchiya and Tagaya reported on viral superinfection of Yaba virus-infected cells (Tsuchiya & Tagaya, 1970), and the improved ability of an enterovirus to form plaques after pretreatment with poxviruses (Tsuchiya & Tagaya, 1972a; Tsuchiya & Tagaya, 1972b). Tysome *et al.* presented a sequential combination applying wildtype adenovirus (Ad5) and the attenuated Lister vaccine strain of vaccinia virus (VVLister) in an immunocompetent Syrian hamster model (Tysome *et al*, 2012). An intratumoral administration of three doses of Ad5 followed by three doses of VVLister eradicated the sub-cutaneously established pancreatic, respectively kidney, Syrian hamster tumor cell lines (Tysome *et al*, 2012). Le Boeuf *et al.*, who combined a vaccinia virus (VV) and a VSV strain, explained their decision to apply VV as a DNA-based virus and VSV as RNA-based component as follows (Le Boeuf *et al*, 2010). Firstly, the risk of virus evolution was effectively prohibited because replication cycles take place at different locations inside the cell (Le Boeuf *et al*, 2010). Secondly, in contrast to one “supervirus” with an unpredictable risk of infection of normal tissue, both attenuated viruses convinced with outstanding safety profiles (Le Boeuf *et al*, 2010). Thirdly, two immunologically distinct agents might have increased the chance to circumvent the antiviral immune response, thus, offering possibilities for multiple virus injections. Furthermore, DNA-viruses offer great packing capacities for additional transgenes. In return, the smaller

RNA-viruses do quickly replicate, which enables them to escape the adaptive immune response (Le Boeuf *et al*, 2010).

In detail, Le Boeuf *et al.* chose a double-deleted VV-version (VVDD), which is contingent upon functional EGFR pathways in E2F-overexpressing cancer cells (Le Boeuf *et al*, 2010). VVDD encodes B*18*R, a soluble type I IFN receptor, which blocks the emerging cellular antiviral response (Le Boeuf *et al*, 2010). Fittingly, the utilized recombinant version of VSV (VSVΔ51) is most sensitive to IFN, which hinders viral replication in normal cells but retargets this virus to cancer cells with a reduced IFN release (Le Boeuf *et al*, 2010). In the course of the work, Le Boeuf *et al.* equipped VSVΔ51 with p14FAST, a gene product that supports VV spreading by induction of cell fusion (Le Boeuf *et al*, 2010). Thus, two supportively acting virus platforms had been generated and provided a great example of how attenuation of oncolytic agents can go hand in hand with enhanced oncolytic potential. VVDD and VSVΔ51 got genetically armed to express fluorescent proteins (VVDD with eGFP, VSVΔ51 with DsRed) in order to observe viral infection and spreading within the infected cell culture (Le Boeuf *et al*, 2010). As observed under fluorescence microscope, the majority of double-treated cells was not coinfected, instead, the initial infection by VVDD sensitized neighboring cells for the following VSVΔ51 treatment (Le Boeuf *et al*, 2010). Le Boeuf *et al.* investigated their coinfection model *in vitro*, both in immunodeficient and –competent murine tumor models, and, *ex vivo*, on human cancer samples (Le Boeuf *et al*, 2010). The researchers were able to demonstrate that “synergistic interaction between oncolytic viruses augments tumor killing” (Le Boeuf *et al*, 2010).

1.4 Selected oncolytic virus platforms and human cancer cell lines of this thesis

1.4.1 Measles virus

The measles virus, first isolated from 11-year old David Edmonston by Enders and Peebles in 1954, belongs to the family of Paramyxoviridae (Enders & Peebles, 1954). Ranging in size from 100-300 nm (Griffin, 2001), the virion is built up of a phospholipid bilayer envelope, which contains the transmembrane

glycoproteins H (haemagglutinin) and F (fusion glycoprotein), and the M- (matrix protein) protein that connects the inner leaflet with the ribonucleoprotein (RNP) complex. This nucleocapsid consists of nucleoprotein (N), phosphoprotein (P), large protein (L) and the negative single-stranded RNA. The measles virus genome also encodes for the nonstructural proteins V and C (Griffin, 2001; Lamb & Kolakofsky, 2001).

Naturally, host cell entry begins with viral H-protein binding the cellular receptor SLAM, which subsequently enables F-protein to initiate membrane fusion (Griffin, 2001; Yanagi *et al*, 2006). While laboratory propagation, wild-type measles virus was forced to adapt to many different human and animal cells lacking SLAM. Resulting, mutants became accustomed to enter host cells via CD46 and nectin-4 (Dorig *et al*, 1993; Naniche *et al*, 1993; Noyce *et al*, 2011). Interestingly, whereas normal cells exhibit only low CD46 receptor densities, many cancer cells overexpress CD46 as possible safeguard mechanism to avoid complement-mediated lysis (Anderson *et al*, 2004; Fishelson *et al*, 2003).

Transcription and all further steps of viral replication take place in the cytoplasm and are coordinated by P-, N- and L-protein. The N-gene is transcribed most frequently because of its upstream position in the genome. This fact is of some importance as it advocates where to place transgenes, for example light-emitting GFP, the best. A sufficient production of negative single-stranded RNAs ends the replication cycle and newly assembled viral progeny begin to spread. Even though the mechanism of virus release is not completely understood, in polarized epithelial cells close contact of the M-protein to the RNP complex seems to be important (Lamb & Kolakofsky, 2001; Nakatsu *et al*, 2013). Syncytia formation, a different cell shape and the appearance of inclusion bodies inside infected cells herald the oncoming cell death (Griffin, 2001).

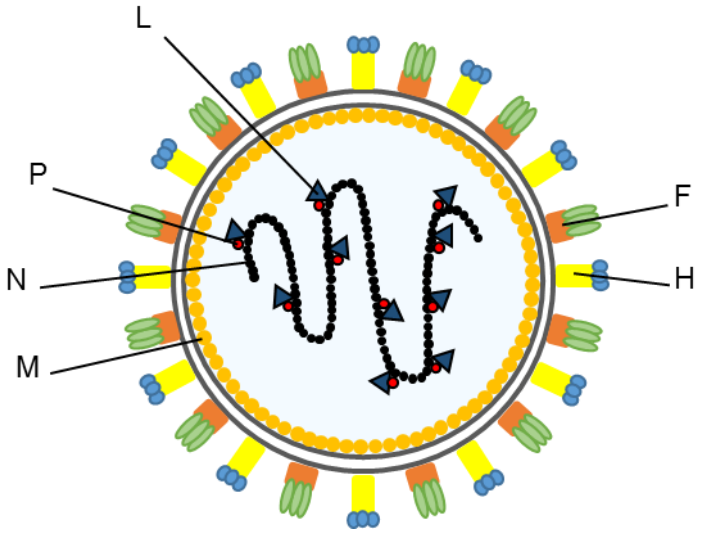

Figure 3. Schematic structure of MeV

The measles virus is built up of a phospholipid bilayer envelope (dark grey), which contains the transmembrane glycoproteins haemagglutinin (H) and fusion (F), and connects to the matrix protein (M). The M-protein surrounds the negative single-stranded RNA (not shown) that is associated with the nucleoprotein (N), the phosphoprotein (P) and the large protein (L).

Wild-type measles virus can lead to severe complications especially when immunosuppressed individuals are infected (Griffin *et al*, 2008; Schneider-Schaulies & ter Meulen, 2002). Attenuated strains, however, convince with similar oncolytic activity while side effects of infection are reduced to flu-like symptoms. The first live attenuated measles vaccine strain, the Edmonston-B-strain, was generated by inoculation of wild-type Edmonston strain to chick embryos (Griffin, 2001). Since 1965, the Schwarz vaccine, a further development of the Edmonston B strain, has been traded as standard measles vaccine in most countries of the world. Until now, more than a billion people have been immunized (Griffin, 2001). Except for recipients with extremely compromised immune system, these attenuated virus strains are safe products and suitable for children from 9 months on (Griffin, 2001; Griffin *et al*, 2008).

In comparison to wild-type MeV, reduced pathogenicity of attenuated versions is achieved by receptor targeting (Russell & Peng, 2009) and mutation of viral nonstructural proteins. Thus, point mutations in the gene encoding nonstructural protein V lead to a reduced suppression of type I interferon upon inoculation with measles vaccine viruses (Ohno *et al*, 2004; Takaki *et al*, 2011). In cells with functional interferon signaling, viral clearance will be initiated immediately. In

cancer cells, however, defects of cell cycle regulating pathways lead to unhindered virus infection and replication of these mutants.

In this thesis we applied MeV-GFP, a vector derived from the Edmonston-B-strain, which carries the marker gene GFP in the leader position next to the N-gene.

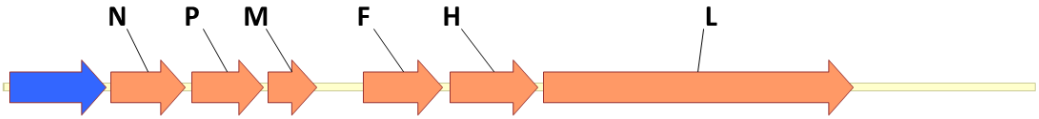

Figure 4. MeV-derived reporter gene vector MeV-GFP, provided by the courtesy of Prof. Dr. Ulrich M. Lauer
The blue arrow encodes green fluorescent protein (GFP).

1.4.2 Vaccinia virus

Vaccinia virus belongs to the Poxvirus family and is a member of the Orthopoxvirus genus. With a diameter of 260-380 nm and a genome capacity of 190 kbp encoding approximately 250 genes, it represents the largest virus we know (Malkin *et al*, 2003; Moss & Earl, 2001). During replication, the double-stranded DNA virus exists in four different forms: the intracellular mature virion (IMV), the intracellular enveloped virion (IEV), the cell-associated enveloped virion (CEV) and the extracellular enveloped virion (EEV) (Schmidt *et al*, 2012; Smith *et al*, 2002). The mature virion is built up of the viral core, which contains the s-shaped double-stranded DNA genome, viral enzymes and proteins, two lateral bodies with unknown function, and a phospholipid bilayer with approximately 25 viral surface proteins incorporated (Moss, 2007; Schmidt *et al*, 2012). The vaccinia virus has the ability to invade lots of different cell types by endocytosis, however, detailed information about host cell entry remains nebulous (Harrison *et al*, 2004; Schmidt *et al*, 2012). Immediately after delivery of the core into the cytoplasm, early viral mRNAs are transcribed (Schramm & Locker, 2005). The translated gene products are essential for the following viral replication (Schramm & Locker, 2005), intermediate gene expression and suppression of an emerging cellular immune response (Moore & Smith, 1992; Thorne *et al*,

2005). Among DNA viruses, poxviruses are unique because they replicate preferentially in the cytoplasm. To replicate almost independently of the cellular replication machinery, VACV brings its own equipment like a virally encoded DNA-dependent RNA polymerase and a multitude of RNA-processing enzymes (Harrison *et al*, 2004; Thorne *et al*, 2005). During replication process, components are sheltered by so called “mini-nuclei”, membranes derived from the rough endoplasmic reticulum (Schramm & Locker, 2005; Tolonen *et al*, 2001). Viral replication is accompanied by transcription and translation of intermediate and late genes, the resulting proteins contribute to the correct assembly of viral progeny (Schramm & Locker, 2005).

Starting as IMV, the most abundantly produced form, vaccinia virus leaves the host cell only via cell lysis. The IEV is additionally wrapped in an intracellular membrane derived from endosome or trans-Golgi network, while the CEV occurs after fusion of an IEV with the cell membrane. Thus, as soon as 6 hours post infection (hpi), a direct cell-to-cell spread becomes feasible (Thorne *et al*, 2005). EEV is the released version of a CEV and able to spread systemically (Thorne *et al*, 2005). While IMV and EEV differ antigenically, CEV moves without entering the extracellular space, thus, VACV escapes host cell immune detection most efficiently (Appleyard *et al*, 1971; Rodriguez *et al*, 1987; Turner & Squires, 1971).

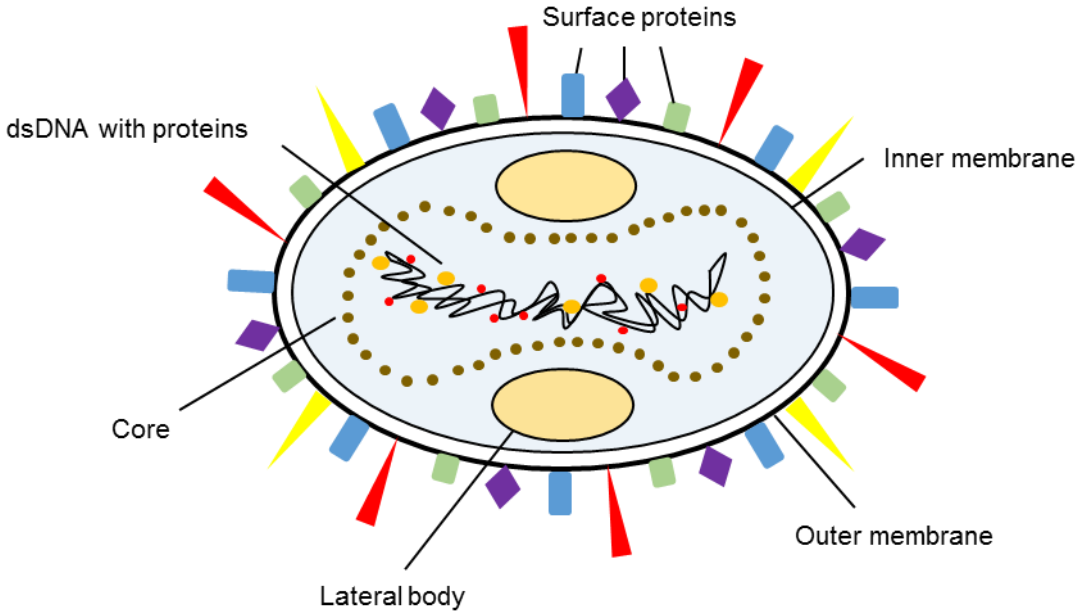

Figure 5. Schematic structure of the intracellular mature virion (IMV) of VACV, modified from Mayer (Mayer, 2014)

An IMV is built up of a viral core, which contains the double-stranded DNA genome associated with viral enzymes and regulatory proteins, two lateral bodies with unknown function, and a phospholipid bilayer (outer and inner membrane) with several viral surface proteins integrated. The use of this modified figure is granted by N. Mayer.

Until now, the real origin of vaccinia virus remains unclear: In the 18th century Edward Jenner, who was looking for a vaccine against smallpox, isolated a virus strain from milkmaids called “vaccinia” (Jenner, 1800). Since 1958 vaccinia virus strains had been applied in a worldwide vaccination campaign leading to a complete eradiation of smallpox in 1978 (Fenner, 1993). In the 1930th, Downie clarified that the applied vaccine strains differ significantly from Jenner´s cowpox isolate (Downie, 1939). Despite this knowledge gap concerning its origin, vaccinia virus is one of the best studied and most applied vaccines we know (Thorne *et al*, 2005). Through years of vaccination program many different vaccinia virus constructs have been developed, not least to reduce adverse effects, which occurred commonly after immunization with first generation vaccines (Lane *et al*, 1969; Walsh & Dolin, 2011). Besides its role in smallpox eradication, engineered vaccinia virus has been applied as a vaccine vector against infectious diseases and cancers (Jager *et al*, 2006; Kanesa-thasan *et al*, 2000; Rochlitz *et al*, 2003), established itself as a “research tool” to

investigate eukaryotic cells and, finally, revealed oncolytic activity (Kirn & Thorne, 2009; Thorne *et al*, 2005).

Wild type vaccinia virus has the ability to adapt host cells for virus replication and spreading by expression of virally encoded vaccinia growth factor (VGF) and thymidine kinase (TK) (Kirn & Thorne, 2009). VGF, as an EGF homologue, activates EGFR-RAS signaling pathways, while viral TK increases the number of nucleotides, which are necessary for virus replication (Buller *et al*, 1985; Buller *et al*, 1988; Kirn & Thorne, 2009). Furthermore, virally encoded immunosuppressive proteins, like B*18*R, block effectively emerging antiviral response (Kirn & Thorne, 2009; Symons *et al*, 1995). In order to reduce pathogenicity of wild type vaccinia virus, numerous attenuated versions miss functional VGF, TK or immunosuppressive protein synthesis. According to these restrictions, mutants are targeted to malignant cells, whereas normal tissue is affected to a limited extent only.

In this thesis we applied GLV-1h254, a relative of well examined GLV-1h68, both derived from the LIVP strain (Lister strain from the Institute for Research on Viral Preparations, Moscow, Russia). LIVP was generated from Lister strain, an attenuated vaccine used extensively during smallpox eradication (Sugimoto & Yamanouchi, 1994). GLV-1h68, established in 2007 by Zhang *et al.*, encodes Renilla luciferase-*Aequorea* green fluorescent protein (RUC-GFP), ß-galactosidase and ß-glucuronidase by genetic engineering of the nonessential gene loci *F14.5L, J2R* (viral TK) and *A56R* (haemagglutinin/HA) (Zhang *et al*, 2007). By deletion of viral TK and inactivation of *A56R*, GLV-1h68 is significantly attenuated but maintains genetic stability and competence of replication (Zhang *et al*, 2007). GLV-1h254 was designed by using GLV-1h71, a RUC-GFP$^-$ version of GLV-1h68, as starting strain (Chen *et al*, 2011; Wang *et al*, 2013). GLV-1h254 itself encodes red light-emitting TurboFP635, a polypeptide, which gene expression cassette was inserted in the HA locus of the parental strain (Wang *et al*, 2013).

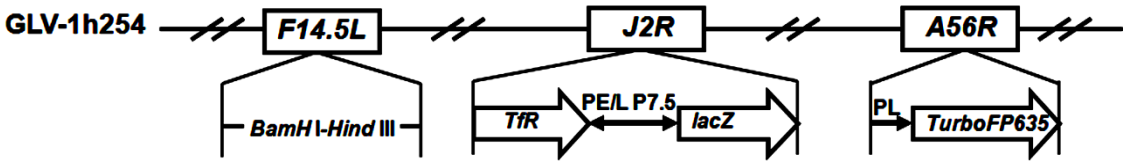

Figure 6. VACV-derived vector GLV-1h254 (encoding TurboFP635), taken from Wang *et al.* (Wang *et al*, 2013).
The unrestricted use of this figure is granted by the publisher.

1.4.3 Evaluated human cancer cell lines

In pretests, ACHN, HCT15 and KM12, three solid human tumor cell lines, received from the U.S. National Cancer Institute´s NCI 60 panel (Shoemaker, 2006), were screened for primary high-grade resistance to both VACV and MeV. These pretests were either conducted by our group ((Noll *et al*, 2013), unpublished data by C. Raff respectively) or by other authors (Ascierto *et al*, 2011). Furthermore, CCS and SRH, two soft-tissue sarcoma cell lines of human origin, which were established and characterized at the University Children´s Hospital Tübingen, were defined resistant towards MeV treatment by Berchtold *et al.* (Berchtold *et al*, 2013). Several preclinical and clinical trials dealt with oncolytic vaccinia virus strains and their potential application to human sarcomas. For example, vaccinia strain GLV-5b451, encoding an Anti-VEGF single-chain antibody, has been brought into place against four canine cancer cell lines including soft-tissue sarcoma (Adelfinger *et al*, 2015). GLV-1h68 has shown promising results when applied to four human sarcoma cell lines *in vitro* and *in vivo* (He *et al*, 2012). Moreover, GLV-1h68 used in combination with chemotherapy, surgery and radiation treatment increased cytotoxic effects to at least some soft-tissue sarcoma cell lines in an animal model (Wilkinson *et al*, 2016). Nevertheless, to our knowledge, sarcoma cell lines SRH and CCS have not been inoculated with oncolytic vaccinia virus strains so far.

In order to evaluate whether there is a synergistic potential of a sequential inoculation applying vaccinia virus GLV-1h254 and Edmonston B vaccine strain-

derived reporter gene vector MeV-GFP, we here established a novel treatment regime.

As outlined before for VV and VSV (section 1.3.4.1), we considered the combined application of DNA-based vaccinia and RNA-based measles virus to be appropriate due to a variety of reasons. VACV and MeV convince with outstanding safety profiles, since both virus constructs have been used in worldwide vaccination programs (Fenner, 1993; Griffin *et al*, 2008). Their oncolytic potency has been demonstrated in numberless preclinical (Blechacz *et al*, 2006; Grote *et al*, 2001; Guo *et al*, 2005; Kim *et al*, 2006; Kirn *et al*, 2007; McCart *et al*, 2001; McDonald *et al*, 2006; Myers *et al*, 2008; Peng *et al*, 2001; Phuong *et al*, 2003; Thorne *et al*, 2007; Zhang *et al*, 2007) and clinical (Downs-Canner *et al*, 2016; Galanis *et al*, 2015; Galanis *et al*, 2010; Gomella *et al*, 2001; Heinzerling *et al*, 2005; Heo *et al*, 2013; Mastrangelo *et al*, 1999; Mell *et al*, 2017; Park *et al*, 2008; Zeh *et al*, 2015) trials.

What is more, VACV and MeV were supposed to complement each other in terms of genetic and immunogenic diversity (Griffin *et al*, 2008; Miller *et al*, 2008; Putz *et al*, 2006; Turner & Squires, 1971), packaging capacities (Smith & Moss, 1983; Zuniga *et al*, 2007), replication time (Kirn & Thorne, 2009; Lamb & Kolakofsky, 2001) and diverse susceptibility to host cellular IFN response (Colamonici *et al*, 1995; Fontana *et al*, 2008; Kirn *et al*, 2007; Ohno *et al*, 2004; Takaki *et al*, 2011).

In fact, Noll *et al.* demonstrated that in ACHN and HCT15 cells, which were found to be high-grade resistant to both MeV-SCD and MeV-GFP treatment, a strong IFN release was initiated upon MeV-SCD infection (Noll *et al*, 2013). Among other findings, like reduced primary infection rates, altered viral growth curves and correspondingly reduced expression of virus-encoded proteins in these cell lines, this finding indicates that the incomplete blockage of the innate cellular immune defense serves as one mechanism of action of reduced sensitivity of high-grade resistant tumor cell lines to measles vaccine virus treatment (Noll *et al*, 2013).

Correspondingly, Berchtold *et al.* screened eight sarcoma cell lines to investigate whether these cells reveal susceptibility to oncolytic MeV-SCD and MeV-GFP treatment (Berchtold *et al*, 2013). Indeed, three cell lines, CCS, SRH and SCOS, were found to be resistant to MeV infection (Berchtold *et al*, 2013). CCS, SRH and SCOS cells showed lower primary infection rates and achieved only poor virus titers in viral growth assays, when compared to susceptible sarcoma cell lines. Although reduced CD46 expression and the absence of SLAM or nectin-4 offered a first explanation for these findings, further data supported the idea that the inhibition of replication accompanied by IFN-dependent host cellular response are of quite more importance (Berchtold *et al*, 2013). Of note, the researchers were unable to identify a clear correlation between the induction of other intracellular receptors, like Toll-like receptor 3 and melanoma differentiation-associated gene 5, and the induction and secretion of IFN-ß upon MeV-SCD infection and resistance patterns (Berchtold *et al*, 2013).

However, to buy into Berchtold *et al.*: “These data suggest that resistance to virotherapy is at least in part due to elevated levels of cytoplasmic pathogen receptors and ISGs” (Berchtold *et al*, 2013).

As described before (section 1.3.4.1), VVDD revealed an IFN-dependent antiviral response mechanism, due to expression of B*18*R, which most effectively supported coinfection by VSVΔ51 (Le Boeuf *et al*, 2010). Tysome *et al.* assumed that synergistic interactions of oncolytic adenovirus and VV are at least in part due to altered IFN signaling (Tysome *et al*, 2012). Although susceptibility of human cancer cell lines to GLV-1h68 seemed to be multifactorial conditioned, Ascierto *et al.* highlighted that downregulated IFN signaling of susceptible cells should be taken into account (Ascierto *et al*, 2011). Consequently, we expected VACV GLV-1h254, as a GLV-1h68 relative, and MeV-GFP to complement each other in any possible way.

1.5 Aim of this thesis

Although oncolytic virotherapy is an exciting new approach in cancer treatment, a wide array of human tumors exhibits primary resistance towards it.

In prior work, ACHN, HCT15 and KM12, three solid human tumor cell lines originating from renal and colon cancer, respectively, were identified highly resistant to both VACV and MeV treatment. Additionally, CCS and SRH, two soft-tissue sarcoma cell lines of human origin, were defined resistant to MeV-derived virotherapeutics.

Here, we investigated whether a combinatorial treatment regime applying two virotherapeutic vectors of completely different origins in the sense of a double-infection, i.e., VACV-derived vector GLV-1h254 (encoding TurboFP635) and MeV-GFP (encoding GFP), was able to overcome remaining limitations.

First, appropriate virus concentrations at which cell masses of ACHN, HCT15, KM12, SRH and CCS cells were reduced less than 25 % were determined in single infection approaches.

Thereafter, different schemes of sequential infections using altering orders of virus treatment, time points of secondary infection and dosages were conducted.

Then, we examined whether synergistic or additive effects explained improved cell death registered upon double-infections and investigated virus-specific marker protein expression by electrophoresis and western blot.

In addition, we also analyzed the impact of plating densities on confluence, virus spreading and oncolysis and described a phenomenon called “viral competition”, which is novel to double-infections combining virotherapeutics of vaccinia virus and measles vaccine virus origin.

2 Material and Methods

2.1 Material

Unless otherwise identified, all mentioned materials and chemicals have been used in the highest possible purity. They were either declared as sterile goods or autoclaved at 121°C and 2 bar for 20 minutes. Deionized and additionally filtered water (H_2O_{dd}) has been used in all experiments, otherwise it is declared differently.

2.1.1 Consumables and Chemicals

Cell scraper	Corning Inc.
Cell strainer 40 µm	BD Falcon
Combitips 2.5/5/12 ml	Eppendorf
Conical tube 1.5 ml	Biozym
Conical tube 2.5 ml	Biozym
Conical tube/Falcon 15 ml	Greiner Bio-one, Corning Inc.
Conical tube/Falcon 50 ml	Corning Inc.
Cryo tubes 1 ml	Corning Inc.
Reaction tubes 500/1500/2000 µl, safe lock	Eppendorf
Flat bottom 96 well plate	Greiner Bio-one
Tissue culture dishes 15 cm	Costar
Tissue culture E-plate 96 well	Roche Applied Science
Tissue culture flask 25/75/150 cm²	Greiner Bio-one, TPP
Tissue culture plate 24 well	TPP
Tissue culture plate 6 well	Falcon, Corning Inc.
Tissue culture plate 96 well	Falcon, TPP
Pasteur pipets	WU Mainz
Pipets 5/10/25/50 ml	Costar, Corning Inc.
Pipet tips 10/100/200/1000 µl	Biozym, PEQLAB
Pipet tips for multichannel pipet 1200 µl	Eppendorf

Descosept	Dr. Schuhmacher GmbH
Isopropanol (70 %)	SAV Lp GmbH
Sekusept	ECOLAB
Sterillium	BODE Chemie Hamburg
Fuji Photo Film	LTD
Hyperfilm^{TM} ECL	Amersham Biosciences
Parafilm	Bemis Company, Inc.
PVDF membrane	Amersham Biosciences
Precision wipes	Kimberley Clark
Latex and nitrile gloves	Ansell, Hartmann
Mycoplasma detection kit	Roche
Sponges	Amersham Biosciences
Whatman papers	Amersham Biosciences
Acetic Acid	Merck
Acrylamide Rotiphorese Gel 30	Carl Roth
APS 10 %	Sigma-Aldrich
Bromophenol blue	Sigma-Aldrich
CMC	Sigma-Aldrich
Crystal violet dye	Carl Roth
DMSO	AppliChem
ECL solution (western blotting detection Reagents and analysis system, 0.125 ml/cm^2)	Amersham Biosciences
Ethanol	Carl Roth
Formaldehyde	Carl Roth
Full Range Rainbow Protein Marker	Amersham Biosciences
Glycerol 86 %	Carl Roth
Glycine	Carl Roth
H_2O_{dd}	MilliQ Synthesis System
HCl	Carl Roth
IGEPAL PA-630 (10 %)	Sigma-Aldrich
KCl	Carl Roth

KH_2PO_4	Carl Roth
Milk powder	Carl Roth
NaCl	Merck
Na_2HPO_4	Carl Roth
NaN3	Sigma-Aldrich
PFA 4.0 %	Otto Fischar GmbH
SDS	Carl Roth
SRB	Sigma-Aldrich
Sucrose	Carl Roth
TCA	Carl Roth
TEMED	Carl Roth
TRIS	Carl Roth
Triton-X-100	Carl Roth
Trypan blue solution 0.4 %	Sigma-Aldrich
Tween-20	Sigma-Aldrich
2-mercaptoethanol	Carl Roth

2.1.2 Antibodies (Western Blot)

Target	***Name, species***	***Dilution, Buffer***	***Source***
GFP	anti-GFP, mouse	1:2500 in 5 % milk in TBS-Tween, NaN3 (0.05 %)	Roche
Human vinculin	V9131, mouse	1:5000 in TBS-Tween, NaN3 (0.05 %)	Sigma
ß-galactosidase	Anti-ß-galactosidase, rabbit	1:200 in TBS-Tween	Invitrogen
ß-actin	Anti-ß-actin, mouse	1:5000 in TBS-Tween, NaN3 (0.05 %)	Sigma
Vaccinia	(Ab35219) Anti-vaccinia virus, rabbit	1:500 in TBS-Tween, NaN3 (0.05 %)	abcam
MeV N-Protein	Ab23974, rabbit	1:1000 in TBS-Tween, NaN3 (0.05 %)	abcam
Mouse IgG	HRP-coupled, goat	1:4000 in TBS-Tween	BioRad
Rabbit IgG	HRP-coupled, goat	1:4000 in TBS-Tween	BioRad

2.1.3 Media, Sera and Buffer

DMEM (with stable L-glutamine, 4.5 g/l glucose)	BIOCHROME, Sigma-Aldrich
EDTA-Trypsin (0.05 % Trypsin)	Lonza, Sigma-Aldrich
FBS	BIOCHROME, Gibco
OPTI-MEM®	Gibco
PBS	PAA, Sigma-Aldrich
Pen/Strep	BIOCHROME

Self-made solutions:

Acidified isopropanol (e.g. 30 ml) *(10 % HCl in Isopropanol)*	HCl	3 ml
	Isopropanol (70 %)	27 ml
CMC medium	CMC	7.5 g
	DMEM	495 ml
	FBS	25 ml
	Pen/Strep	5 ml
Crystal violet stain *(Crystal violet 0.13 %, Ethanol 5 %, Formaldehyde 11.1 %)*	Crystal violet (408.6 g/mol)	1.3 g
	Formaldehyde 37 %	300 ml
	Ethanol 100 %	50 ml
	H_2O_{dd}	filled up to 1 l
2 % FBS-supplemented DMEM Inactivated at 56 °C for 30 minutes:	DMEM	500 ml
	FBS	10 ml
	Storage at	4 °C

10 % FBS-supplemented DMEM	DMEM	500 ml
Inactivated at 56 °C for 30 minutes:	FBS	50 ml
	Storage at	4 °C
22 % FBS-supplemented DMEM	DMEM	50 ml
Inactivated at 56 °C for 30 minutes:	FBS	11 ml
Prepared prior to use	Storage at	4 °C
26 % FBS-supplemented DMEM	DMEM	50 ml
Inactivated at 56 °C for 30 minutes:	FBS	13 ml
Prepared prior to use	Storage at	4 °C
Freezing medium (e.g. 25 ml)	DMEM	17.5 ml
(70 % DMEM, 20 % FBS and 10 % DMSO)	FBS	5 ml
	DMSO	2.5 ml
Loading buffer (6x)	TRIS 1 M pH 6.8	37.5 ml
	Glycerol 86 %	30 ml
	SDS	12.3 g
	Bromophenol blue	60 mg
	H_2O_{dd}	filled up to 100 ml
Prior to use:	2-mercaptoethanol	60 µl/ml
Lysis buffer stock solution (50 ml)	TRIS 1 M pH 7.6	50 mM (5 ml)
	NaCl 5 M	150 mM (3 ml)
	IGEPAL PA-630 (10 %)	1% (10 ml)
	H_2O_{dd}	32 ml
	Storage at	4 °C
MTT stock solution (30 ml)	MTT 75 mg	(2.5 mg/ml)
	colorless DMEM	30 ml

	filtered (pore size 0.45 µm) and dissolved at 37 °C water bath	
PAGE buffer (1x)	TRIS	125 mM (15.1 g/l)
	Glycine	72 g/l
	SDS	5 g/l
	H_2O_{dd}	filled up to 1 l
	pH	8.3
PBS (not used in cell culture)	NaCl	137 mM (8 g)
	KCl	2.7 mM (0.2 g)
	Na_2HPO_4	10 mM (1.44 g)
	KH_2PO_4	1.8 mM (0.24 g)
	H_2O_{dd}	filled up to 1 l
8 % resolving gel (15 ml)	H_2O_{dd}	6.9 ml
	30 % acrylamide mix	4.0 ml
	1.5 M TRIS pH 8.8	3.8 ml
	SDS 10 %	0.15 ml
	APS 10 %	0.15 ml
	TEMED	0.009 ml
15 % resolving gel (15 ml)	H_2O_{dd}	3.4 ml
	30 % acrylamide mix	7.5 ml
	1.5 M TRIS pH 8.8	3.8 ml
	SDS 10 %	0.15 ml
	APS 10 %	0.15 ml
	TEMED	0.006 ml
SRB dye *(0.4 % in 1 % acetic acid)*	SRB	4 g
	Acetic acid	10 ml
	H_2O_{dd}	filled up to 1 l

5 % stacking gel (10 ml)	H_2O_{dd}	6.8 ml
	30 % acrylamide mix	1.7 ml
	1.0 M TRIS pH 6.8	1.25 ml
	SDS 10 %	0.1 ml
	APS 10 %	0.1 ml
	TEMED	0.01 ml
Stripping buffer	TRIS	1.0 M (3 ml)
	SDS 10 %	10 ml
	2-Mercaptoethanol	100 mM (340 µl)
	H_2O_{dd}	47.5 ml
10 x TBS	NaCl	1.5 M (438.3 g)
	TRIS	0.5 M (302.85 g)
	pH	7.4, adjusted with HCl
	H_2O_{dd}	filled up to 5 l
TBS-Tween (0.02 %)	Tween-20	5 ml of 20 %
	10 x TBS	500 ml
	H_2O_{dd}	filled up to 5 l
TCA solution (10 %)	TCA	100 g
	H_2O_{dd}	filled up to 1 l
Transfer buffer (10x)	Glycine	390 mM (146.25 g)
	TRIS	435 mM (264 g)
	H_2O_{dd}	filled up to 5 l
Transfer buffer (1x)	Transfer buffer (10x)	280 ml
	MeOH	560 ml
	H_2O_{dd}	filled up to 2.8 l

TRIS base buffer (10 mM, pH 9, 5 % sucrose) sterile-filtered	TRIS	10 mM (1.21 mg/100 ml)
	H_2O_{dd}	filled up to 100 ml
	Sucrose	5 g
	pH	9, adjusted with HCl
TRIS solution (10 mM, pH 10.5)	TRIS	10 mM (1.21 g/l)
	H_2O_{dd}	filled up to 1 l
	pH	10.5, adjusted with HCl
TRIS solution (1.0 M, pH 6.8)	TRIS	1 M (121 g/l)
	H_2O_{dd}	filled up to 1 l
	pH	6.8, adjusted with HCl
TRIS solution (1.0 M, pH 7.6)	TRIS	1 M (121 g/l)
	H_2O_{dd}	filled up to 1 l
	pH	7.6, adjusted with HCl
TRIS solution (1.5 M, pH 8.8)	TRIS	1.5 M (181.71 g/l)
	H_2O_{dd}	filled up to 1 l
	pH	8.8, adjusted with HCl

2.1.4 Cell lines

2.1.4.1 Human tumor cell lines

ACHN

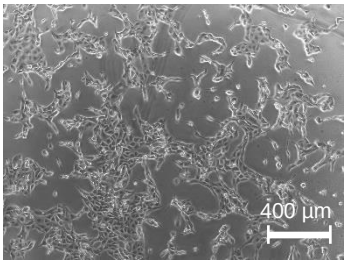

human kidney cancer
Source: U.S. National Cancer Institute´s NCI 60 panel

Bright-field picture

HCT15

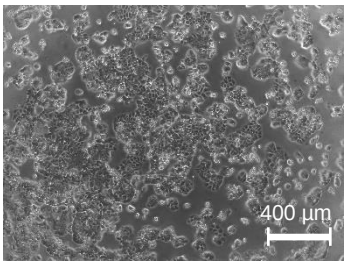

human colorectal adenocarcinoma
Source: U.S. National Cancer Institute´s NCI 60 panel

Bright-field picture

KM12

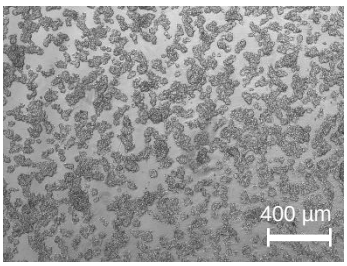

human colorectal adenocarcinoma
Source: U.S. National Cancer Institute´s NCI 60 panel

Bright-field picture

SRH

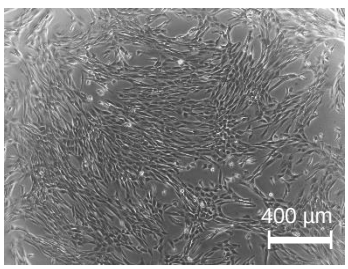

sclerosing spindle cell rhabdomyosarcoma
Species: human
Source: established and characterized at the University Children´s Hospital Tübingen

Bright-field picture

CCS

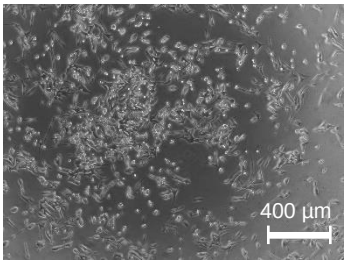

clear cell sarcoma
Species: human
Source: established and characterized at the University Children´s Hospital Tübingen

Bright-field picture

2.1.4.2 Other cell lines

Vero

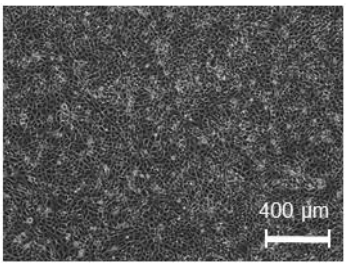

African green monkey kidney epithelial cells
Species: simian
Source: German Collection of Microorganisms and Cell Cultures (DSMZ, Braunschweig)
Bright-field picture

CV-1

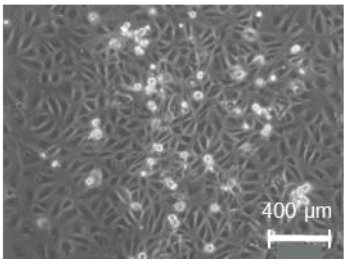

African green monkey kidney fibroblasts
Species: simian
Source: ATCC® CCL-70™

Bright-field picture, modified from Mayer (Mayer, 2014). The use of this picture is granted by N. Mayer.

All cell lines were cultivated as permanent cell cultures, and grew as adherent monolayers in Dulbecco´s modified Eagles medium (DMEM) supplemented with 10 % fetal bovine serum (FBS) in culture flasks.

2.1.5 Viruses

MeV-GFP	Wolfgang Neubert
VACV GLV-1h254	Genelux Corp.

2.1.6 Laboratory Equipment

All-in-one BZ-9000 fluorescence microscope	KEYENCE
Autoclave 3850 EL	Systec
Autoclave VARIOKLAV	HP Medizintechnik GmbH
Banded ear protectors	Peltor
Blotting system	BioRad
Centrifuge	Eppendorf, Heraeus
Counter	LVP
Cylinder & beaker 500/1000/2000 ml	Hirschmann, VITLAB, VWR
Cryo Freezing Container (Mr. Frost)	Nalgene
Laboratory bottle, Duran	Schott
Electronic pipet	Eppendorf
Electrophoresis chamber	Amersham Biosciences
Fluorescence microscope	Olympus
Forceps	Servoprax
Freezing cabinet (-150 °C)	Sanyo
Gel caster	Amersham Biosciences
Haemocytometer	Hecht Assistant
Heating cabinet	Binder
High-definition camera, F-view	Soft Imaging System GmbH
lncubator	Heraeus, Memmert
Laminar Flow Work Bench	Heraeus
Light microscope	Olympus
Magnetic stirrer	IKA Labortechnik
Manual repeating pipet (Multistep)	Brand
Microchronometer	Oregon Scientific
Microtiter plate reader (Tecan GENios)	Tecan

Multichannel pipette	Eppendorf
pH controller	Hanna instruments
Photo cassette	Dr. GOOS Suprema GmbH
Pipet Boy	Integra
Pipets	Eppendorf
Precision scale	Sartorius
Refrigerator (-20 °C)	Liebherr
Refrigerator (-80 °C)	Heraeus, Forma Scientific, Skadi
Shaker	Heidolph
Thermostatic circulator 2219 Multitemp II	LKB Bromma
Ultrasound Sonifier 450	Branson
Vortexer Vibrofix Electronics	Janke+Kunkel IKA Labortechnik
Water bath 342 (37 °C)	Köttermann
xCELLigence SP system	Roche Applied Science
15-pocket comb	Amersham Biosciences

2.2 Methods

2.2.1 Safety

All experimental work was done in laboratories with Biosafety Level 2 approval (BSL2, Directive 2000/54/EC). Infectious virus particles or precarious organics were treated under laminar flow hoods. All materials and laboratory equipment were both disinfected and inactivated by UV ray (at least 15 minutes) as well as autoclaved whenever possible.

2.2.2 Cell culture

All cell lines were cultured in 75 cm^2 tissue culture flasks with vented caps in DMEM supplemented with 10 % FBS without any antibiotics added. Flasks were incubated at 37 °C in a humid atmosphere containing 5 % CO_2. All work was done in a laminar flow work bench under sterile conditions. Cell lines were tested for mycoplasma contamination at regular intervals with a mycoplasma detection kit. During cultivation, cell lines were examined regularly under a light microscope with a 4 - 10 x objective to ensure subconfluent growth of the monolayer and to detect any lack of nutrients or contamination.

Before use, FBS and EDTA-Trypsin were stored at -20 °C and FBS was heat-inactivated at 56 °C for 30 minutes. Open bottles of FBS, EDTA-Trypsin, media and PBS were stored in the fridge at 4 °C. Prior to use, media, PBS and EDTA-Trypsin were warmed in the water bath at 37 °C unless otherwise specified.

2.2.3 General cell culture

For harvesting of cells, DMEM was removed with a pipet and cells were washed with PBS. Thereafter, cells were incubated with 1 ml EDTA-Trypsin at 37 °C and flasks were agitated gently until the cell layer came off. Subsequently, EDTA-Trypsin was inactivated with 9 ml 10 % FBS-supplemented DMEM and cells were resuspended by using a pipet. If necessary, the cell suspension was additionally filtered through a 40 µm cell strainer. To split cells, one half of the generated single cell suspension was transferred to a new tissue culture flask

and filled up with fresh medium supplemented with 10 % FBS. Split ratios of different cell lines diversified and were empirically determined. Culture flasks were stored in the incubator at 37 °C.

2.2.3.1 Counting cells with a haemocytometer

In order to plate cells, it was necessary to define the number of viable cells in the created cell suspension. Accordingly, 10 µl of the cell suspension were added to 90 µl of Trypan blue solution, a diazo dye, to generate a 1:10 dilution. Trypan blue is used to differentiate between dead and viable cells. As living cells appear highlighted, dead cells appear dark blue, when analyzed under a light microscope. Unless otherwise specified, Trypan blue was used for all counting.

Cells were counted by using an improved Neubauer counting chamber. The Newton ring, a light reflection that appears when the covering glass is rubbed against the chamber, indicates that the covering glass is fixed accurately, which is essential to guarantee a gap of no more than 0.1 mm. Accordingly, one square contains a define volume of 0.1 µl. After the chamber was assembled correctly, 10 to 12 µl of the prepared 1:10 dilution were transferred to one corner of the chamber. Depending on capillary forces, the volume now distributed equally over the squares. Every living cell in a large square, consisting of 16 smaller squares, was now counted properly under a light microscope with a 10 x objective. The factor of dilution was taken under consideration by multiplication by 10. Accordingly, the concentration of cells was calculated as follows:

$$\frac{cells}{ml} = \frac{total\ amount\ of\ viable\ cells}{number\ of\ large\ squares\ counted}\ x\ 10^4\ x\ 10$$

2.2.3.2 Plating of cells

After calculating the concentration of viable cells via haemocytometric technique, the desired concentration for plating was diluted using 10 % FBS-supplemented DMEM. Most cell lines were plated in 0.5 ml cell suspension/well at a density of 5 x 10^4 cells per well in 24-well plates. Cells were seeded with a manual repeating pipet and incubated at 37 °C for one to two nights depending on the cell line processed.

2.2.3.3 Confluence trials

Tumor cell confluence, which is required for optimal virus spreading, was analyzed for each cell line in separate pretests. Thus, cells were plated at different densities in 24-well plates and examined under a light microscope with a 4 - 10 x objective up to 6 days. The extent of the reached confluence, expressed as percentage, as well as the consumption of media and the detachment of cells were documented daily.

2.2.3.4 xCELLigence system for monitoring of cell viability and virus spreading

The xCELLigence system allows to monitor real-time cell viability and cell proliferation by the measurement of electrical impedance. Interdigitated micro-electrodes, which are integrated in special 96-well E-plates, register changes of electrical impedance. The readout, displayed as cell index, provides information about cell viability and correlates well with the actual cell number. Thereby, the xCELLigence system helps to review the chosen cell counts and selected time points to run cell viability assays like SRB and MTT assay (Ke *et al*, 2011). In addition, it may clarify the impact of cell confluence on the efficiency of virus spreading.

In order to determine suitable cell numbers for the following xCELLigence trial, cells were plated in sextuplicates in 200 µl 10 % FBS-supplemented DMEM at various densities in a 96-well plate. The next day, cells were either infected with VACV GLV-1h254 or mock-treated in 20 µl 2 % FBS-supplemented DMEM.

Cells were incubated until 96 hpi. Virus infection and spreading, as well as the development of confluence were evaluated under a fluorescence microscope. Virological methods are described in detail in section 2.2.4.1.1.

For xCELLigence trial, cells were split one day before plating to avoid growth inhibition. The following day, 50 µl of 10 % FBS-supplemented DMEM were added to each well of a 96-well E-plate and a background measurement was performed. Thereafter, cells were plated at the selected densities in 100 µl 2.5 % FBS-supplemented DMEM. Thus, a final concentration of 5 % FBS was obtained. The E-plate was incubated at 37 °C overnight. At 22.5 hrs after plating, cells got either infected in triplicates with VACV GLV-1h254 in 10 µl DMEM or were mock-treated. Triton 0.1 % X-100, which was used as a positive control for cell death, was applied to three wells of each plating density. At 1.5 hpi, 50 µl of 26 % FBS-supplemented DMEM were added to each well to receive a final concentration of 10 % FBS in a total volume of 210 µl. Electrical impedance was measured every 30 minutes, starting after seeding of the cells until the experiment was ended (after an observation period of approximately 130 hrs). Electrical impedance was measured using the xCELLigence SP system. RTCA Software 1.2 was applied to calculate cell index values. All values were normalized.

2.2.3.5 Cryoconservation and thawing of cells

Cells in tissue culture flasks were first examined under a light microscope with a 4 - 10 x objective to evaluate the density of the cell layer. Confluent but not overgrown cells were favorite to generate a concentrated cell suspension.
Freezing medium, containing 70 % DMEM, 20 % FBS and 10 % DMSO, was prepared next. Cells were harvested as outlined above and settled by centrifuging at 1200 rpm for 3 minutes at 22 °C. Cell supernatant was discarded, the cell pellet was resolved in the prepared freezing medium and the cells were resuspended carefully with a 25 ml pipet. The volume was distributed to cryo tubes, 1 ml each. The last cryo tube served as a sterility check and was labelled. Cryo tubes were frozen with an isopropanol bath at -80 °C for one day and transferred afterwards to a freezing cabinet at -145 °C or into liquid nitrogen

for long time storage. The labelled cryo tube was thawed the next day and checked for growth behavior and contamination.

For thawing, frozen cryo tubes were shortly dipped into the water bath (37 °C). The defrosted cell suspension was transferred with 9 ml of FBS-supplemented DMEM into a conical tube and resuspended carefully. Thus, DMEM inactivates the cytotoxic DMSO. Cells were now centrifuged at 1200 rpm for 2 minutes, supernatant was removed and the remaining cell pellet was resuspended in 10 ml fresh FBS-supplemented DMEM. The cell suspension was then transferred into a fresh culture flask.

2.2.4 Virological methods

2.2.4.1 Infection of cells

2.2.4.1.1 Single virus infection with VACV GLV-1h254

Plates were labelled with the assay number, plate number and date. Cells were seeded in 0.5 ml cell suspension/well at the determined plating density in 24-well plates. Plates were incubated at 37 °C for one to two nights depending on the cell line processed. On the infection day, the plates were examined under a light microscope to check for sufficient cell adherence and a subconfluent monolayer. The current cell count of each cell line was determined via haemocytometer technique, as described above, and calculated as an average of four wells.

$$\frac{cells}{well} = (\frac{total\ number\ of\ viable\ cells}{number\ of\ large\ squares\ counted} x\ 10^4\ x\ factor\ of\ dilution)/4$$

The following calculation of multiplicity of infection (MOI) based on the received cell count. To exemplify, MOI 1 stands for one infectious virus particle per cell at the time point of infection. The following formula calculates the required volume (amount of virus in µl) of the virus stock which is needed to create a virus dilution that fit the counted cell number/well at the determined MOI:

$$amount\ of\ virus\ (\mu l) = \frac{\frac{cells}{well} * \frac{1000}{\frac{virus\ suspension}{well}(\mu l)} * MOI}{virus\ titer\ (pfu/ml)} * total\ volume\ (\mu l)$$

Virus aliquots were thawed carefully for a few seconds in the water bath (37 °C). Subsequently, aliquots were vortexed and sonicated three times 30 seconds each and intercalated on ice again. Now, the calculated amount of virus was diluted in 2 % FBS-supplemented DMEM. Since cells were infected at various MOIs, a serial dilution, starting with the calculated virus dilution, was prepared. Therefore, virions were diluted in DMEM supplemented with 2 % FBS.

DMEM was removed from the cells and each well was washed carefully with 0.5 ml PBS. Next, 100 or 150 µl 2 % FBS-supplemented DMEM were added to each well to prevent cells from drying out. Now, cells were either infected with GLV-1h254 at ascending viral concentrations in 100 or 150 µl 2 % FBS-supplemented DMEM or mock-treated (only medium was added). Plates were incubated at 37 °C and agitated gently every 20 minutes to allow the virus suspension to disperse equally. At 1.5 hpi, the inoculum was removed and every well was filled with 500 µl 10 % FBS-supplemented DMEM. Respectively, in experiments where it was important to keep the inoculum on the cells, 200 µl 22 % FBS-supplemented DMEM were added without removing the inoculum to receive a final concentration of 10 % FBS-supplemented DMEM. Plates were stored in the incubator for maximum 96 hpi.

2.2.4.1.2 Single virus infection with MeV-GFP

Plates were labelled as described above. Cells were seeded confluence-optimized in 24-well plates and incubated overnight, respectively for two nights. Cell adherence and confluence were evaluated under a light microscope prior to infection. The current cell count was calculated as detailed in section 2.2.3.1 for each cell line separately.

The measles vaccine virus (MeV-GFP) was thawed on ice and vortexed briefly. Every aliquot was used only once after thawing. To infect cells at various MOIs, a serial dilution with room-tempered OPTI-MEM® was prepared. Next, the medium was removed carefully from the wells, cells were washed with PBS and 150 µl of OPTI-MEM® were pipetted to the cells. The infection medium or only OPTI-MEM® were added in 100 µl suspension per well. Plates were incubated at 37 °C and agitated gently every 20 minutes until 1.5 hpi. After 1.5 hrs absorption period, the inoculum was removed and replaced by 500 µl of 10 % FBS-supplemented DMEM. Plates were placed in the cell culture incubator for 96 hpi.

2.2.4.1.3 Combined infection with VACV GLV-1h254 and MeV-GFP

For each experiment we needed at least four 24-well plates and an additional plate for cell counting, labelled as mentioned above. For Keyence microscopy, cells were plated in an open µ-Slide with 8 wells, respectively. After plating, cells were incubated at least overnight. The next day, the plates were examined for cell adherence and extent of confluence. On the infection day, the current cell count was calculated as explained above. Each virus and its serial dilution was prepared separately. VACV was treated as described in section 2.2.4.1.1. A serial dilution of measles vaccine virus was performed by the use of 2 % FBS-supplemented DMEM instead of OPTI-MEM®.

Now, medium was removed from the plates, cells were washed with PBS and 150 µl of 2 % FBS-supplemented DMEM were added to each well. Cells were inoculated with the first virus at various MOIs in a volume of 100 µl/well or mock-treated. The plates were stored in the incubator and swayed in 20-minutes periods. The second virus was added in a volume of 50 µl at diverse time points, while mock-treated and single-infected cells were inoculated with 50 µl 2 % FBS-supplemented DMEM.

At 1.5 hpi with the second virus, 200 µl DMEM + 22 % FBS were added. Culture plates were stored in the incubator for 96 hpi with the first virus.

2.2.4.2 Amplification of MeV

To produce a sufficient amount of measles vaccine viruses, Vero cells were plated in 10 % FBS-supplemented DMEM in 15 cm culture dishes, each dish containing 1 x 10^7 cells. Culture dishes were incubated overnight at 37 °C. Vero cells were chosen for amplification, as they guarantee an optimal environment for the replication of measles vaccine virus (Griffin, 2001).

On the infection day, medium was removed from subconfluent monolayers, cells were washed once with PBS and incubated with 9 ml OPTI-MEM®. Subsequently, Vero cells were infected with MeV-GFP at MOI 0.03 in 1 ml OPTI-MEM® and incubated for 3 hrs at 37 °C. During this incubation period, dishes were gently agitated for an equal disperse of the virus suspension. The inoculum was discarded at 3 hpi, and culture dishes were filled with 20 ml 10 % FBS-supplemented DMEM. Dishes were stored in the incubator for another 48 hrs.

Best conditions for harvest were indicated on the one hand by the extent of syncytia building, and on the other hand by the attachment of virus particles to the cell surface. Accordingly, virus spreading and syncytia building were examined under both a light and a fluorescence microscope daily. On the harvesting day, supernatant was removed and 1 ml OPTI-MEM® was added to each dish. The cell layer was popped off with a cell scraper and cells were assembled in a 50 ml conical tube. The tube was quickly frozen in liquid nitrogen at -160 °C and subsequently stored at -80 °C. This freezing process broke off the cell membranes and released the virus particles. Next, the frozen tube was thawed quickly in a water bath at 37 °C, vortexed and centrifuged at 4000 x g for 15 minutes at 4 °C. The centrifugation process separated the cell remnants, which accumulate in a cell pellet, from the virus particles in the supernatant. The virus suspension was aspirated and transferred into a fresh tube, vortexed and distributed to cryo tubes at various volumes (100 µl, 200 µl and 500 µl). Finally, the virus aliquots were stored at -80 °C. The amplification of MeV-GFP was kindly supported by Irina Smirnov.

2.2.4.3 Production of vaccinia virus aliquots out of a stock solution

The vaccinia virus stock solution (VACV GLV-1h254) was kindly provided by Genelux Corp., San Diego, USA.
To yield a more diluted virus suspension, the highly-concentrated virus stock solution needed to be diluted and distributed to smaller aliquots. TRIS base buffer (10 mM, pH 9), containing 5 % sucrose, was used as dilution volume. Accordingly, the virus stock solution was thawed quickly at 37 °C in the water bath, vortexed and sonicated 3 x 30 seconds. Thereafter, the stock was stored on ice again. Next, 45 µl of the stock solution were pipetted into a 1.5 ml conical tube, filled up with 855 µl of sucrose-supplemented TRIS base buffer and vortexed again. The obtained virus dilution was now allocated to approximately 29 cryo tubes, 30 µl each, and stored at -80 °C.

2.2.4.4 Titration of viruses

To identify the virus titer of an unknown virus solution, it is essential to perform titration assays, both for oncolytic vaccinia and measles vaccine virus.

2.2.4.4.1 Titration of vaccinia virus

For the titration of virus aliquots, CV-1 cells were plated in 24-well plates at a density which resulted in a confluent monolayer (in this case 4 x 10^4 cells/well) after 24 hrs incubation time. The CV-1 cell line was chosen as it provides a suitable environment for the replication of vaccinia virus particles (Liu *et al*, 2017). The next day, three virus aliquots were thawed quickly at 37 °C in a water bath, vortexed and sonicated 3 x 30 seconds before stored on ice again. Serial dilutions with factors from 10^{-2} to 10^{-7} were prepared in 2 % FBS supplemented DMEM. All tubes were stored on ice again. To guarantee a reliable value of the mean, the experimental steps described so far were repeated in a second approach using the same aliquot. Furthermore, aliquot two and three were processed likewise. Additionally, the whole titration assay was repeated using another three aliquots some days later.

DMEM was removed from the wells and CV-1 cells were infected in 200 µl/well at various dilutions in duplicates. Inoculated plates were stored in the incubator at 37 °C for one hour, interrupted only by gentle agitation every 20 minutes. Subsequently, 1 ml of CMC medium was added to each well, and plates were stored in the incubator for another 48 hrs. The CMC medium prohibits a further virus spreading through the medium. As a consequence, virus dispersion is limited to direct cell-to-cell contact, which forms plaque units (Baer & Kehn-Hall, 2014). At 49 hpi, 250 µl crystal violet stain were brought carefully to each well using a manual repeating pipet. Thereafter, plates were stored overnight at room-temperature. Crystal violet terminates the virus infection and stains the wells (Baer & Kehn-Hall, 2014). The next day, supernatants were removed, plates were washed with H_2O_{dd} and dried under UV light. For titration, every well was examined with the naked eye under a light source for plaque forming units (pfu). These pfu appeared as pale spots on the violet stained background. In order to obtain a reliable result, plaques were only counted in wells, which showed 10 to 100 pale spots. For the determination of the virus titer, expressed in plaque forming units per ml (pfu/ml), we used the following calculation:

$$VACV\ titer\ (pfu/ml) = \frac{average\ plaque\ count\ (pfu) * 5}{dilution\ factor * 0.2\ ml\ (volume\ of\ infection) * 5}$$

The volume of infection (200 µl/well) and the average plaque count were multiplied by 5 to obtain the pfu in a volume of 1 ml virus suspension per dilution factor (titer is expressed in pfu/ml). The titration of VACV GLV-1h254 was kindly supported by Dr. Martina Schell and Dr. Julia Beil.

A

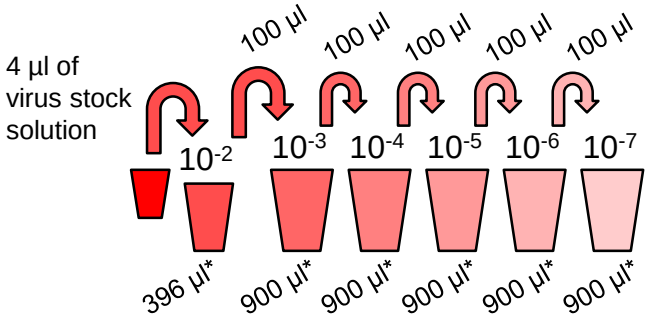

* 2 % FBS-supplemented DMEM

B

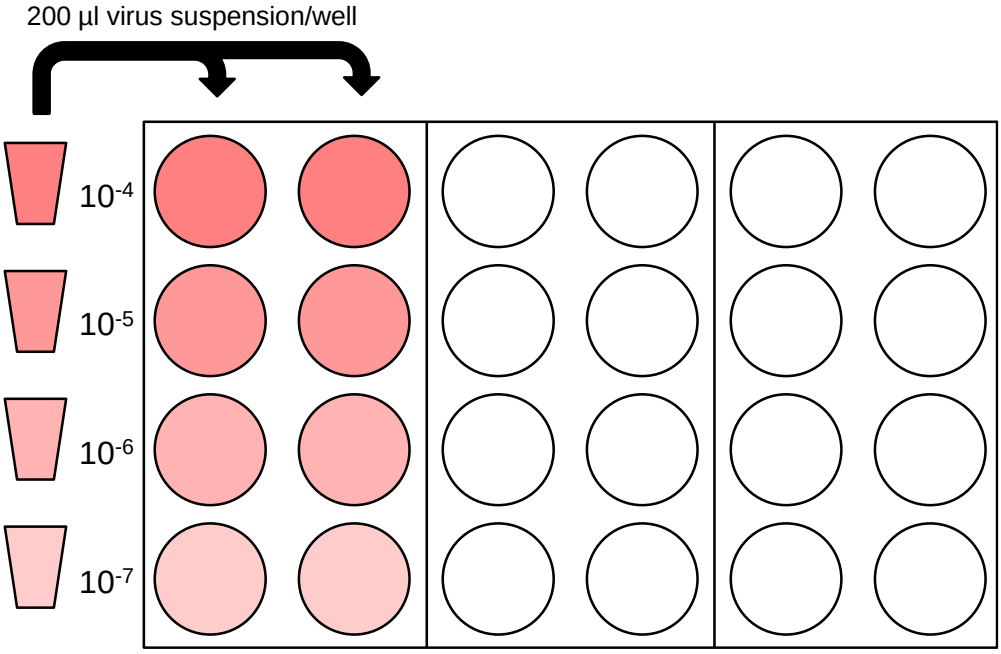

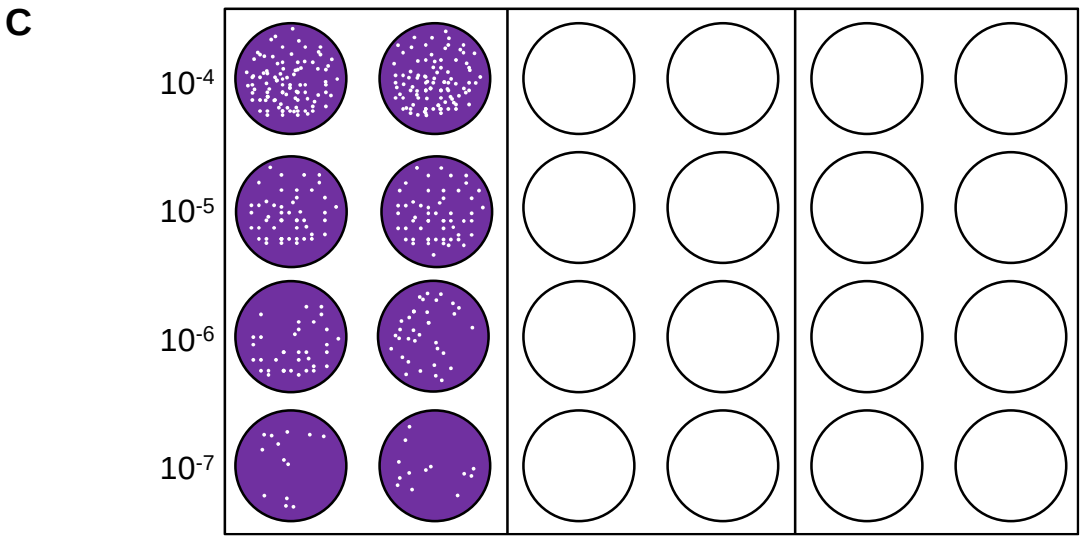

Figure 7. Performance of a serial dilution of vaccinia virus stock solution (A), infection of CV-1 cells at various dilution factors (B) and crystal violet stained plate (C)

First, 4 µl of the virus stock solution were pipetted to a 1 ml conical tube prepared with 396 µl 2 % FBS-supplemented DMEM. The volume was resuspended and vortexed rigorously, then 100 µl were transferred to the next tube, which was already filled with 900 µl medium. Resuspending and vortexing were repeated, before 100 µl virus suspension were transferred to the next tube. This way a serial dilution with six dilution factors (10^{-2} to 10^{-7}) was established (**A**). For titration assay, CV-1 cells, plated in a 24-well plate, were infected in 200 µl virus suspension/dilution factor (from 10^{-4} to 10^{-7}) in duplicates and incubated at 37 °C (**B**). For plaque counting, the inoculated plate was dyed using crystal violet stain. After a 48 hrs-incubation period with CMC medium, 250 µl crystal violet stain were brought to each well, the plate was stored at room-temperature. The next day, supernatant was discarded and plates were washed and dried under UV light. After drying, plaque forming units appeared as pale spots on the violet stained background (**C**).

2.2.4.4.2 Titration of measles vaccine virus

To identify the unknown titer of a measles vaccine virus stock, we performed a $TCID_{50}$ (tissue culture infective dose 50, (Rabenau *et al*, 2015)) endpoint dilution assay, using calculations by Spearman and Kärber (Kärber, 1931; Spearman, 1908). Due to reasons of convenience, the received $TCID_{50}$ unit was subsequently converted into pfu/ml.

First, a sufficient amount of Vero cells was harvested from culture flasks. The gained cell suspension was incubated at 37 °C in the water bath before further processed. Next, eight wells of a 96-well plate were filled with 270 µl OPTI-MEM® each. One aliquot of the measles vaccine virus stock was thawed carefully as described above (section 2.2.4.1.2). Subsequently, 30 µl of the virus suspension were pipetted into the first cavity of the prepared 96-well plate and resuspended 5 x. Furthermore, 30 µl of this well were aspirated and transferred into the next and resuspended 5 x. This step was repeated until a serial dilution with eight dilution factors (10^{-1} to 10^{-8}) was performed. Now, using an 8-channel electric pipet and fresh 200 µl pipet tips, the prepared serial dilution was transferred in sextuplicates (30 µl/well) into a fresh 96-well plate. The experimental steps described so far were repeated in a second approach.

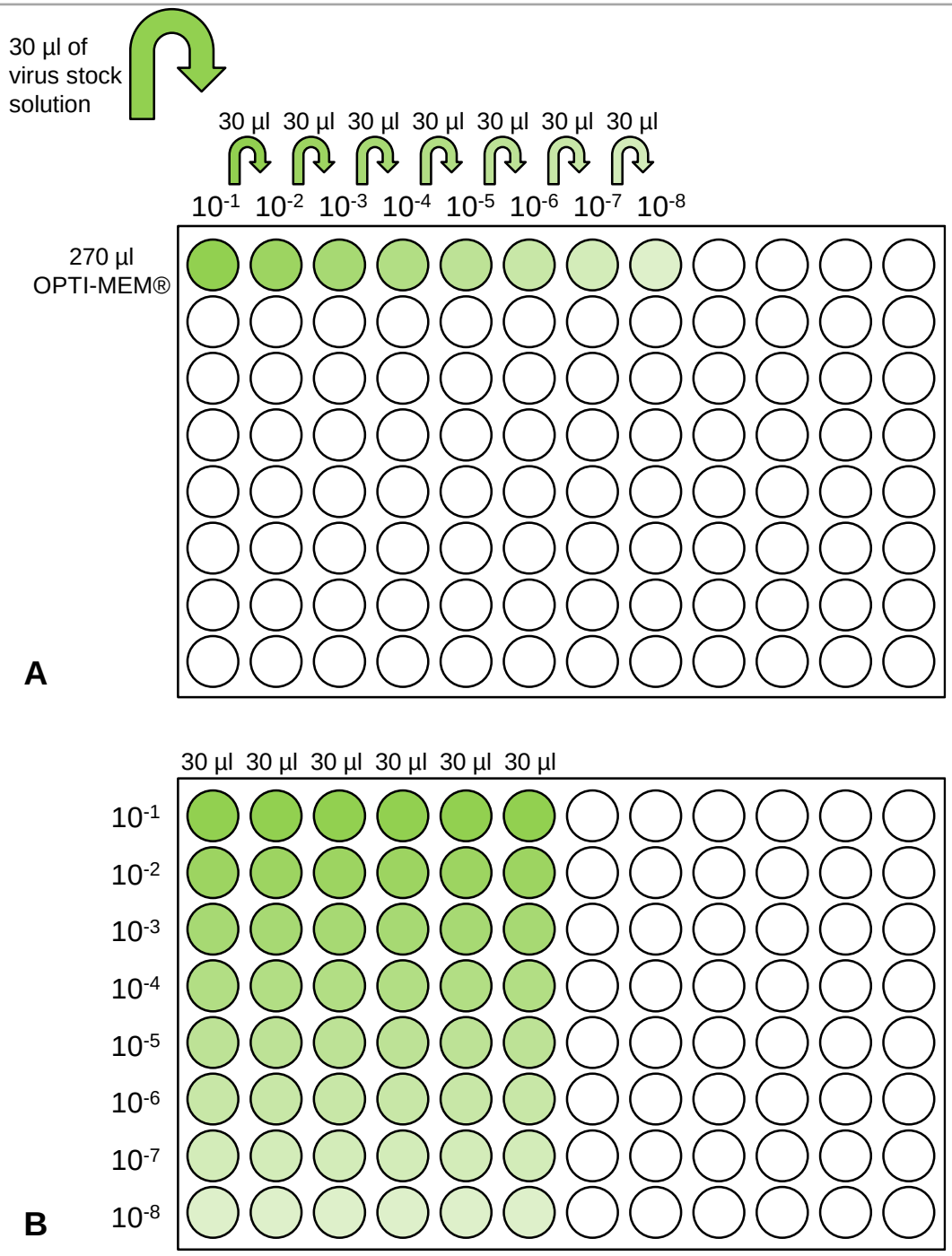

Figure 8. Performance of a serial dilution of measles vaccine virus stock solution (A) and preparation of a 96-well plate for titration (B)

Eight wells of a 96-well plate (**A**) were filled with 270 µl OPTI-MEM®. Next, 30 µl of the thawed virus stock solution were pipetted to the first well, resuspended 5 x and transferred to the proximate well, until a serial dilution with eight dilution factors (10^{-1} to 10^{-8}) was completed. Now, using an 8-channel electric pipet, the prepared serial dilution was transferred in sextuplicates (30 µl/well) into a fresh 96-well plate (**B**).

Vero cells were now transferred in 200 µl 5 % FBS-supplemented DMEM/well at a density of 2 x 10^4 cells/well to the inoculated 96-well plate. Cells and measles virus particles were incubated for four days at 37 °C and observed under a fluorescent microscope. The $TCID_{50}$ was now determined by counting every fluorescent cavity as “positive”, irrespective of the extent of cytopathic effect.
To gain a stable value of the stock titer, another virus aliquot was titrated in the described manner. The $TCID_{50}$, or rather the pfu/ml, was expressed as average of the mean.

$$\frac{\mathrm{TCID}_{50}}{ml}\left(\frac{pfu}{ml}\right) = \frac{10^{1+\sum infected\ wells - 0.5\ x \log 10}}{30\ \mu l\ (inserted\ viral\ stock\ solution)}$$

$TCID_{50}$-formula by Spearman and Kärber

The titration of measles vaccine virus was performed by Dr. Martina Schell.

2.2.5 Microscopy

Before plating and on the infection day, cells were observed at various magnifications with a light microscope to check for contamination, cell distribution and confluence. During trials, virus-encoded GFP and TurboFP635 expression were visualized several times under a fluorescence microscope with suitable excitation and emission wavelengths, or observed constantly in a separate trial (section 3.5.2) using the All-in-One BZ-9000 fluorescence microscope.

A high-definition camera (F-view, Soft Imaging System GmbH) was connected to the microscope (IX50, Olympus) to take fluorescence pictures by applying the Olympus U-RFL-T function. Bright-field pictures were taken with a 4–10 x objective with the PhL, respectively the Ph1/PhC ocular. Captured images were processed with the Analysis 3.1 software (Soft Imaging System GmbH) and merged to yield overlays by Adobe Photoshop 7.0 (Adobe Systems, Mountain View, CA). Digital images (All-in-one BZ-9000 fluorescence microscope) were further processed with the BZ-II software. Here, haze reduction, black balance and the superimposing function were applied in order to receive sharp-cut

images. All images were adjusted with Microsoft PowerPoint 2010, respectively Microsoft PowerPoint 2013.

2.2.6 Determination of cell mass and cytotoxic effects

After incubation with oncolytic viruses, we needed to quantify the cytotoxic effect of virus infection. Therefore, Sulforhodamine-B (SRB) assay (Skehan *et al*, 1990) was performed. The SRB assay measures the residual cell mass, but it does not differentiate between viable and dead cells (Vichai & Kirtikara, 2006). Therefore, results obtained by SRB were compared to those of MTT, a cell viability assay.

2.2.6.1 SRB assay

The SRB assay uses the characteristics of Sulforhodamine-B as an acid dye for cell staining. Thus, the remaining cell mass can be quantified in drug-toxicity trials. SRB binds to cellular proteins when cells were fixed with TCA or comparable acids before. After dissolution under mild basic conditions, the optical density (OD) is measured by using a microtiter plate reader (Tecan GENios). The OD correlates linear with the protein content and therefore with the remaining cell count (Skehan *et al*, 1990).

The exact procedure includes the following steps. Medium was removed from the wells at 96 hpi the longest and cells were washed with cold (4 °C) PBS. Thereafter, cells were fixed with 250 µl cold (4 °C) TCA (10 % w/v) per well. Plates were incubated at 4 °C for at least 30 minutes. After this time period, TCA was removed and discarded, plates were washed three times with tap water, before dried under UV light for approximate 15 minutes. Subsequently, plates were stored in a heating cabinet (40 °C) for at least 12 hrs or overnight to ensure the drying process.

In a next step, SRB dye and 1 % acetic acid needed to be prepared. 250 µl of room-tempered SRB dye/well were added to the cells and incubated for 10 minutes. Thereafter, plates were washed accurately with 1 % acetic acid until no unbound staining solution remained. To double-check, plates were

tapped firmly on absorbent paper. Next, plates were ranged in the heating cabinet (40 °C) until they were dried completely and either measured directly or stored in a dark place for a couple of days.

For the measurement of OD at 550 nm, 500 or 1000 µl/well TRIS base (10 mM, pH 10.5), depending on the colour intensity, were pipetted to the cells. Plates were stored on ice and agitated gently until the stain was dissolved completely. Subsequently, 80 µl/well in duplicates were transferred into a 96-well plate consistent with a microtiter plate reader. Results were further calculated with Microsoft Excel 2010. The following statistical analysis was performed with GraphPad Prism4 and GraphPad Prism6 (GraphPad Software). Values of treated cells were normalized on mock-treated cell data (set as 100 %) unless otherwise specified.

2.2.6.2 MTT assay

As another colorimetric assay, the MTT assay quantifies cell metabolic activity and therefore cell viability. Only viable cells convert 3-(4,5-dimethylthiazol-2-yl)-2,5-diphenyltetrazolium bromide, a pale yellow tetrazolium salt, into blue colored formazan crystals. The OD, measured by a microtiter plate reader, is directly proportional to the amount of living cells (Mosmann, 1983).

First, MTT stock solution needed to be prepared and protected from light, thus, the tube was wrapped with aluminum foil at any time. After various incubation periods with oncolytic viruses, plates were washed carefully with PBS. Next, 250 µl MTT solution/well were added for 2 hrs at 37 °C. Thereafter, the supernatant was aspirated carefully and discarded. Plates were wrapped quickly with a strip of parafilm and stored in the refrigerator at -20 °C. For measurement, 1 ml of acidified isopropanol (1 N HCl in isopropanol) was added to each well and plates were placed on a shaker until the dye dissolved thoroughly. Next, 200 µl of each well were transferred to a 96-well plate consistent with a microtiter plate reader. Measurement was now performed using a 570 nm test wavelength and a 650 nm reference wavelength. The received data was calculated with Microsoft Excel 2010 and Microsoft Excel

2013. The following statistical analysis was performed with GraphPad Prism4 and GraphPad Prism6 (GraphPad Software).

2.2.7 Polyacrylamide gel electrophoresis (PAGE) and western blot

2.2.7.1 Production of protein lysates

Cells were plated in 24-well plates and incubated overnight as described before. The next day, wells were either infected by VACV at defined MOIs in 50 µl/well 2 % FBS-supplemented DMEM, or cells were mock-treated. Thereafter, plates were sequentially infected at 6 hpi with MeV-GFP. At the end of the incubation period, supernatant was removed and wells were washed carefully with PBS. PBS was not discarded but pooled to reduce cell loss due to this washing step. Next, 125 µl EDTA-Trypsin/well were applied for the detachment of the cell layer. Identically treated cells were now collected in tubes. Wells were washed with 500 µl 10 % FBS-supplemented DMEM and the volume was transferred to the belonging tube to inactivate the EDTA-Trypsin. PBS and collected cells were merged, before tubes were centrifuged at 1200 rpm for 3 minutes at 22 °C. In the meantime, the prepared lysis buffer was completed by adding one tablet complete mini, a protease inhibitor. Accordingly, supernatant was discarded from the centrifuged tubes, 450 µl of the finished lysis buffer were pipetted to each cell pellet and resuspended thoroughly, before the tubes were sonicated 3 x 30 seconds. Subsequently, the obtained protein lysates were centrifuged at 4600 rpm for 10 minutes at 4 °C. The supernatant was aspirated and distributed to the prepared reaction tubes, 150 µl per tube. Lysates were then stored at -20 °C.

2.2.7.2 Discontinuous SDS-Polyacrylamide gel electrophoresis

Electrophoresis, a method to investigate the mobility of macromolecules in an electric field, is widely used to categorize proteins according to their size, confirmation and charge. By using Sodium-Dodecyl-Sulfate polyacrylamide gel electrophoresis (SDS-PAGE), proteins are separated exclusively according to their size. 2-mercaptoethanol and SDS are attached to linearize proteins, SDS

additionally charges polypeptides equally negative dependent on their molecular weight. In order to sharpen bands, a discontinuous SDS-PAGE (Laemmli, 1970), containing a 1.5 mm stacking gel with 5 % acrylamide and a resolving gradient gel with 8 to 15 % acrylamide, was performed.

First, the gel caster was assembled and the resolving gradient gel was compounded using 8 % and 15 % resolving gel solutions. APS and TEMED were added at last because they start the polymerization. Approximately 10 ml of both approaches (8 and 15 % resolving gel solutions) were poured between the two glass plates using a pulsatile pump, which is necessary to provide a controlled mixture. Next, 1 ml isopropanol was pipetted on top to flatten the gel. After the resolving gel was polymerized, isopropanol remnants were outpoured and the gel was overlaid with the prepared stacking gel. Before the stacking gel was polymerized completely, a 15-pocket comb was inserted.

Prior to use, the loading buffer was adjusted by adding 2-mercaptoethanol to cleave disulfide bonds. Now, an appropriate volume of each protein lysate was transferred to 1.5 ml reaction tubes. Subsequently, a calculated volume of the loading buffer (1/5 of the volume of each protein lysate) was added to each sample, and lysates were stored on ice or at -20 °C. Now, the loaded lysates were centrifuged at 13000 rpm for 1 minute, denatured at 95 °C for 10 minutes and once again centrifuged. Tubes were stored on ice before reaching room-temperature.

The gel cassette was now placed in a vertical electrophoresis chamber, which was filled with PAGE buffer (1 x). The inserted comb was removed carefully and the remaining cavities were flushed out with PAGE buffer (1 x). Each sample was pipetted at a defined volume into the slots. The first slot was reserved for the rainbow marker (Full Range Rainbow Protein Marker), which was used as molecular weight standard. All filled slots were covered with a small layer of PAGE buffer (1 x). Now, the assembly of the electrophoresis chamber was completed and the tank was filled up with PAGE buffer (1 x) to the rim. Electrophoresis was started at a higher voltage (100 V) for 30 minutes.

Thereafter, 55 V were applied overnight until the bromophenol blue front reached the edge of the resolving gel.

2.2.7.3 Western Blot

To visualize macromolecules, separated by discontinuous SDS-PAGE, proteins were transferred from the resolving gel to a membrane by blotting technique and afterwards detected by linked antibodies (Burnette, 1981; Towbin *et al*, 1992).

A PVDF membrane, which is often preferred when compared to nitrocellulose membranes (Mahmood & Yang, 2012), was slewed in methanol, rinsed with filtered water (H_2O_{dd}) and incubated with transfer buffer (1 x) on a shaker for 15 minutes. Additionally, two sponges and three Whatman papers, which are necessary to assemble the blot sandwich, were soaked in transfer buffer (1 x). The glass plates of the gel caster (section 2.2.7.2) were removed carefully and the stacking gel was separated from the resolving section. Next, the resolving gel was placed upon the prepared membrane, air bubbles were prevented by the aid of a glass rod. Covered by transfer buffer (1 x), the blot sandwich was assembled and fixed accurately in a suitable blotting system. Blotting was performed at 400 mA for 90 minutes at 4 °C. Since the membrane was oriented in direction of the anode, negative loaded proteins were transferred to the membrane.

After blotting, unspecific binding of antibodies was prohibited by blocking the PVDF membrane with 5 % milk in TBS-Tween (2.5 g milk powder, resolved in 50 ml TBS-Tween) for at least 90 minutes. Thereafter, the membrane was rinsed thoroughly with TBS-Tween for 5 minutes, wrapped in transparent film and cut into various pieces dependent on the expected positions of the bands. The visible rainbow marker served as a landmark, since each coloured line of the marker stands for a specific molecular weight.

Next, antibody solutions were diluted as detailed in section 2.1.2. Primary antibodies were incubated with their belonging pieces of the PVDF membrane on a shaker at 4 °C overnight. The following day, diluted antibody solutions

were recycled and the pieces of the membrane were washed 3 x 10 minutes with TBS-Tween to remove unstable bounded antibodies. For binding of secondary antibodies, directed against mouse IgG or rabbit IgG, matching pieces were incubated at room-temperature for 45 minutes under gentle agitation.

The secondary antibody is linked to an enzyme called horseradish peroxidase (HRP). This enzyme converts ECL solution, which contains luminol, under basic conditions into a reaction product generating luminescence. The light intensity, which is dependent on the amount of bound protein, exposes and develops an X-ray film (Hyperfilm^{TM} ECL), and thereby visualizes the antibody-linked proteins on the membrane.

Accordingly, after incubation with the secondary antibody, the pieces were rinsed 4 x 15 minutes with TBS-Tween. By avoiding air-bubbles, detection reagent 1 and 2 of the ECL solution were mixed at equal volumes and incubated with the pieces for 1 minute. Thereafter, the pieces were fixed in a photo cassette and exposed to a sensitive photo film (Fuji Photo Film).

For detection of proteins with similar molecular weights, it was necessary to remove the linked primary and secondary antibodies. In order to do so, the pieces of the membrane were incubated for 30 minutes at 50 °C with a stripping buffer, washed 6 x 10 minutes with TBS-Tween and blocked with 5 % milk in TBS-Tween as described above. The detection process was then repeated with the application of the suitable primary antibody.

3 Results

The aim of this thesis was to test a novel approach for overcoming resistance of tumor cells against virotherapy by performing sequential infections applying two completely different virus types, i.e., oncolytic vaccinia virus together with measles vaccine virus.

Accordingly, preliminary tests with both viral vectors were performed to determine “appropriate” multiplicities of infection (MOIs), defined as viral concentrations at which the tumor cell mass was reduced less than 25 % in a single infection approach. Thus, highly resistant human tumor cell lines, such as ACHN, HCT15, KM12, SRH and CCS, were seeded at equal plating density and infected first with oncolytic VACV GLV-1h254 at various MOIs (section 3.1.1).

Based on the observation that each tumor cell line required different plating densities to reach confluence, we compared several initial cell counts to identify the most suitable one (section 3.1.2.1). As a proof of principle, xCELLigence trials with ACHN and KM12 cells were performed (section 3.1.2.2). Single infection approaches with VACV were repeated at confluence-optimized plated cells (section 3.1.3) and executed with MeV-GFP for the first time (section 3.1.4).

In order to guarantee survival of untreated cells until the end of the trial, single infection approaches with VACV were modified and repeated for ACHN, HCT15 and KM12 cells (section 3.1.5). Eventually, we were able to examine different orders of virus treatment and different time points for secondary virus infection in sequential infection approaches (section 3.2). To further investigate whether an improved susceptibility to virus infection of double-infected cells was due to synergistic or additive effects, we performed sequential infections at different dosages of the second virus (section 3.3).

In addition, a Keyence microscope was implemented to get a closer look at the observed phenomenon of “viral competition” (section 3.5.2). Moreover, data

obtained from SRB assays were compared to those from MTT assay to confirm the results and detect potential sources of error (section 3.4).
Finally, electrophoresis and western blot were implemented to investigate the expression of virus-specific proteins (section 3.6).

3.1 **Identification of a suitable MOI for both viral vectors by single infections**

The resistance of human tumor cell lines such as ACHN, HCT15, KM12, SRH and CCS upon virotherapy is relative. Here, highly resistant cell lines were defined by cell mass reduction of less than 25 % compared to uninfected controls at 96 hpi. In order to determine an appropriate MOI, single virus infections were performed with both viral vectors. Prior to infection trials, vaccinia and measles vaccine virus titers were determined according to the methods described in section 2.2.4.4.

3.1.1 Preliminary tests for vaccinia virus GLV-1h254 infection

As suggested in previous work from C. Raff (unpublished data) and M. Noll (Noll *et al*, 2013), all three selected cell lines of the NCI-60 panel (ACHN, HCT15 and KM12) as well as a sarcoma (CCS) and a rhabdomyosarcoma (SRH) cell line were seeded equally in 24-well plates. Cells were incubated overnight and 5×10^4 cells/well were assumed to comply with current cell counts. On the infection day, cells were either infected in quadruplicates with VACV GLV-1h254 at MOI 0.0001, 0.001, 0.01, 0.1 and 1 or mock-treated. During the incubation period, expression of virus-encoded TurboFP635 was observed daily under a fluorescence microscope (Figure 9). At 96 hpi, plates were analyzed by SRB assay (Figure 10).

As visualized in Figure 9, we noticed differences between the cell lines referring their reached extent of confluence one day post infection (1 dpi). Whereas ACHN cells grew subconfluent, and HCT15 cells reached approximately 50 % confluence, KM12, SRH and CCS cells revealed a slower growth behavior. For CCS cells there were no pictures archived at 1 dpi.

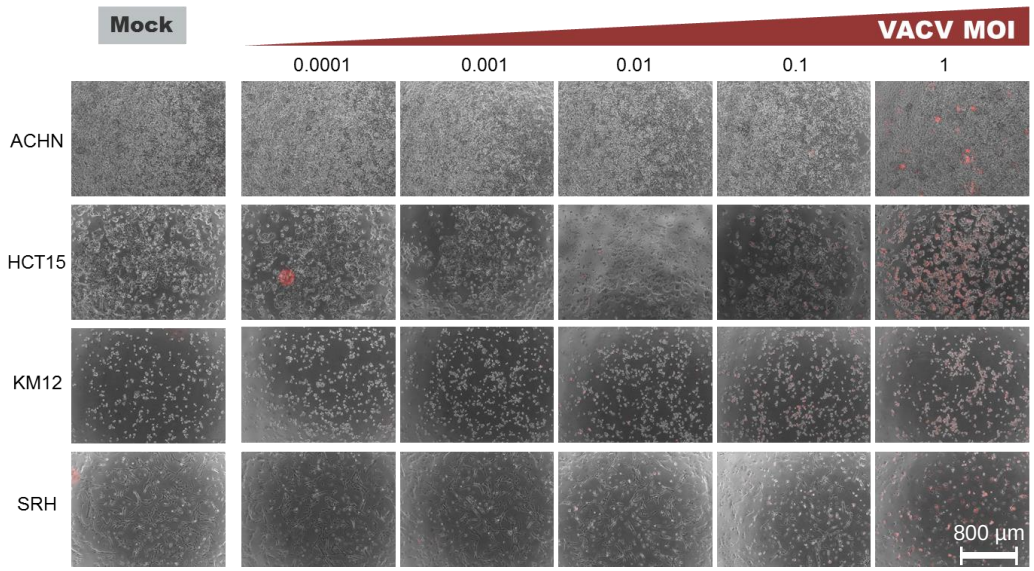

Figure 9. Overlays of fluorescence and bright-field pictures from VACV single-infected human tumor cell lines, 1 dpi

Cells were seeded at equal plating densities (5 x 10^4 cells/well in 24-well plates). Cells were either infected with VACV GLV-1h254 at MOI 0.0001, 0.001, 0.01, 0.1 and 1 or mock-treated. Fluorescence and bright-field pictures were taken at 1 dpi and overlaid afterwards. Infected cells show TurboFP635 expression as VACV marker for viral gene expression (HCT15 at MOI 0.0001: red signal is based on an artifact). Scale bar in the right lower corner applies to all panels.

As detailed in Figure 10, ACHN and HCT15 cells were defined highly resistant at MOI 0.01, according to the specification given above, when analyzed by SRB assay. At higher MOIs cell masses were reduced more than 25 %. For KM12, SRH and CCS cells it was difficult to make a statement because of large standard deviations of means of three independent experiments. As a consequence, the development of confluence dependent on plating densities was evaluated next.

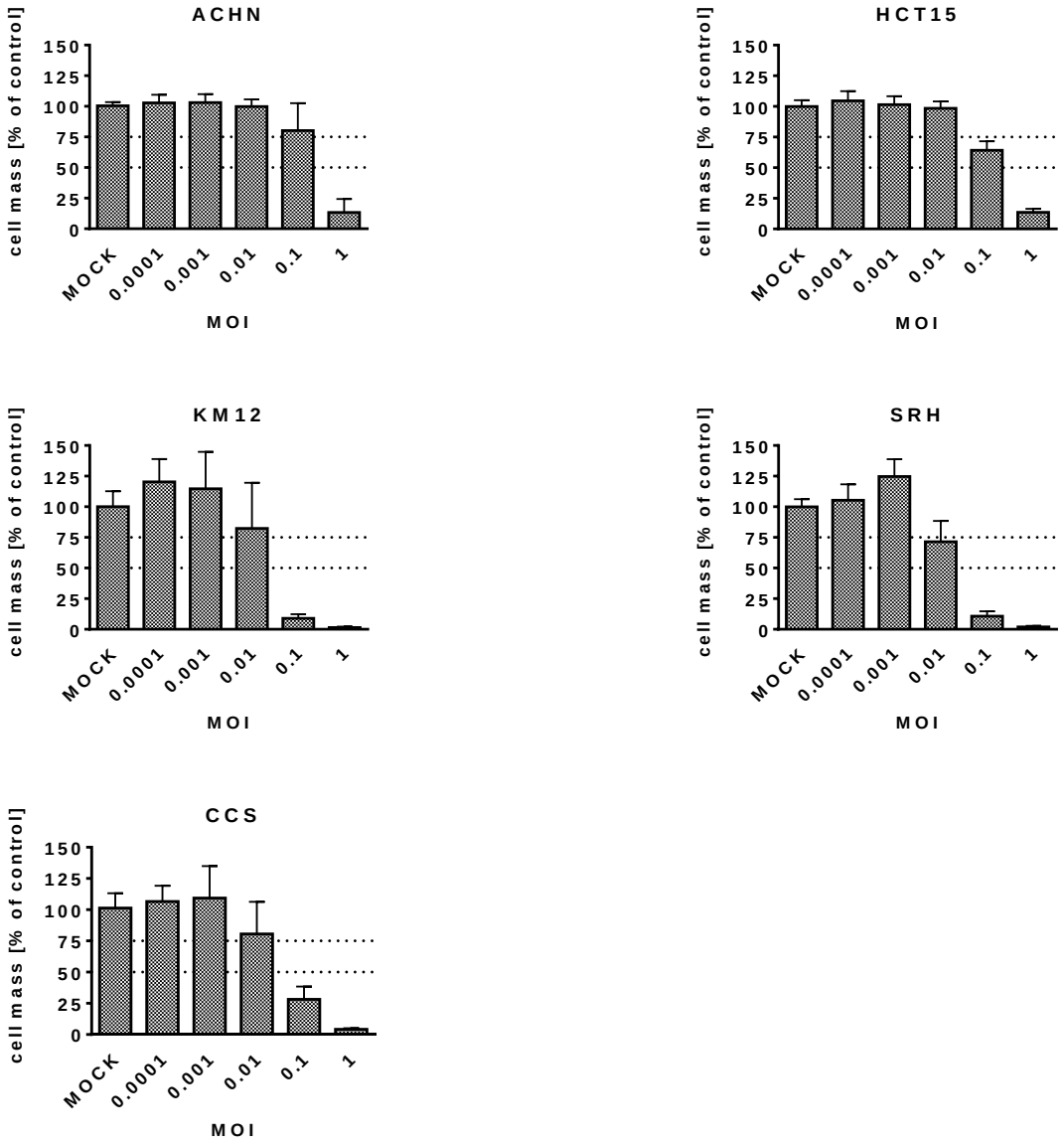

Figure 10. Identification of a suitable MOI in equally plated tumor cell lines infected with VACV GLV-1h254 in SRB assays

Cells were plated at 5 x 10^4 cells/well. The next day (except CCS: one data set was obtained from cells infected 2 days after plating), cells were either infected in quadruplicates with VACV at MOI 0.0001, 0.001, 0.01, 0.1 and 1 or mock-treated. At 96 hpi, cells were fixed and the remaining cell mass was analyzed by SRB assay. Mock-treated (uninfected) controls were set 100 %. Dotted lines highlight the 50 and 75 % remaining cell mass. Values are means of three independent experiments (except ACHN: Values until MOI 0.1 are means of four independent experiments, for MOI 1 two data sets are integrated). Error bars: SD.

3.1.2 Evaluation of cell density and confluence

To guarantee optimal conditions for uninhibited cell growth, as well as for virus infection and spreading, the development of confluence was analyzed. Thus, so called “confluence trials” were performed for each cell line. Additionally, a proof of principle was generated by xCELLigence trials using ACHN and KM12 cells.

3.1.2.1 Confluence trials

We evaluated the development of confluence, dependent on several plating densities, and studied cell adherence and growth rate. Furthermore, we took note of medium color change. ACHN, HCT15, KM12, SRH and CCS cells were plated at densities of 5×10^4, 1×10^5 and 2×10^5 (except SRH) cells/well in 24-well plates. KM12 cells were additionally seeded at 4×10^5 cells per well. Cells were incubated for 6 days and observed daily under a light microscope. The reached extent of confluence was documented, expressed as an estimated percentage (Figure 11).

At a plating density of 5×10^4 cells/well, ACHN cells adhered overnight and reached approximately 50 % confluence within two days. At this plating density, HCT15 and CCS cells stuck to the bottom not until two days after plating. At a density of 1×10^5 cells/well, ACHN, HCT15 and SRH cells reached a plateau at day 4 (ACHN, HCT15), respectively at day 3 (SRH). At day 5, ACHN and HCT15 cells showed medium color change from red to yellow, which indicated reduced pH values. CCS and KM12 cells, however, adhered insufficiently to the bottom and tended to detach at higher densities although cells did not reach total confluence. Additionally, KM12 cells agglomerated quickly and independent of the initial cell count and the medium color turned yellow at day 4 (2×10^5 cells/well), respectively at day 5 (1×10^5 cells/well).

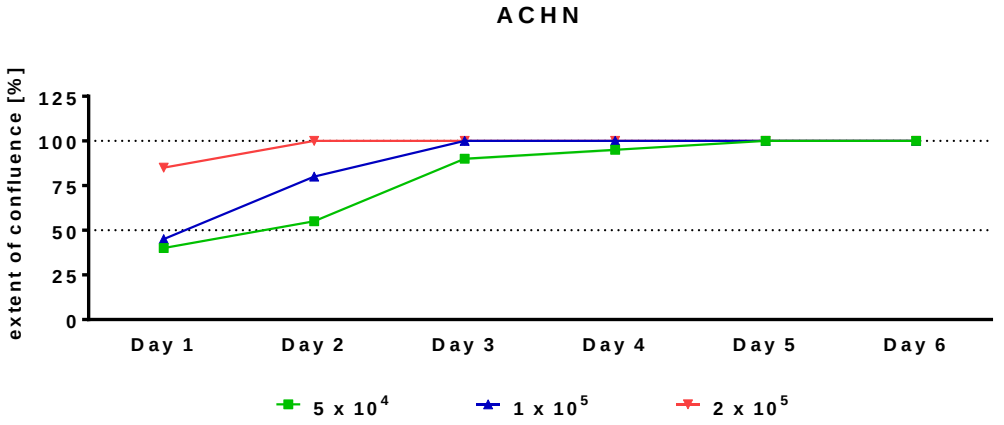
ACHN
extent of confluence [%]
125
100
75
50
25
0
Day 1
Day 2
Day 3
Day 4
Day 5
Day 6
5 x 10^4
1 x 10^5
2 x 10^5

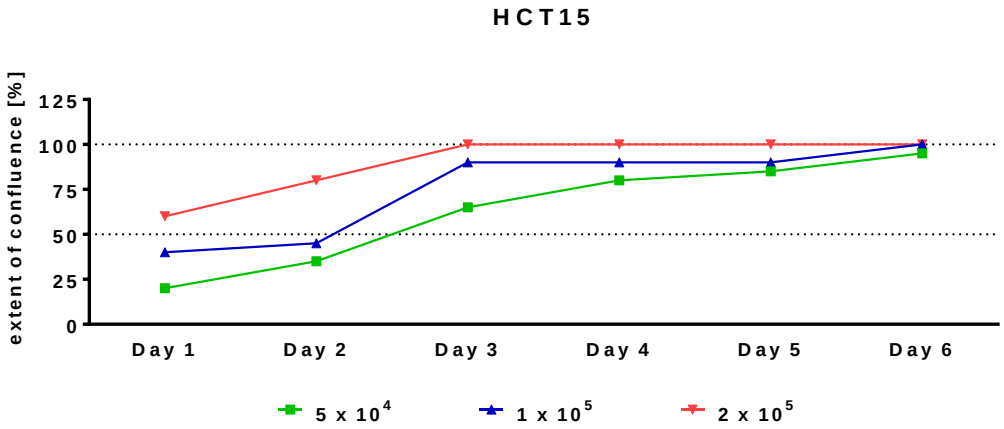
HCT15
extent of confluence [%]
125
100
75
50
25
0
Day 1
Day 2
Day 3
Day 4
Day 5
Day 6
5 x 10^4
1 x 10^5
2 x 10^5

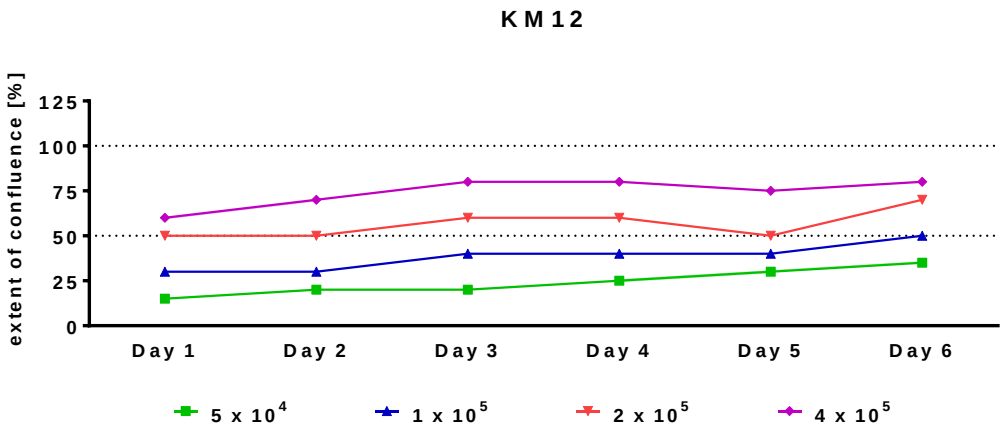
KM12
extent of confluence [%]
125
100
75
50
25
0
Day 1
Day 2
Day 3
Day 4
Day 5
Day 6
5 x 10^4
1 x 10^5
2 x 10^5
4 x 10^5

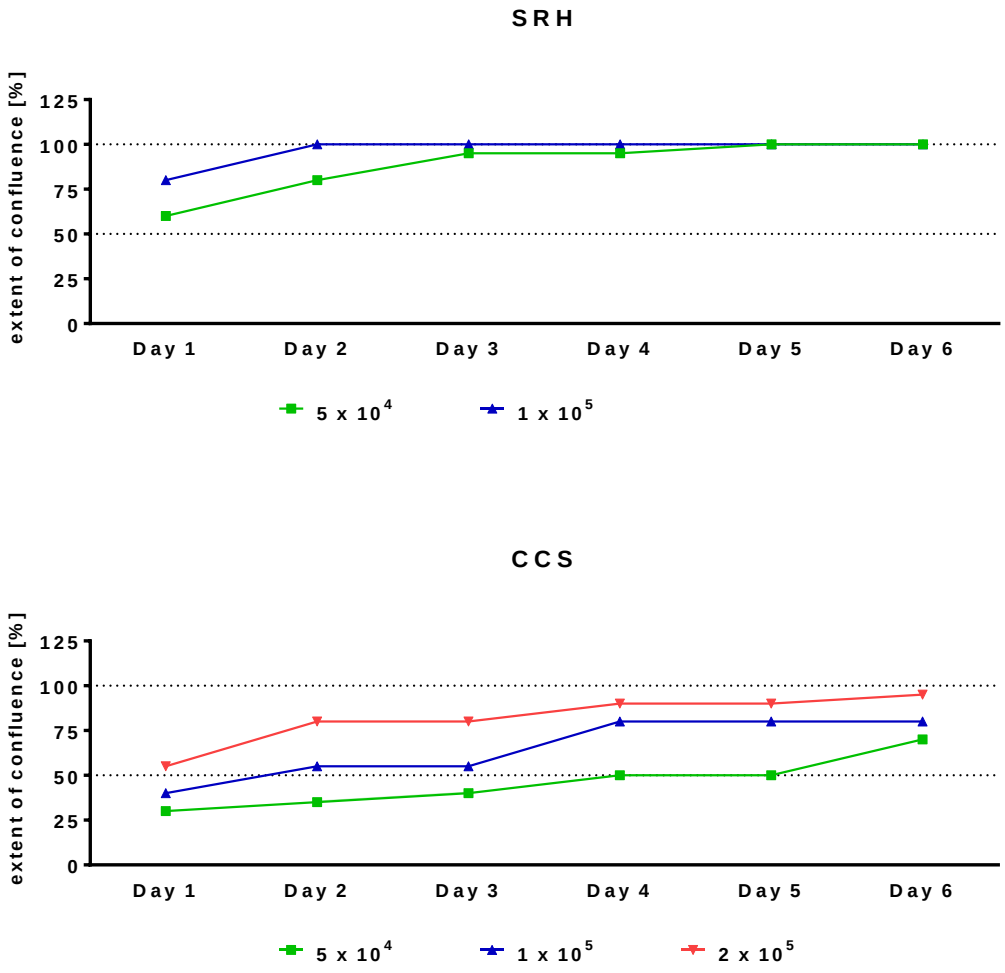

Figure 11. Extent of confluence during 6 days of incubation

ACHN, HCT15, KM12**,** SRH and CCS cells were plated at 5 x 10^4, 1 x 10^5 and 2 x 10^5 (except SRH) cells/well in 24-well plates. KM12 cells were additionally seeded at 4 x 10^5 cells/well. Cell lines were examined under a light microscope for six days and evaluated by the naked eye. The extent of confluence related to initial cell counts is diagrammed (expressed as a percentage). Dotted lines highlight 50 and 100 % confluence of the cell layer.

Accordingly, initial cell counts were retrospectively determined for each cell line in order to optimize survival of uninfected controls until 96 hpi. Unless otherwise specified, cells were seeded as detailed in Table 1 for all following experiments.

Table 1. Recommended plating densities for each cell line to build optimal confluence in 24-well plates

The table shows the recommended number of days before infection and plating densities at which cells should be plated in 24-well plates. dbi = days before infection.

Cell line	*Days before infection (dbi), plating densities*
ACHN	1 dbi, 5 x 10^4 cells/well
HCT15	2 dbi, 5 x 10^4 cells/well
KM12	2 dbi, 4 x 10^5 cells/well
SRH	2 dbi, 5 x 10^4 cells/well
CCS	2 dbi, 2 x 10^5 cells/well

3.1.2.2 xCELLigence trial

Confluence trials, as depicted in section 2.2.3.3, were necessary to determine suitable initial cell counts in 24-well plates. Nevertheless, the development of confluence was evaluated by the naked eye only. Consequently, cells were further analyzed by xCELLigence system to demonstrate a proof of principle. If the plating density is chosen too high, uninfected controls will grow over, which induces growth inhibition and cell death. Additionally, the initial cell count, and therefore the extent of confluence, affects efficiency of infection and spreading of vaccinia virus particles.

Prior to xCELLigence trial, initial cell counts suitable for 96-well plates needed to be identified. Thus, several plating densities (1 x 10^5, 5 x 10^4, 2.5 x 10^4, 1 x 10^4, 5 x 10^3, 2.5 x 10^3 and 1 x 10^3 cells/well) of ACHN and KM12 cells were seeded in 96-well plates, and cells thereafter infected with VACV GLV-1h254 at MOI 0.1, 1 or mock-treated. Virus spreading and the development of confluence were monitored under a fluorescence microscope until 96 hpi.

As a result, ACHN cells were plated at 1 x 10^3, 2 x 10^3, 4 x 10^3 and 8 x 10^3 cells/well, KM12 cells at 2.5 x 10^3, 5 x 10^3, 1 x 10^4, 2 x 10^4 cells/well in the following xCELLigence trial. After 22.5 hrs, cells were infected with VACV GLV-1h254 at MOI 0.1, 1 or mock-treated. Triton 0.1 % X-100 was used as a positive

control for cell death. Electrical impedance was measured at 30-minute intervals and all curves were normalized. Unfortunately, KM12 cells did not adhere firmly enough; thus, electrical impedance could not be measured sufficiently and values were neglected.

As shown in Figure 12, uninfected controls of ACHN cells plated at low densities did still proliferate at 96 hpi. However, mock-treated cells, which were seeded at higher cell numbers, hit a plateau (4 x 10^3 cells/well 90 hpi) or even levelled off (8 x 10^3 cells/well 60 hpi). Interestingly, with higher cell numbers the disparity of the normalized cell index between mock treated and virus infected cells increased. In particular, this was evident for the MOI 0.1 treatment group. The xCELLigence trial was kindly supported by Dr. Dr. Sascha Venturelli, Christian Leischner and Dr. Martina Schell.

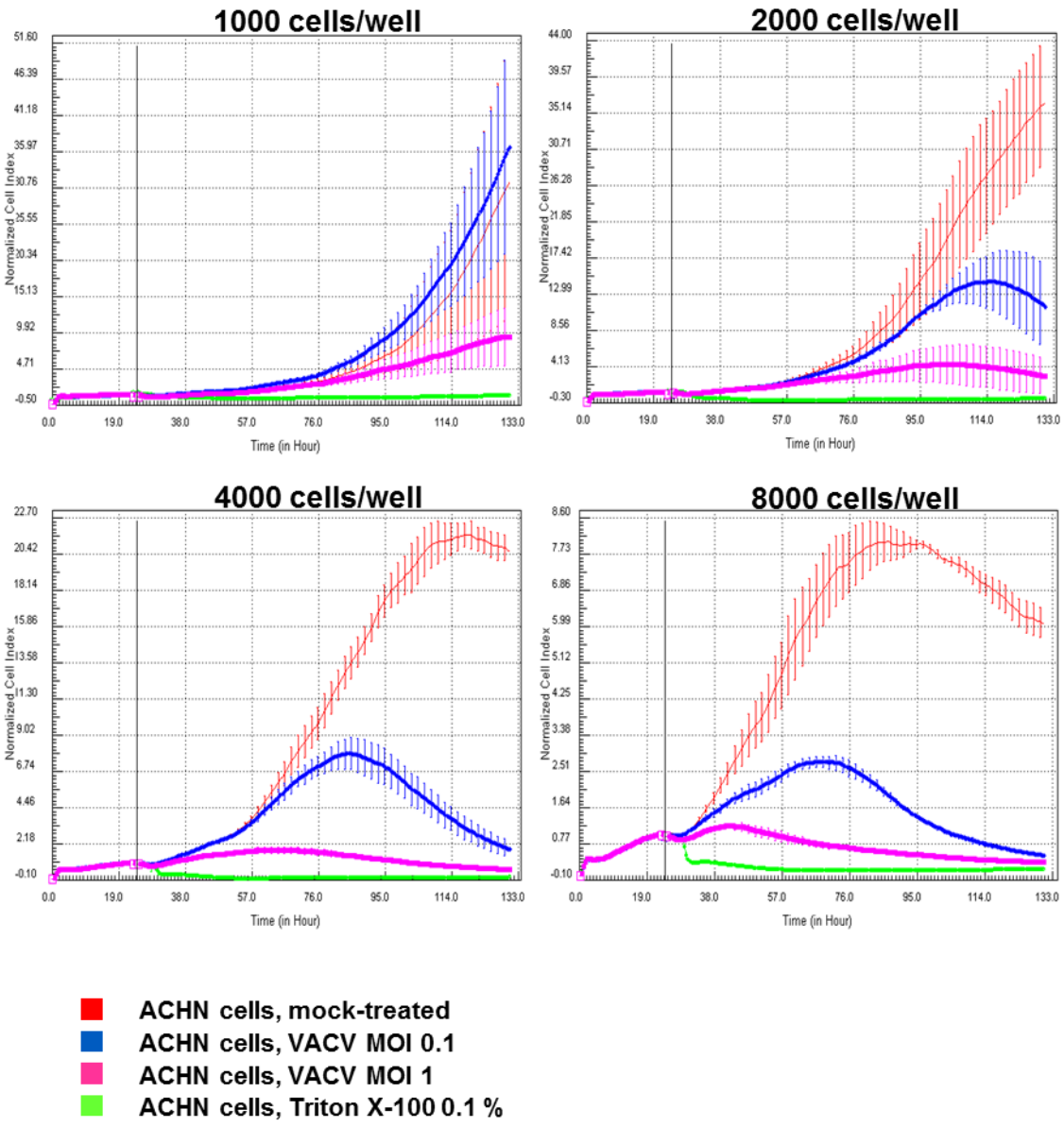

Figure 12. xCELLigence in real-time monitoring of cell proliferation

ACHN cells were plated in triplicates at densities of 1 x 10^3, 2 x 10^3, 4 x 10^3 and 8 x 10^3 cells/well. At 22.5 hrs after seeding, cells were either infected with VACV GLV-1h254 MOI 0.1, 1 or mock-treated. Triton X-100 0.1 % was used as positive control for cell death. Cell index was continuously monitored in 30-minute intervals, starting after plating the cells. All values were normalized (line mark). Error bars: SD. This figure was kindly generated by Dr. Dr. Sascha Venturelli.

3.1.3 Identification of a suitable MOI for vaccinia virus GLV-1h254 in confluence-optimized plated cells

As specified above, appropriate MOIs should be determined by infection of confluence-optimized plated cells. Thus, HCT15, KM12, SRH and CCS cells were seeded as detailed in Table 1. Due to the fact that test conditions for ACHN cells did not changed, approaches were not repeated for this cell line.

On the infection day, cells were inoculated in quadruplicates with VACV at MOI 0.0001, 0.001, 0.01 and 0.1 or mock-treated. MOI 1 was no longer applied, since cell masses of infected cells were eradicated completely in preliminary tests (section 3.1.1). During the incubation period, cells were observed daily under a fluorescence microscope. At 96 hpi, cells were fixed and analyzed by SRB assay (plates were washed once with tap water before washed approximately three times with 1 % acetic acid).

As shown in Figure 13, virus infection and spreading were monitored by observation of virus-encoded TurboFP635. As assumed, the number of infected cells increased at ascending viral concentrations and led to plaque forming units (HCT15, CCS). Interestingly, although GLV-1h254 formed large plaque forming units at MOI 0.01 and 0.1 in HCT15 cells, analysis by SRB assay revealed less cell mass reduction than expected (Figure 14). KM12, SRH and CCS cells were almost completely infected and subsequently erased at higher MOIs.

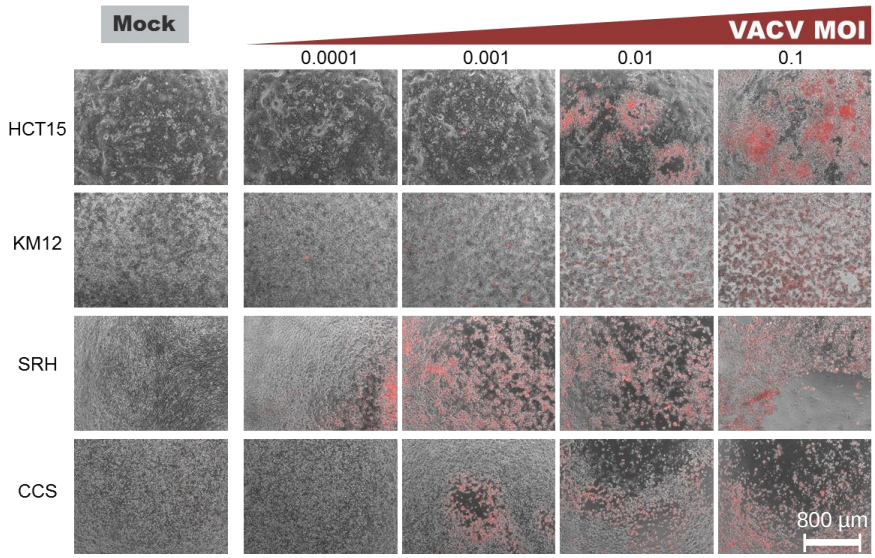

Figure 13. Overlays of fluorescence and bright-field pictures from VACV single-infected human tumor cell lines, confluence-optimized, 4 dpi

HCT15, KM12, SRH and CCS cells, seeded at confluence-optimized plating densities (Table 1), were either single-infected with VACV GLV-1h254 at MOI 0.0001, 0.001, 0.01, 0.1 or mock-treated. Fluorescence and bright-field pictures were taken at 4 dpi and overlaid afterwards. Infected cells show TurboFP635 expression as VACV marker for viral gene expression. Scale bar in the right lower corner applies to all panels.

As represented in Figure 14, HCT15 and KM12 cells were defined highly resistant at MOI 0.01. At MOI 0.1, however, cell counts were decreased to the critical value of 75 % (HCT15) or even lower (KM12). SRH and CCS cells were erased almost completely at ascending viral concentrations (MOI 0.01, 0.1).

When compared to results obtained from SRB assay in section 3.1.1, here, means of KM12 cells show lower standard deviations, whereas those of SRH and CCS were unimproved. Anyhow, cell masses from SRH and CCS cells infected at MOI 0.001, 0.01 and 0.1 were reduced compared to those obtained from equally plated cells (Figure 10). Resulting, SRH and CCS cells were defined as resistant at MOI 0.0001 according to the definition given above.

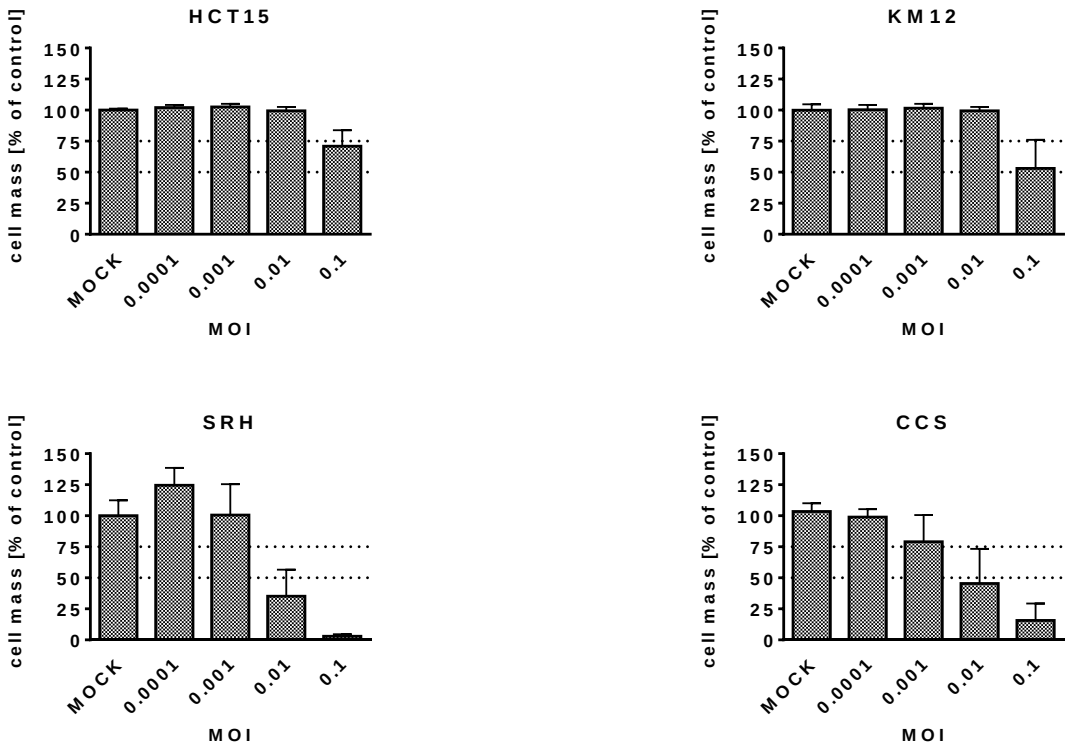

Figure 14. Identification of a suitable MOI in confluence-optimized plated cell lines infected with VACV GLV-1h254 in SRB assays

Cells were plated as detailed in Table 1. Cells were either infected in quadruplicates with VACV at MOI 0.0001, 0.001, 0.01 and 0.1 or mock-treated. At 96 hpi, cells were fixed and the remaining cell mass was analyzed by SRB assay. Mock-treated (uninfected) controls were set 100 %. Dotted lines highlight the 50 and 75 % remaining cell mass. Values are means of three independent experiments. Error bars: SD.

3.1.4 Identification of a suitable MOI for measles vaccine virus MeV-GFP in confluence-optimized plated cells

All five cell lines were seeded according to Table 1 and infected in quadruplicates at ascending viral concentrations (MOI 0.001, 0.01, 0.1, 1 and 10) with MeV-GFP or were mock-treated. Cells were incubated until 96 hpi and virus-encoded GFP was observed daily under a fluorescence microscope. At 96 hpi, infected cells were analyzed via endpoint SRB assay (plates were washed once with tap water before washed approximately three times with 1 % acetic acid).

The number of infected cells, visualized by virus-encoded GFP expression and syncytia formation, increased at ascending viral concentrations in all cell lines, except for SRH cells where only few infected cells could be visualized (Figure 15). At MOI 10, HCT15 cells were barely infected, whereas ACHN, KM12 and CCS cells represented the mentioned signs of infection especially at higher MOIs.

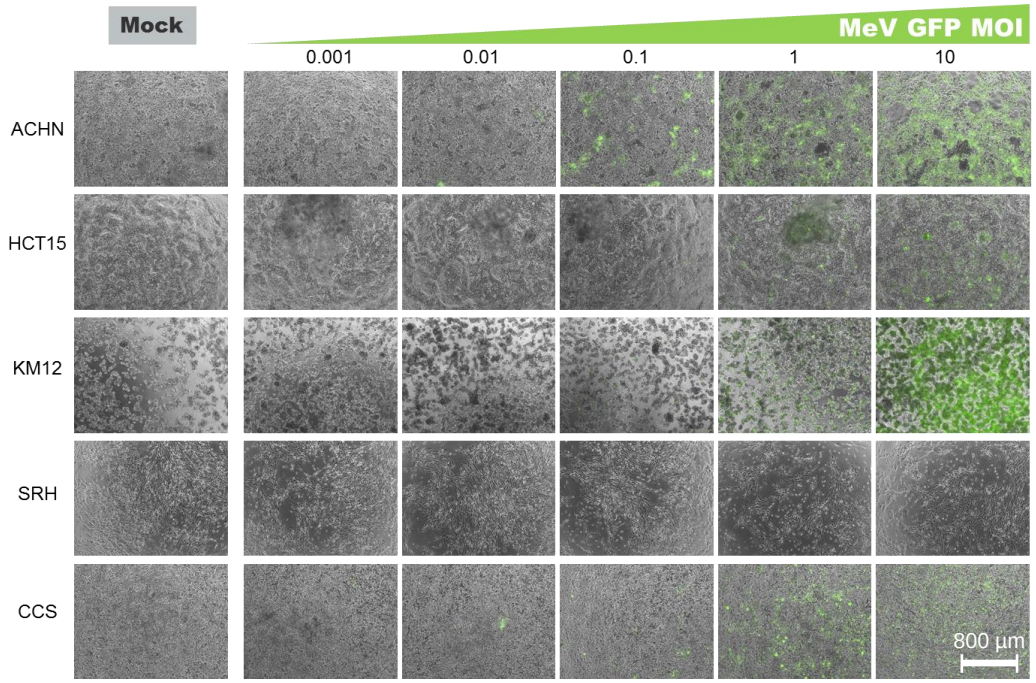

Figure 15. Overlays of fluorescence and bright-field pictures from MeV-GFP single-infected human tumor cell lines, confluence-optimized, 4 dpi

ACHN**,** HCT15, KM12, SRH and CCS cells, seeded at confluence-optimized plating densities (Table 1), were either single-infected with MeV-GFP at MOI 0.001, 0.01, 0.1, 1, 10 or mock-treated. Fluorescence and bright-field pictures were taken separately at 4 dpi and overlaid afterwards. Infected cells show GFP expression as marker for viral gene expression and syncytia formation as cytopathic effect. Scale bar in the right lower corner applies to all panels.

When ACHN, HCT15, KM12, SRH and CCS cells were analyzed by SRB assay regarding oncolysis (Figure 16), these cell lines responded barely to virus infections at MOI 0.001, 0.01 or 0.1. At MOI 1, ACHN, SRH and CCS cells showed a cell mass reduction but less than 25 %, whereas HCT15 and KM12 cells showed almost no tumor cell lysis. It has to be mentioned that cell counts of SRH and CCS cells revealed large standard deviations between three

independent experiments. At MOI 10, ACHN cells were reduced to nearly 50 %, HCT15 and SRH cells showed an increased cytopathic effect above the critical value of 75 % but with large standard deviations.

Cell numbers of KM12 and CCS cells, however, collapsed almost completely at the highest MOI. Consequently, MOI 1 was defined as the critical multiplicity of infection for MeV-GFP for further experiments concerning ACHN, HCT15 and KM12 cells.

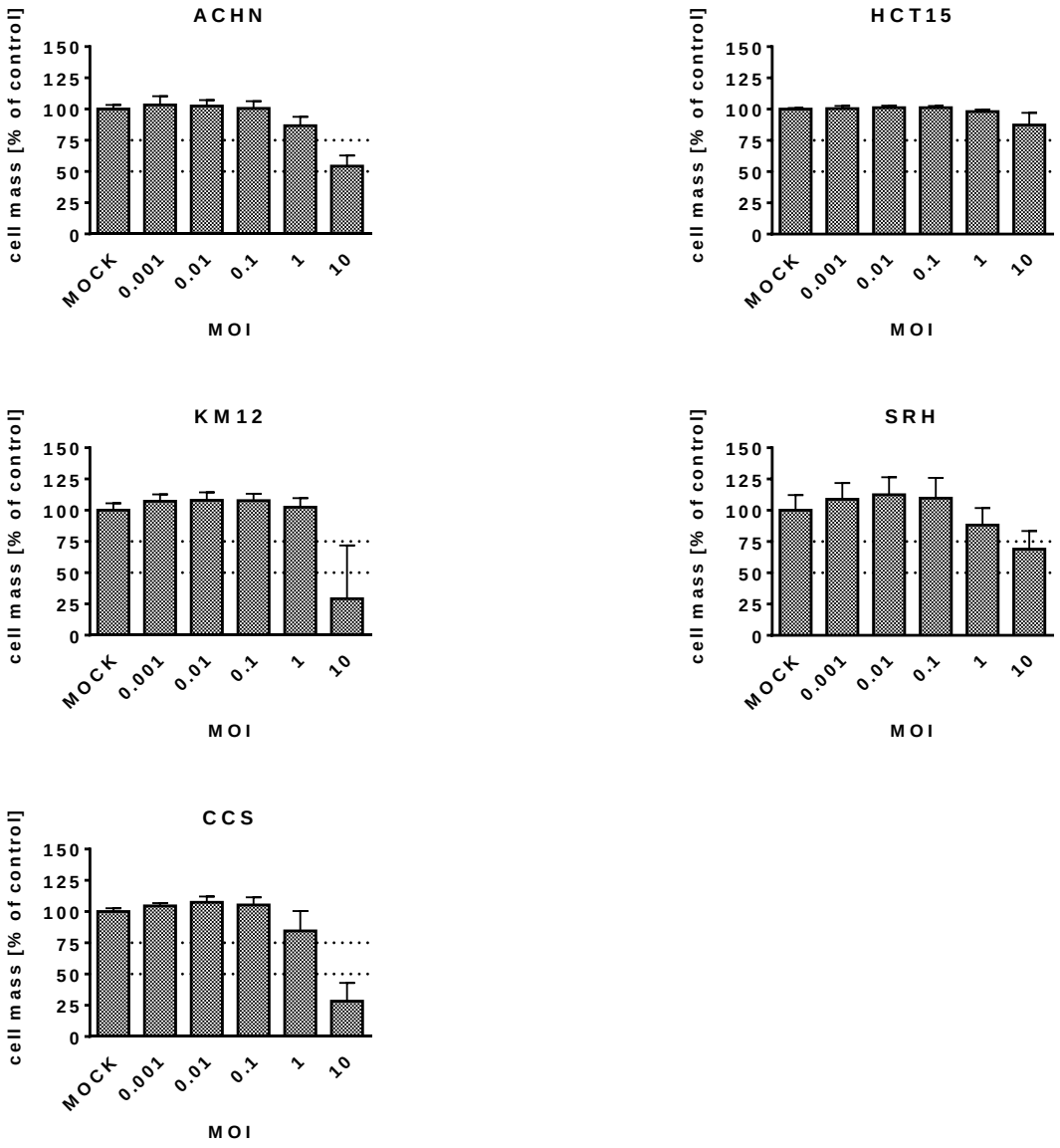

Figure 16. Identification of a critical MOI for each cell line infected with MeV-GFP in SRB assays

ACHN, HCT15, KM12, SRH and CCS cells were plated as described in Table 1, and infected in quadruplicates with MeV-GFP at MOI 0.001, 0.01, 0.1, 1 and 10 or mock-treated. At 96 hpi, cells were fixed and the remaining cell mass was analyzed by SRB assay. Uninfected controls were set 100 %. Dotted lines highlight the 50 and 75 % remaining cell mass. Values are means of three independent experiments. Error bars: SD.

3.1.5 Identification of a critical MOI for vaccinia virus (GLV-1h254) - plotted as relative to mock and relative to 0 hrs of infection

As detailed in section 3.1.3, critical MOIs for vaccinia virus were identified by infection of confluence-optimized plated cells. As cell indices of infected cells were related to those of uninfected controls, it was essential to guarantee cell survival of mock-treated cells at 96 hpi. Until now, we were unable to ensure the survival of controls, since plating densities were recommended on data which were collected with the naked eye only (section 3.1.2.1).

Here, single infection approaches with VACV were modified in order to evaluate growth characteristics of ACHN, HCT15 and KM12 cells from day to day by SRB assay and fluorescence microscopy. We focused on ACHN, HCT15 and KM12 cells in all further experiments, since these cell lines were resistant to VACV single infection at higher MOIs in contrast to SRH and CCS cells (section 3.1.3).

ACHN and HCT15 cells were plated according to recommended initial cell counts, listed in Table 1, in 24-well plates. KM12 cells were seeded at several densities (5×10^4, 1×10^5 and 2×10^5 cells/well). Cells were incubated overnight (ACHN), respectively for two nights (HCT15, KM12). One plate of each cell line was fixed prior to infection to obtain an output value (0 hpi). Adhered ACHN, HCT15 and KM12 cells (plated at 5×10^4 and 2×10^5 cells/well) were either infected with VACV GLV-1h254 in quadruplicates at MOI 0.001, 0.01, 0.05, 0.1 and 0.5 or mock-treated. KM12 cells plated at 1×10^5 cells/well were either infected at MOI 0.001, 0.005, 0.01, 0.05 and 0.1 or mock-treated. Here, MOIs were adjusted to obtain the possibility to survey differences between treatment groups reliant on minor alterations of virus concentration. At 1.5 hpi, 200 µl 22 % FBS-supplemented DMEM were added to the wells. Plates were incubated for 24, 48, 72 or 96 hpi.

Virus-encoded TurboFP635 expression was monitored under a fluorescence microscope, pictures (Figure 17) were taken prior to analysis by SRB assay. Values were plotted either as relative to 0 hrs or as relative to mock at 96 hpi.

As visualized in Figure 17, virus infection and spreading were monitored daily. At ascending viral concentrations and days post infection, the number of infected cells increased in all cell lines and the characteristic formation of virus plaques was detected (ACHN (**A**), HCT15 (**B**)). For KM12 (**C-E**), it became obvious that cells agglomerated quickly at all seeding densities. As a consequence, for this cell line total confluence was impossible to reach, as described before. Additionally, from 2 dpi on, mock-treated KM12 cells overgrew when plated at 2 x 10^5 cells/well (**E**).

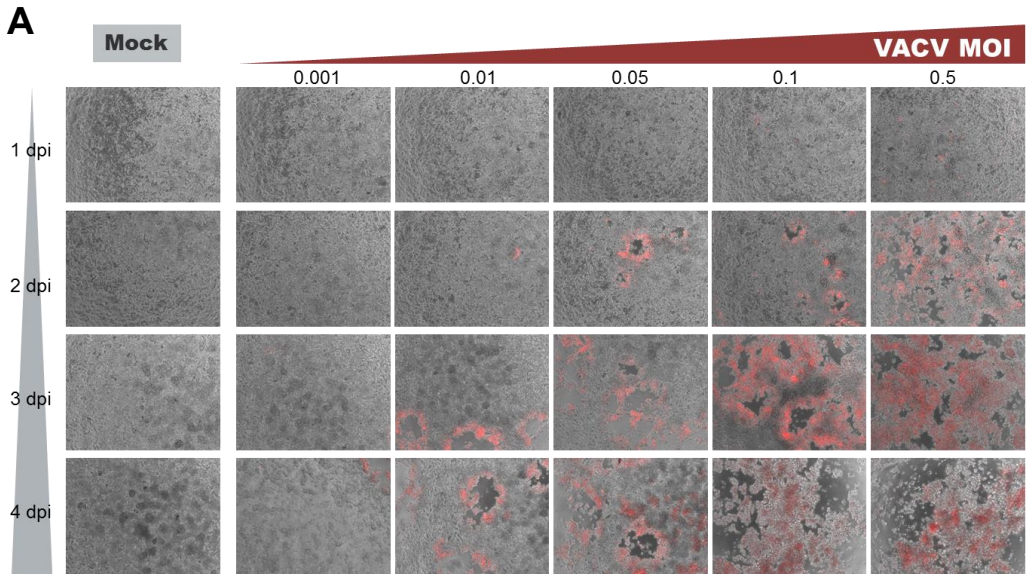

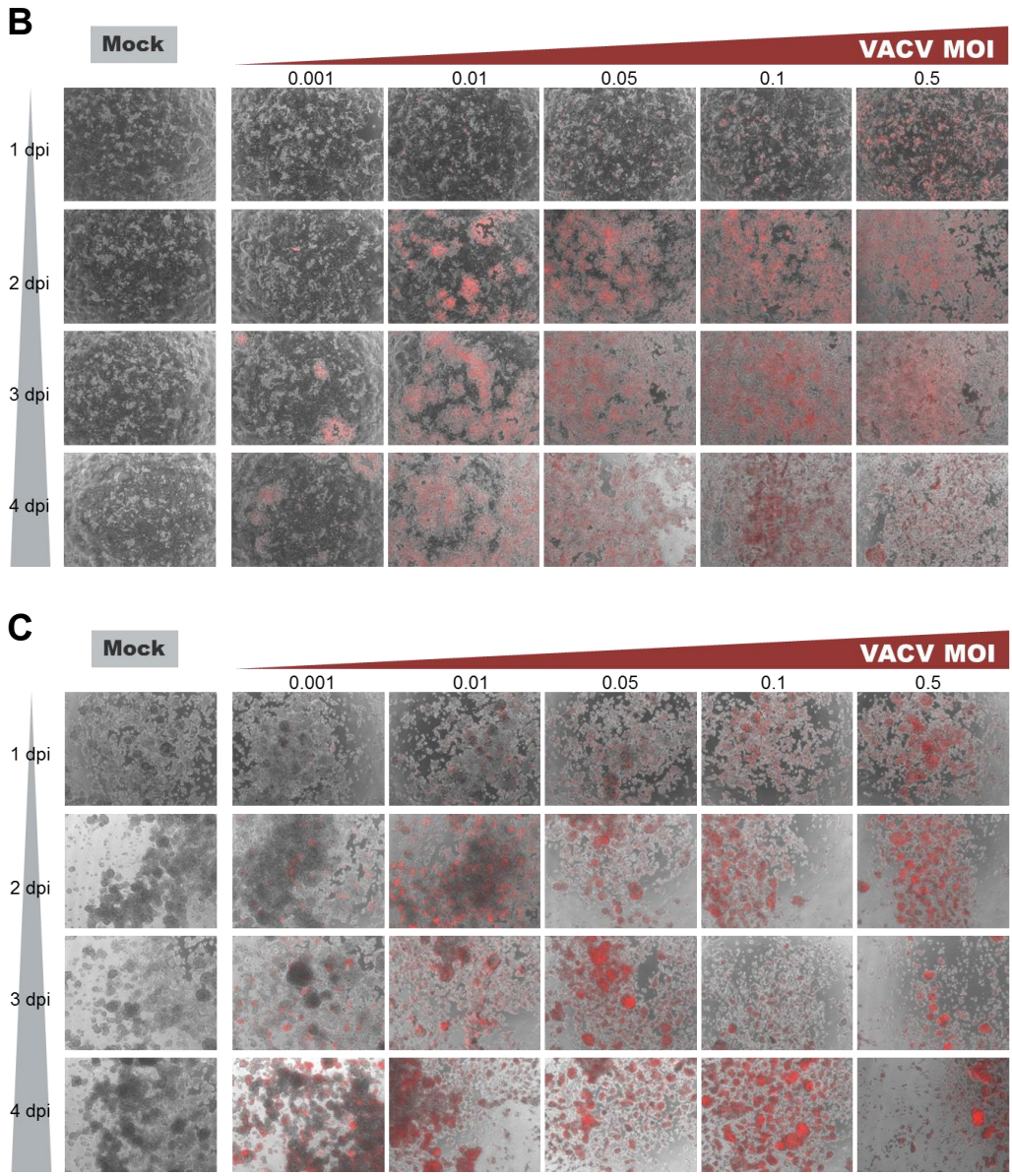
B
Mock
VACV MOI
0.001
0.01
0.05
0.1
0.5
1 dpi
2 dpi
3 dpi
4 dpi
C
Mock
VACV MOI
0.001
0.01
0.05
0.1
0.5
1 dpi
2 dpi
3 dpi
4 dpi

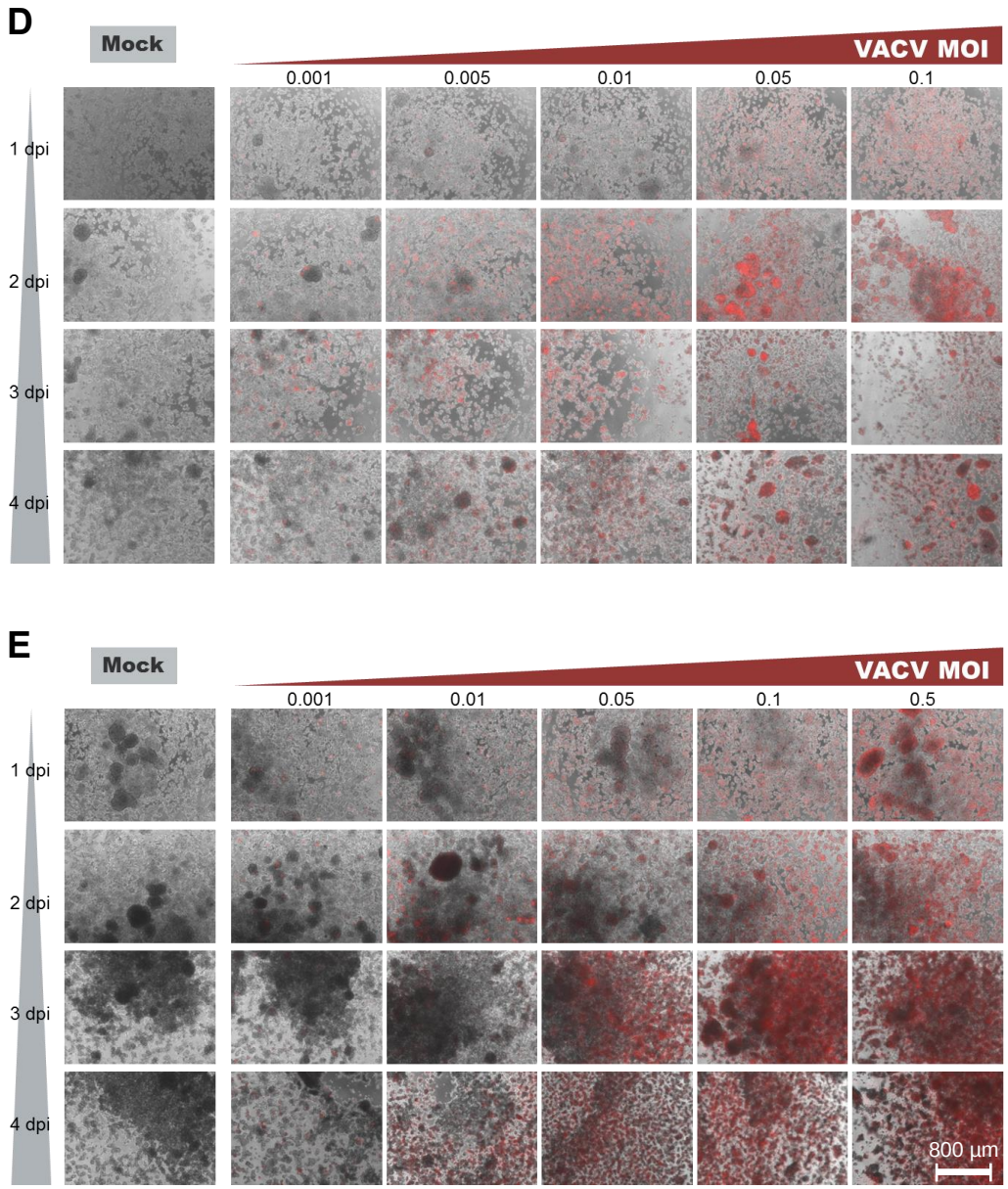

Figure 17. Overlays of fluorescence and bright-field pictures from VACV single-infected human tumor cell lines, confluence-optimized, 1-4 dpi

Cells were infected with VACV at MOI 0.001, 0.01, 0.05, 0.1 and 0.5 (ACHN (**A**), HCT15 (**B**), KM12 plated at 5 x 10^4 (**C**) and 2 x 10^5 cells/well (**E**)), respectively at MOI 0.001, 0.005, 0.01, 0.05 and 0.1 (KM12 plated at 1 x 10^5 cells/well) (**D**) or mock-treated. Fluorescence and bright-field pictures were taken every day (1-4 dpi) and overlaid afterwards. Infected cells show TurboFP635 expression as VACV marker for viral gene expression and plaque formation. Scale bar in the right lower corner applies to all panels.

The corresponding analysis of the treated cells by SRB viability assay revealed that mock-treated controls of ACHN and HCT15 cells still proliferated at 96 hpi (Figure 18 on the left (0 hrs)). Cell indices of uninfected KM12 cells, however,

hit a plateau when plated at 5 x 10^4 (at 96 hpi) and 1 x 10^5 cells/well (at 72 hpi) or even leveled off (2 x 10^5 cells/well at 96 hpi). It has to be noted that results from KM12 cells were either means of three independent experiments (1 x 10^5 cells/well) or of two experiments (2 x 10^5 cells/well), respectively one data set (5 x 10^5 cells/well). As a result, recommended plating densities for ACHN and HCT15 cells (Table 1) were maintained. For KM12 cells, 1 x 10^5 cells/well was chosen as new plating density.

As expressed in Figure 18 on the right, MOI 0.01 was verified as suitable value in single infection approaches for ACHN and HCT15 cells, whereas MOI 0.005 was determined as appropriate MOI for KM12 cells applied in all further experiments.

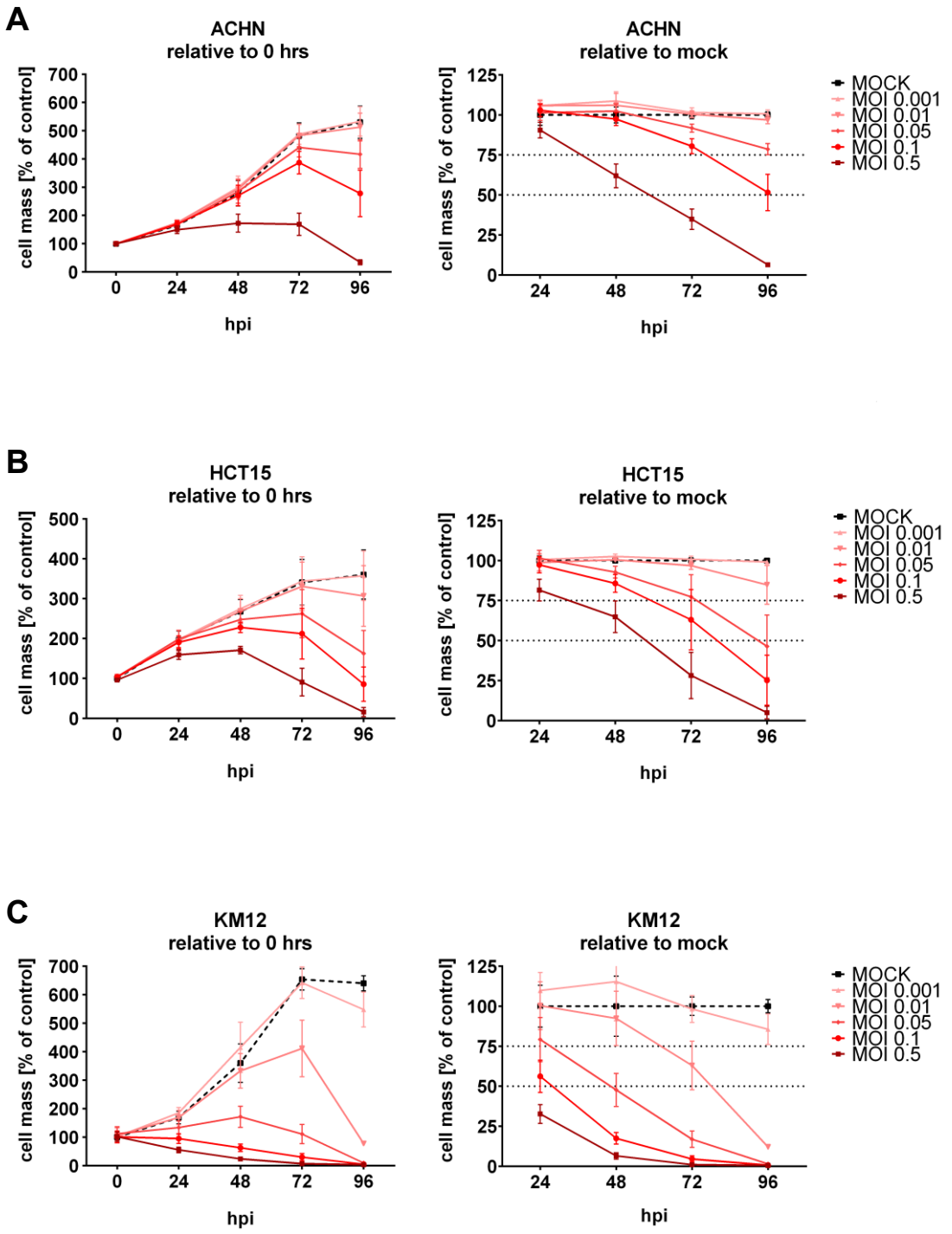
A
ACHN
relative to 0 hrs
cell mass [% of control]
hpi
ACHN
relative to mock
MOCK
MOI 0.001
MOI 0.01
MOI 0.05
MOI 0.1
MOI 0.5
B
HCT15
relative to 0 hrs
HCT15
relative to mock
C
KM12
relative to 0 hrs
KM12
relative to mock

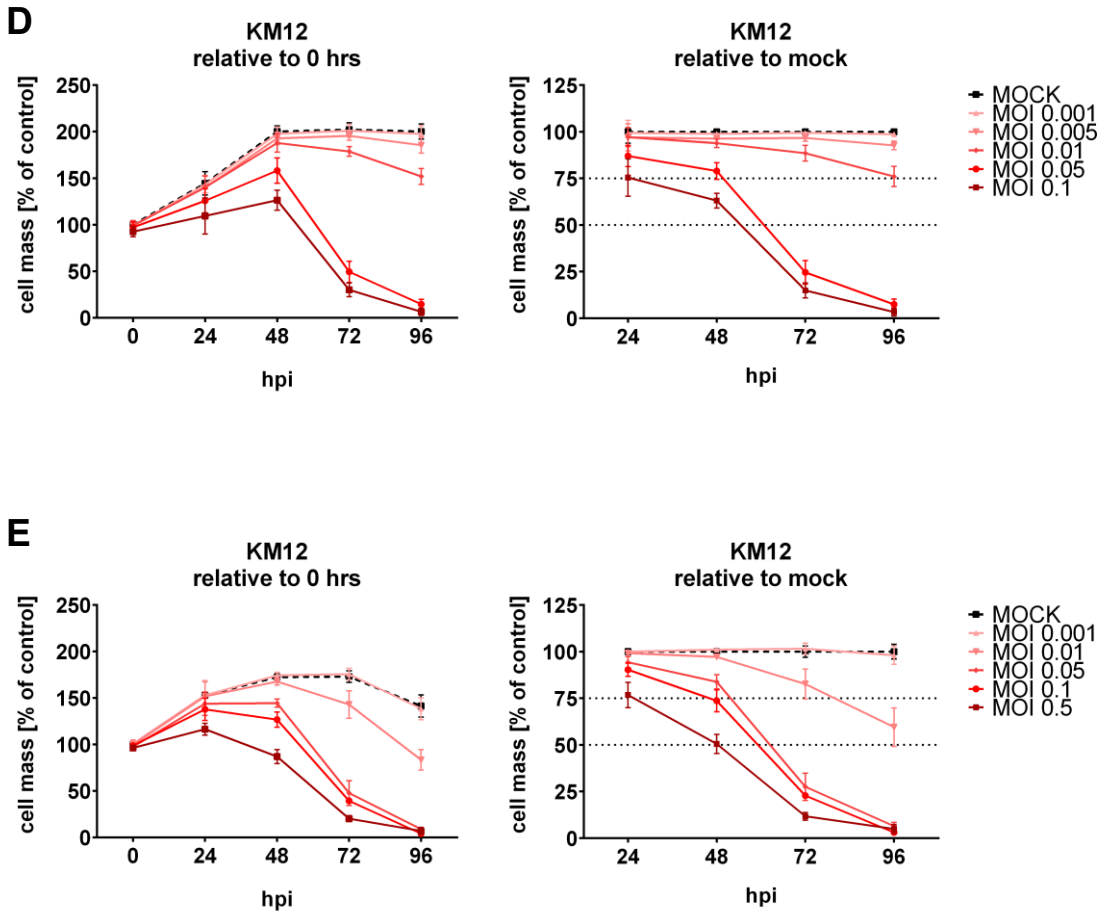

Figure 18. Identification of a suitable MOI for each cell line infected with VACV GLV-1h254 in SRB assays, blotted relative to 0 hrs and relative to mock

Cells were infected in quadruplicates with VACV at MOI 0.001, 0.01, 0.05, 0.1 and 0.5 (ACHN (**A**), HCT15 (**B**), KM12 plated at 5 x 10^4 (**C**) and 2 x 10^5 cells/well (**E**)), respectively at MOI 0.001, 0.005, 0.01, 0.05 and 0.1 (KM12 plated at 1 x 10^5 cells/well) (**D**) or mock-treated. At 0, 24, 48, 72 and 96 hpi, cells were fixed and the remaining cell mass was analyzed by SRB assay. Values were either plotted as relative to 0 hrs (on the left), or as relative to mock 96 hpi (on the right) with uninfected controls set 100 %. Dotted lines highlight the 50 and 75 % remaining cell mass on the right. Values are means of three independent experiments (except KM12 plated at 5 x 10^4 cells/well: means of one experiment, plated at 2 x 10^5 cells/well: means of two experiments). Error bars: SD.

3.2 **Double infection trials**

After threshold MOIs were determined successfully in single infection approaches for both viral vectors, application schemes for double infection trials were established.

Here, different orders of viruses, time points of secondary virus infection and multiplicities of infection were investigated in order to identify the most effective application scheme. Accordingly, ACHN, HCT15 and KM12 cells were seeded at adapted plating densities and incubation periods (Table 2).

Table 2. Adapted plating densities for ACHN, HCT15 and KM12 cells in 24-well plates
The table shows the adapted and recommended number of days and plating densities at which tumor cells were plated in 24-well plates prior to infection.

Cell line	***Days before infection (dbi), plating densities***
ACHN	1 dbi, 5 x 10^4 cells/well
HCT15	2 dbi, 5 x 10^4 cells/well
KM12	2 dbi, 1 x 10^5 cells/well

3.2.1 **Combinatorial treatment - VACV infection prior to infection with MeV**

ACHN, HCT15 and KM12 cells were either infected by VACV GLV-1h254, as detailed in section 3.1.5, without application of the highest MOI (0.5 for ACHN and HCT15, 0.1 for KM12), or mock-treated.

At 2, 6 or 12 hpi, cells were either double-infected by MeV-GFP at MOI 1 or medium was added to mock-treated and single-infected wells. MeV-GFP single-infected controls were executed for each time point (2, 6, 12 hpi). Additionally, another plate was single-infected by VACV and MeV-GFP to generate single-infected controls at 0 hrs.

The expression of virus-encoded marker genes GFP and TurboFP635 was monitored daily under a fluorescence microscope. At 96 hpi (in relation to the

infection with the first virus), cells were fixed and analyzed by SRB assay. Application schemes are attached below.

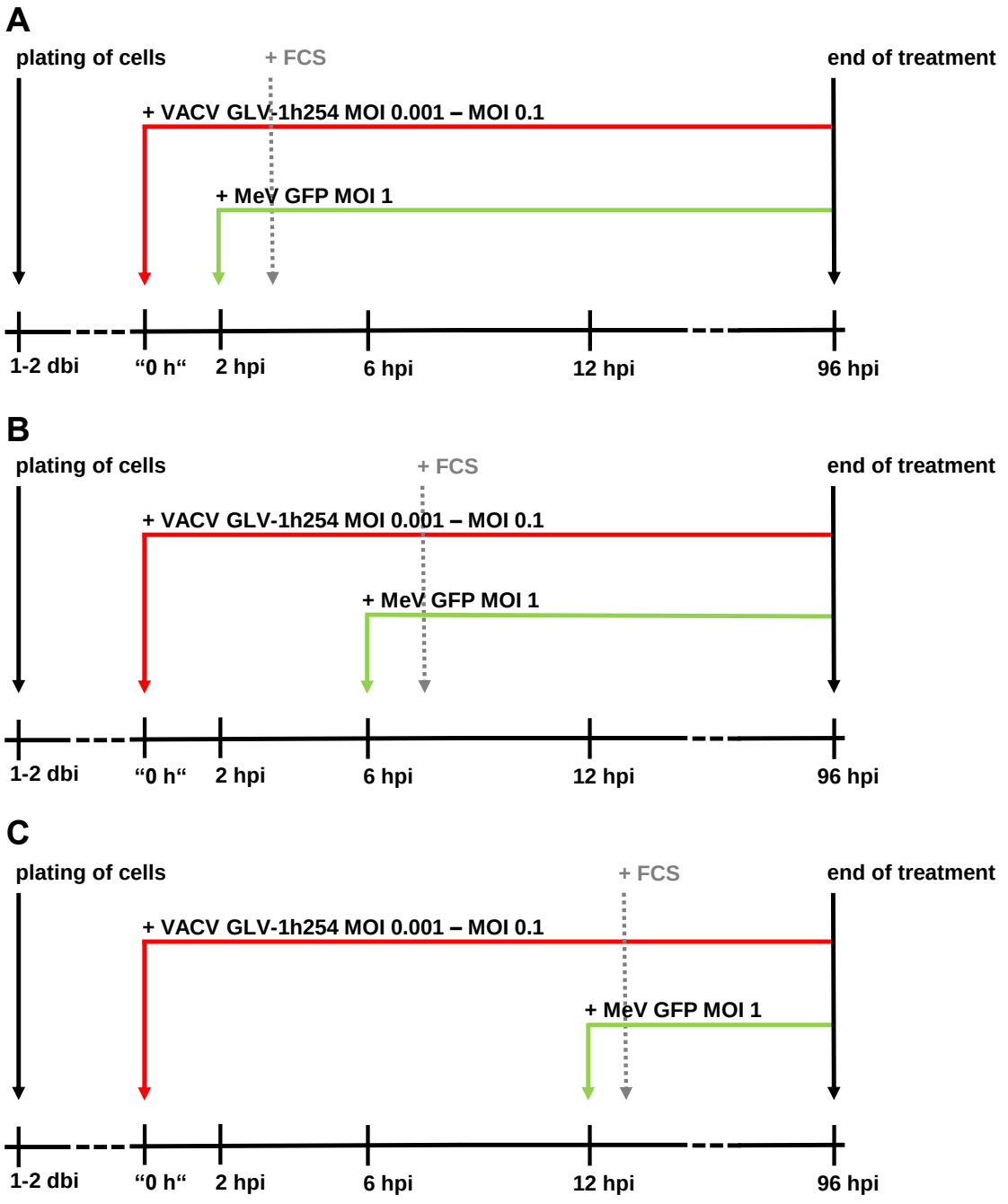

Figure 19. Application scheme for double-infections, VACV GLV-1h254 prior to MeV-GFP

Cells were plated in 24-well plates 1 dbi (ACHN), respectively 2 dbi (HCT15 and KM12 cells). On the infection day, cells were inoculated in quadruplicates with VACV GLV-1h254 at ascending MOIs from 0.001 to 0.05 (KM12), respectively 0.001 to 0.1 (ACHN, HCT15),

or mock-treated. Secondary virus infection with MeV-GFP at MOI 1 took place at 2 (**A**), 6 (**B**) or 12 hpi (**C**) with the first virus. At each time point (0, 2, 6, 12 hpi), single virus infections with MeV-GFP were performed as controls (not shown). Plates were incubated until 96 hpi with the first virus. The remaining cell mass was measured by SRB assay.

Infected cells were visualized by vaccinia virus-encoded TurboFP635 and measles vaccine virus-encoded GFP expression (Figure 21). Additionally, the resulting cytopathic effect, demonstrated by plaque formation and syncytia building, was observed in bright-field microscopy.

At ascending viral concentrations the number of infected cells increased in all cell lines (ACHN, HCT15 and KM12). Major differences between the time points of infection with the second virus (2, 6 or 12 hpi with MeV) were not perceived.

However, we made a peculiar observation concerning combinatorial treated cells:

Exemplified by ACHN cells infected at MOI 0.001 (VACV), followed by inoculation with MeV-GFP at MOI 1 (at 2 hpi), we noticed that most of the cells were infected “only” in a singular manner, either by VACV or by MeV-GFP (Figure 20).

- When VACV was applied at a low MOI (0.001), the majority of the cells was infected by the second virus, i.e. MeV-GFP, and consequently expressed primarily the GFP marker protein.
- When compared to double-treated ACHN cells at higher MOIs (0.01, 0.05, 0.1 of VACV), it was just the other way round. Now, most of the cells expressed the TurboFP635 marker protein.

We called this phenomenon “viral competition” and followed it up in further trials.

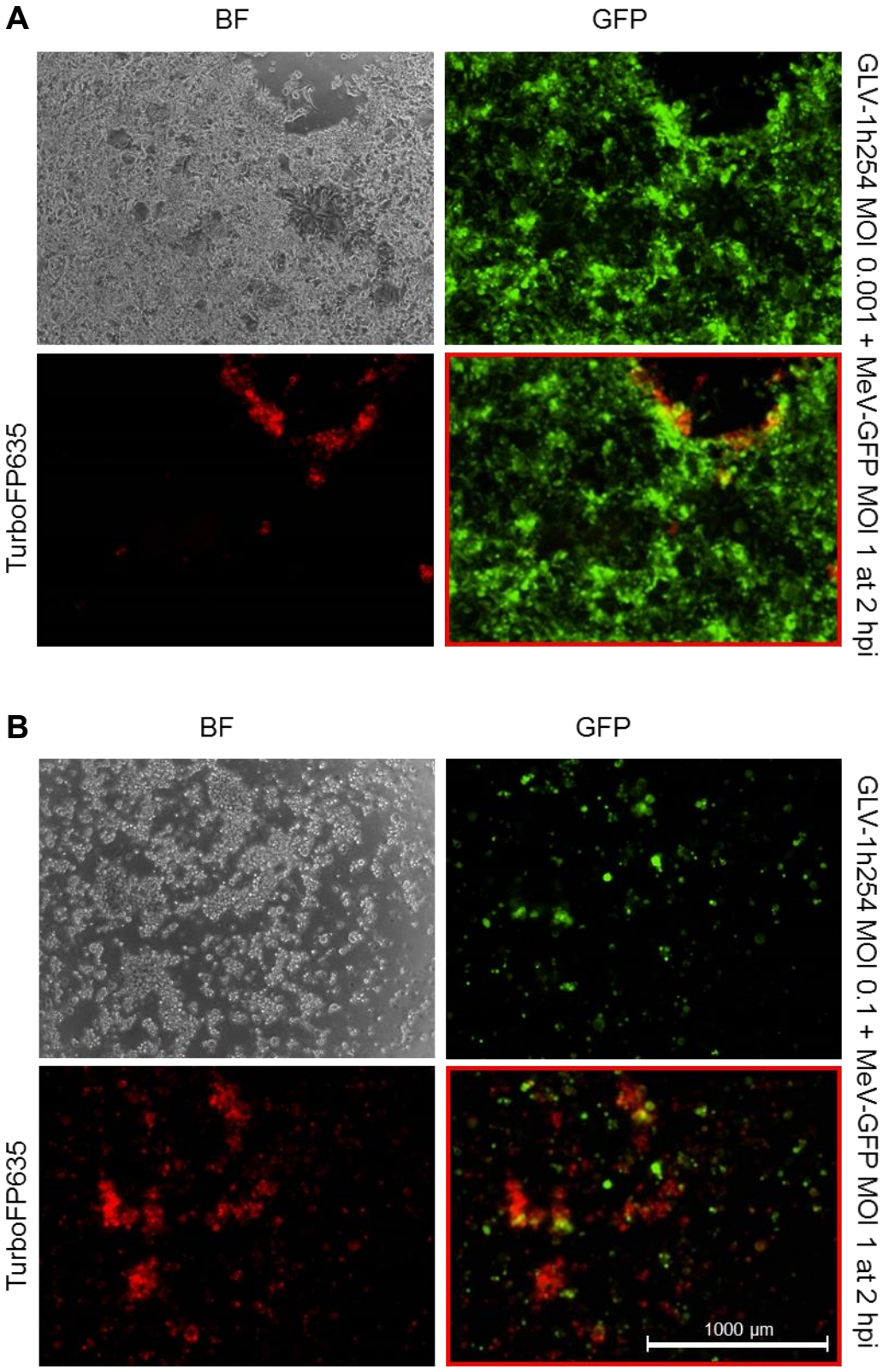

Figure 20. Fluorescence and bright-field pictures from combinatorial infected ACHN cells, VACV GLV-1h254 prior to MeV-GFP at 2 hpi. Selection of Figure 21

ACHN cells were seeded in 24-well plates and either infected by VACV at MOI 0.001 (**A**) or MOI 0.1 (**B**), respectively. At 2 hpi, cells were additionally inoculated with MeV-GFP at MOI 1. At 4 dpi, fluorescence (TurboFP635, GFP) and bright-field (BF) pictures were taken using Olympus IX50 fluorescence microscope. The image in the bottom right corner shows the overlay of both fluorescence pictures. Infected cells showed TurboFP635 and GFP expression as marker for VACV and MeV-GFP viral gene expression. Scale bar in the right lower corner applies to all panels.

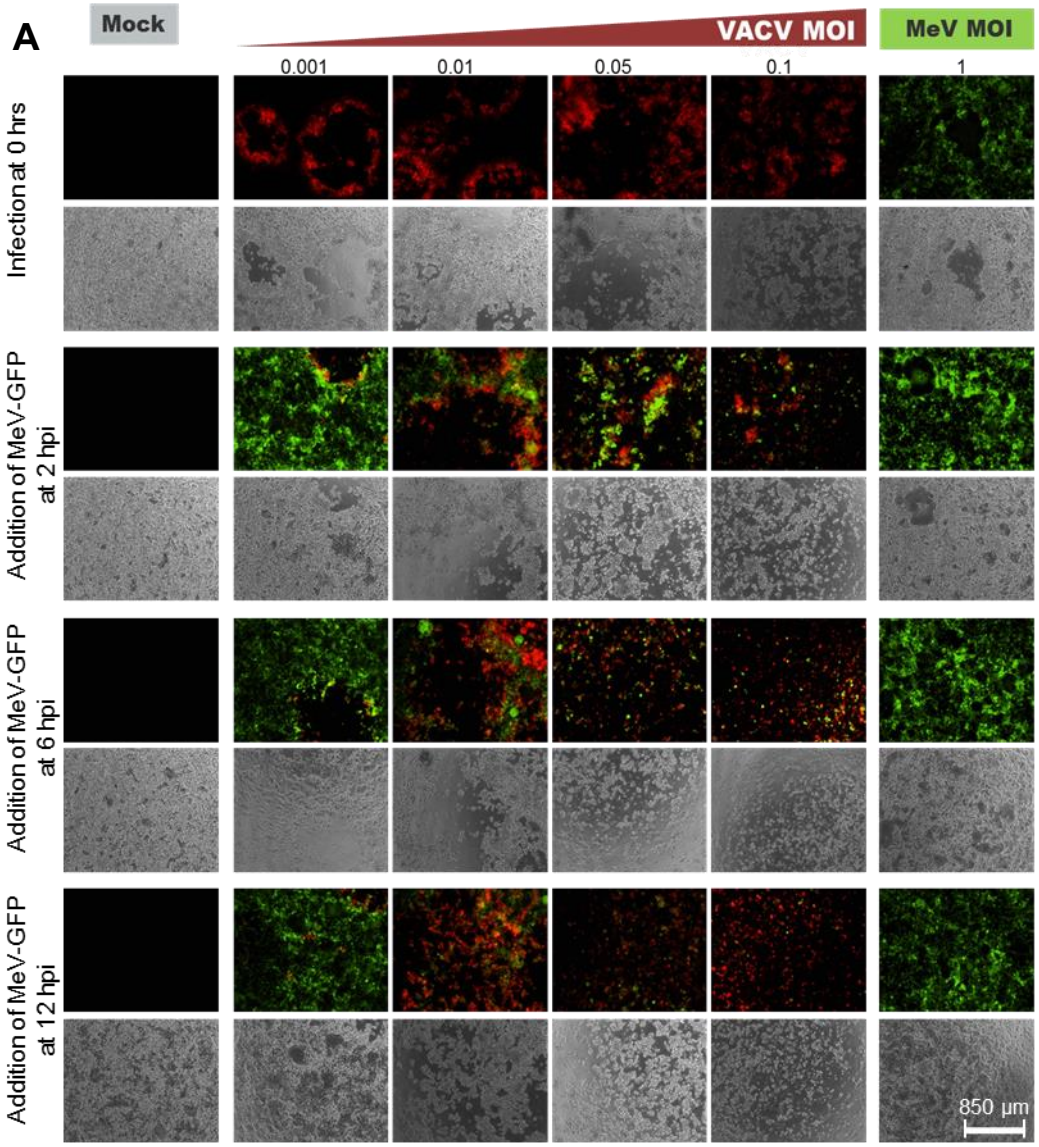

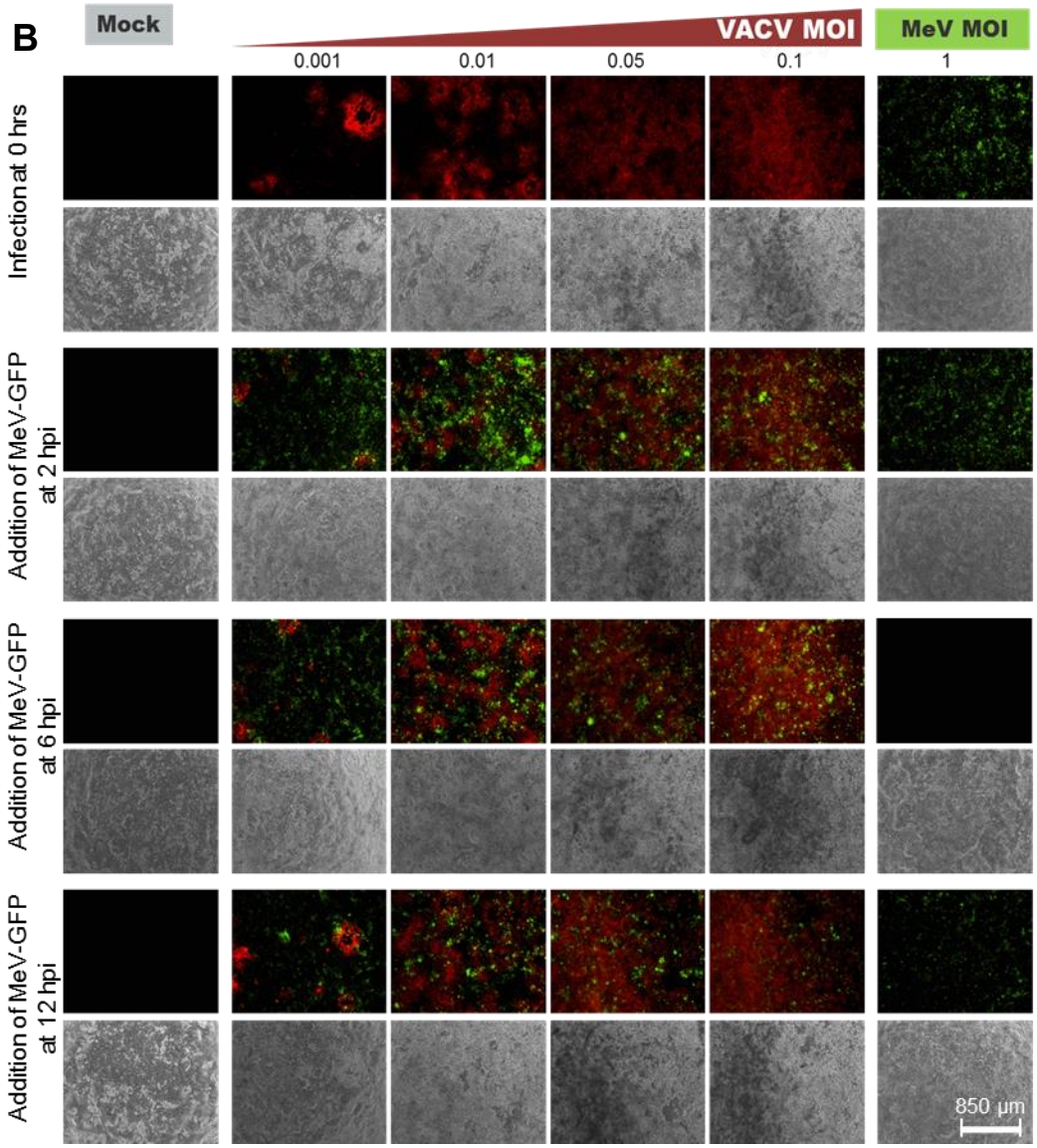
B
Mock
VACV MOI
MeV MOI
0.001
0.01
0.05
0.1
1
Infection at 0 hrs
Addition of MeV-GFP at 2 hpi
Addition of MeV-GFP at 6 hpi
Addition of MeV-GFP at 12 hpi
850 µm

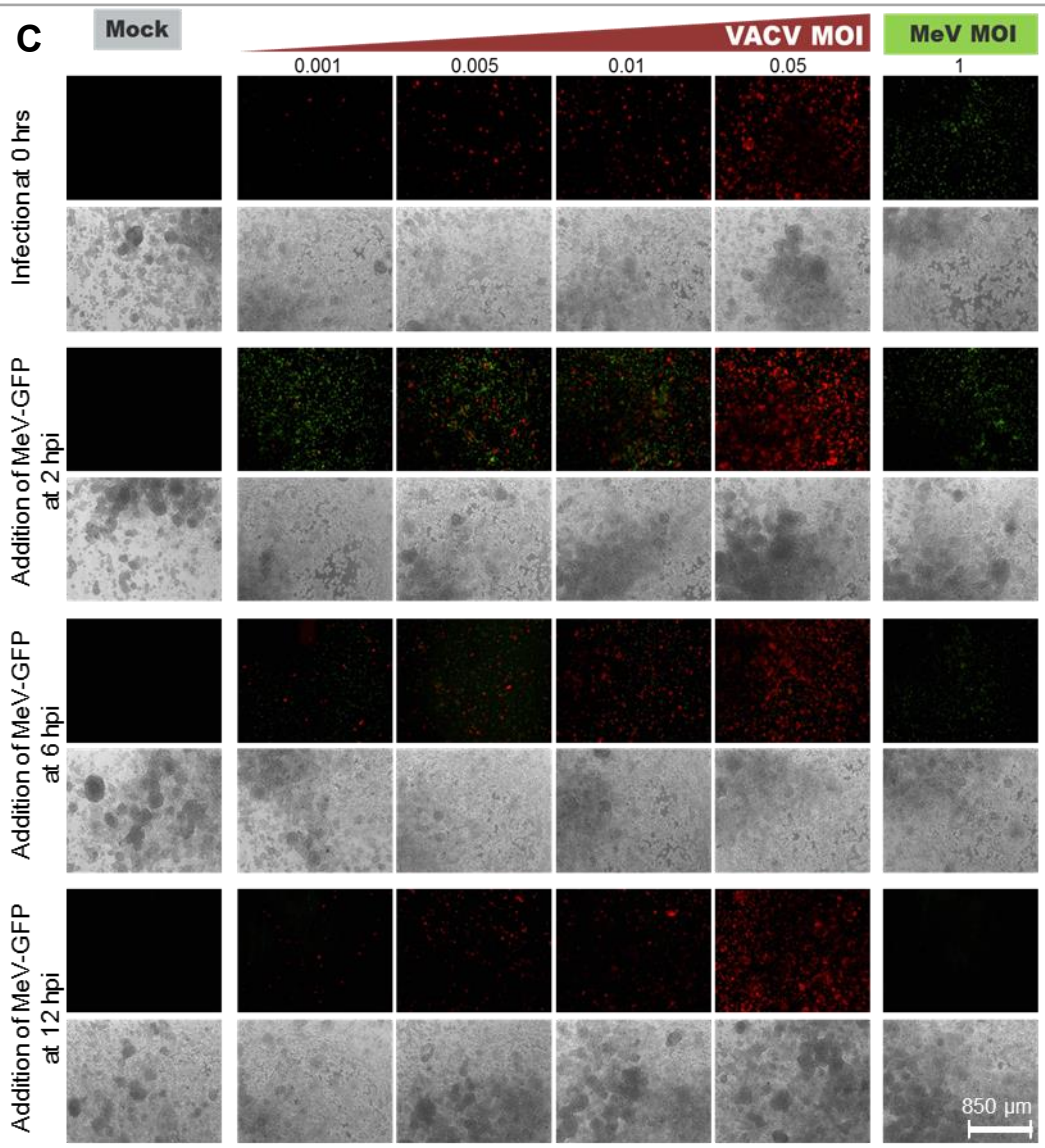

Figure 21. Overlays of fluorescence and bright-field pictures from double-infected human tumor cell lines, VACV GLV-1h254 prior to MeV-GFP

ACHN (**A**), HCT15 (**B**) and KM12 (**C**) cells were plated in 24-well plates as listed in Table 2. Cells were either infected by VACV GLV-1h254 at ascending MOIs from 0.001 to 0.05 (KM12), respectively up to 0.1 (ACHN, HCT15), or mock-treated. Secondary virus infection with MeV-GFP at MOI 1 took place at 2, 6 or 12 hpi (row three to eight). Single virus infections as controls were performed with MeV-GFP (right column) at each time point (0, 2, 6, 12 hpi), respectively with VACV (first and second row) at 0 hrs. Pictures were taken at 4 dpi (ACHN, HCT15) prior to SRB assay analysis, respectively at 1 dpi (KM12). Fluorescence pictures are overlays. Infected cells show TurboFP635 and GFP expression as marker for viral gene expression, as well as plaque (VACV) and syncytia (MeV) formation. Scale bar in the right corner applies to all panels.
Of note: One overlay picture of HCT15 (**B**) shows a place holder (right column, 4th picture from bottom).

Analysis by SRB assay (Figure 22) revealed that all three cell lines single-infected by VACV GLV-1h254 at MOI 0.001 and 0.01, respectively at 0.005 (KM12) (columns in red), and by MeV-GFP at MOI 1 (columns in green) showed no or only slight oncolytic effects.

In contrast, double-treated cells presented a convincing oncolytic effect, when infected by VACV at MOI 0.001 or 0.01, respectively 0.005 (KM12), followed by MeV-GFP at MOI 1 (columns in yellow).

In ACHN and KM12 cells differences between time points of secondary virus infection were negligible (neighboring columns in yellow did not reveal any major differences); for HCT15 cells, however, best results were achieved at 6 hpi.

In the single-infection treatment group, the application of higher MOIs of VACV led to cell mass reduction below 75 % remaining cell mass. Accordingly, we further on concentrated on VACV infections employing only one definite MOI; i.e., MOI 0.01 for tumor cell lines ACHN and HCT15, and MOI 0.005 for tumor cell line KM12, used for any further investigations.

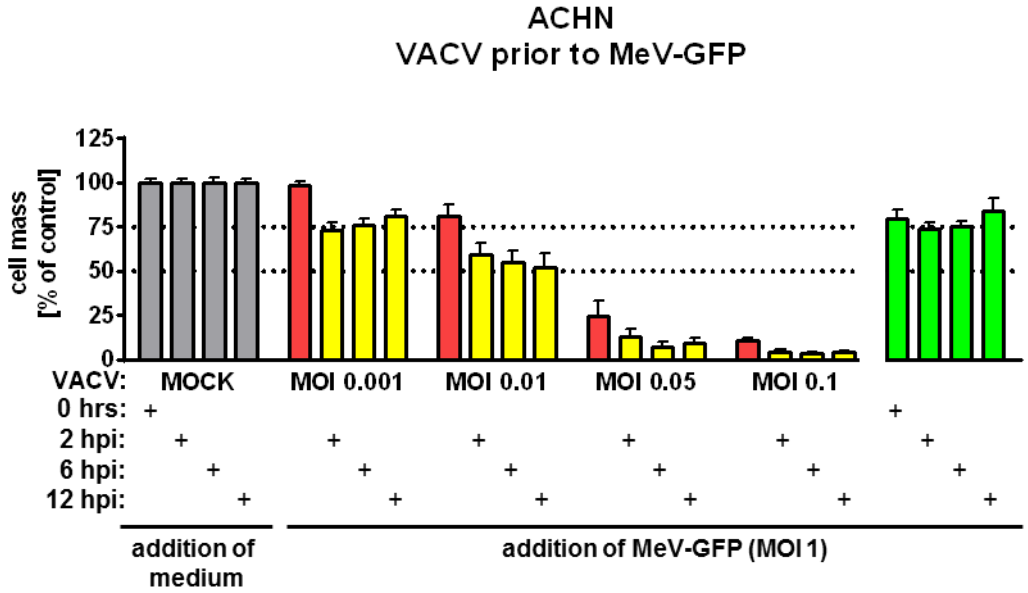

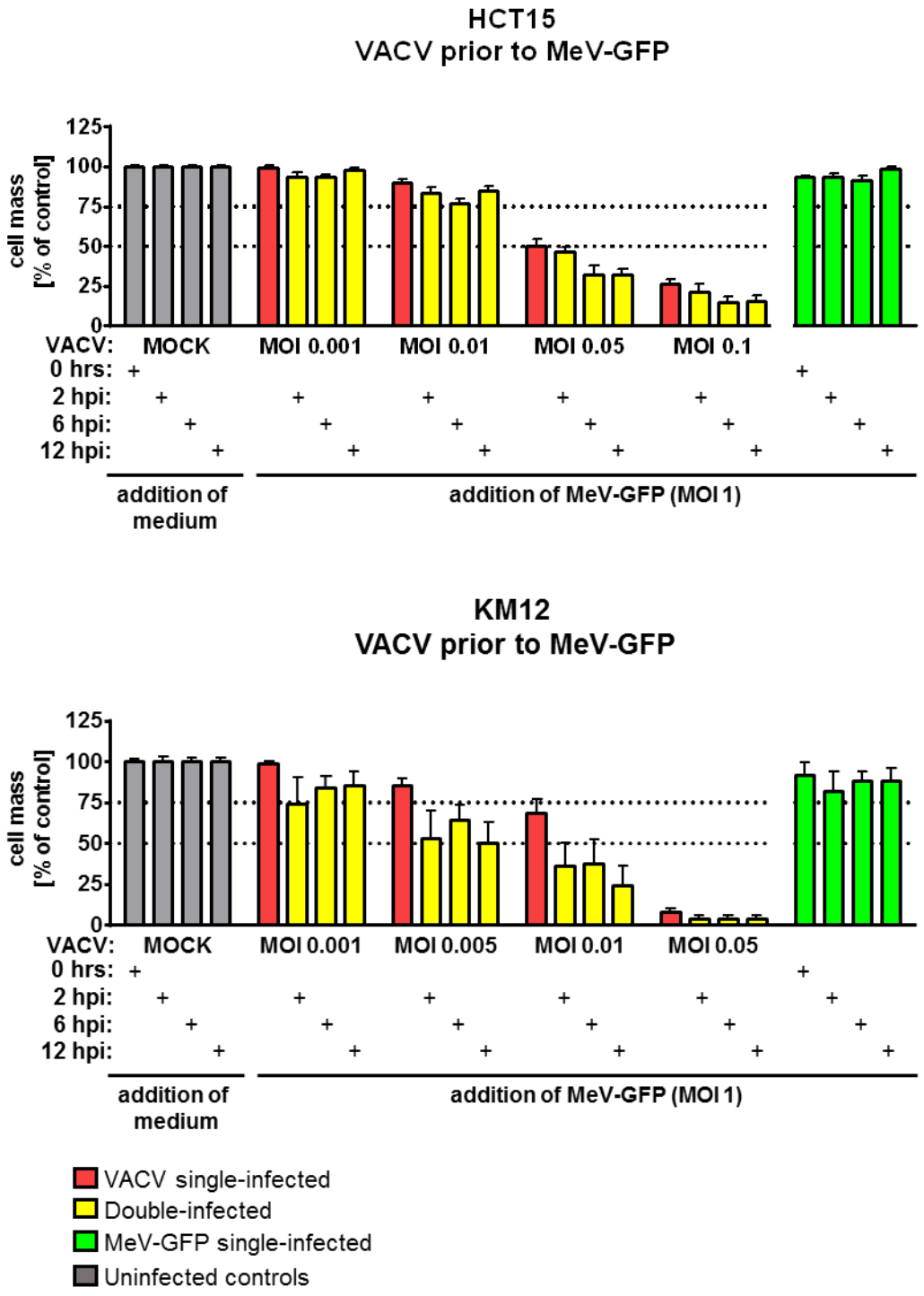

Figure 22. Cytopathic effects of combinatorial treatments with VACV GLV-1h254 prior to MeV-GFP in SRB viability assay.

ACHN, HCT15 and KM12 cells were plated in 24-well plates 1 dbi (ACHN), respectively 2 dbi (HCT15 and KM12 cells) as listed in Table 2. Cells were either inoculated in quadruplicates with VACV GLV-1h254 at ascending MOIs from 0.001 to 0.05 (KM12), respectively from 0.001 to 0.1 (ACHN, HCT15), or mock-treated. Single-infected controls at all applied MOIs were implemented (red columns). Secondary virus infection with MeV-GFP at MOI 1 took place at 2, 6 or 12 hpi (yellow columns) with the first virus. At each time point (2, 6, 12 hpi and additionally

at 0 hrs), single virus infections with MeV-GFP were performed as controls (green columns). Plates were incubated until 96 hpi with the first virus, the remaining cell mass was measured by SRB assay. Mock-treated controls were set 100 %. Dotted lines highlight the 50 and 75 % remaining cell mass. Values are means of three independent experiments. Error bars: SD.

3.2.2 **Combinatorial treatment - MeV infection prior to infection with VACV**

In section 3.2.1, tumor cells were infected with VACV first. Here, we infected vice versa and inoculated initially with MeV-GFP at ascending viral concentrations.

For this purpose, ACHN, HCT15 and KM12 cells were either infected by MeV-GFP at MOI 0.001, 0.01, 0.1 and 1, or mock-treated.

Secondly, tumor cells were either infected by VACV GLV-1h254 at MOI 0.01 (ACHN, HCT15), respectively MOI 0.005 (KM12), at 2, 6 or 12 hpi or medium was added to mock-treated and single-infected wells.

VACV single-infected controls were performed for each time point (2, 6, 12 hpi). Additionally, one plate was single-infected by VACV and MeV-GFP at “0 hrs” to generate a 0 hrs reference. Plates were incubated until 96 hpi.

Virus-encoded fluorescent proteins were observed daily under a fluorescence microscope. At the end of viral treatment, plates were fixed and analyzed by SRB viability assay. Application schemes are attached below.

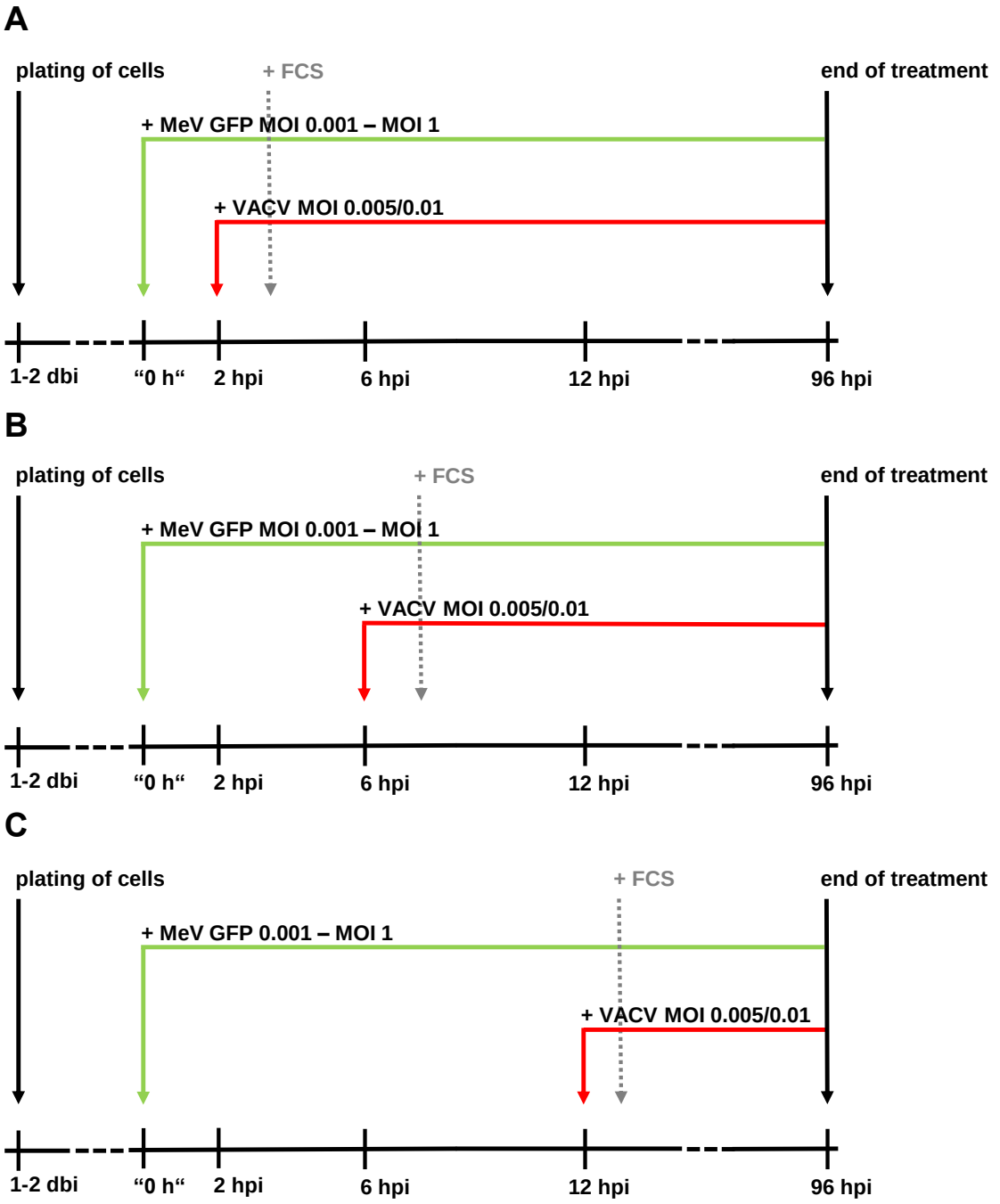

Figure 23. Application scheme for double-infections, MeV-GFP prior to VACV GLV-1h254

Cells were plated in 24-well plates as listed in Table 2. On the infection day, cells were inoculated in quadruplicates with MeV-GFP at ascending MOIs from 0.001 to 1, or mock-treated. Secondary virus infection with VACV at MOI 0.01 (ACHN, HCT15), respectively 0.005 (KM12) took place at 2 (**A**), 6 (**B**) or 12 (**C**) hpi. At each time point, single virus infections with VACV were performed as controls. Plates were incubated until 96 hpi with the first virus. The remaining cell mass was measured by SRB assay.

As shown in Figure 25, infected cells were detected by vaccinia virus-encoded TurboFP635 and measles vaccine virus-encoded GFP expression. In bright-field microscopy pictures, the resulting cytopathic effect was visualized by plaque formation (VACV) and syncytia building (MeV-GFP).
Expectedly, at ascending viral concentrations the number of MeV-infected cells increased in all tumor cell lines (ACHN, HCT15 and KM12).

For HCT15 and KM12 cells, we noticed differences in TurboFP635-expression. Thus, at 6 hpi, less HCT15 cells expressed the fluorescent, at 12 hpi, much more KM12 cells glowed red compared to cells inoculated at other time points. For ACHN cells, no major differences were perceived.

Furthermore, the phenomenon of “viral competition” was observed again, now for the combinatorial order “MeV infection prior to infection with VACV”: Sequentially treated ACHN and HCT15 cells (rows three to eight of each picture collection, Figure 25) were found to be either infected by VACV or by MeV, but not by both viral vectors.

- According to the concentration of the viral vector being applied first, tumor cells were either already “occupied” (when infected at high MOIs) or “free” for secondary virus infection with the other virus type (see also Figure 24 as a closeup view).
- In KM12 tumor cells, however, this phenomenon was not observed. Quite the contrary, coinfected KM12 tumor cells at 6 and 12 hpi expressed TurboFP635, the viral marker protein of the second virus, to a great extent.

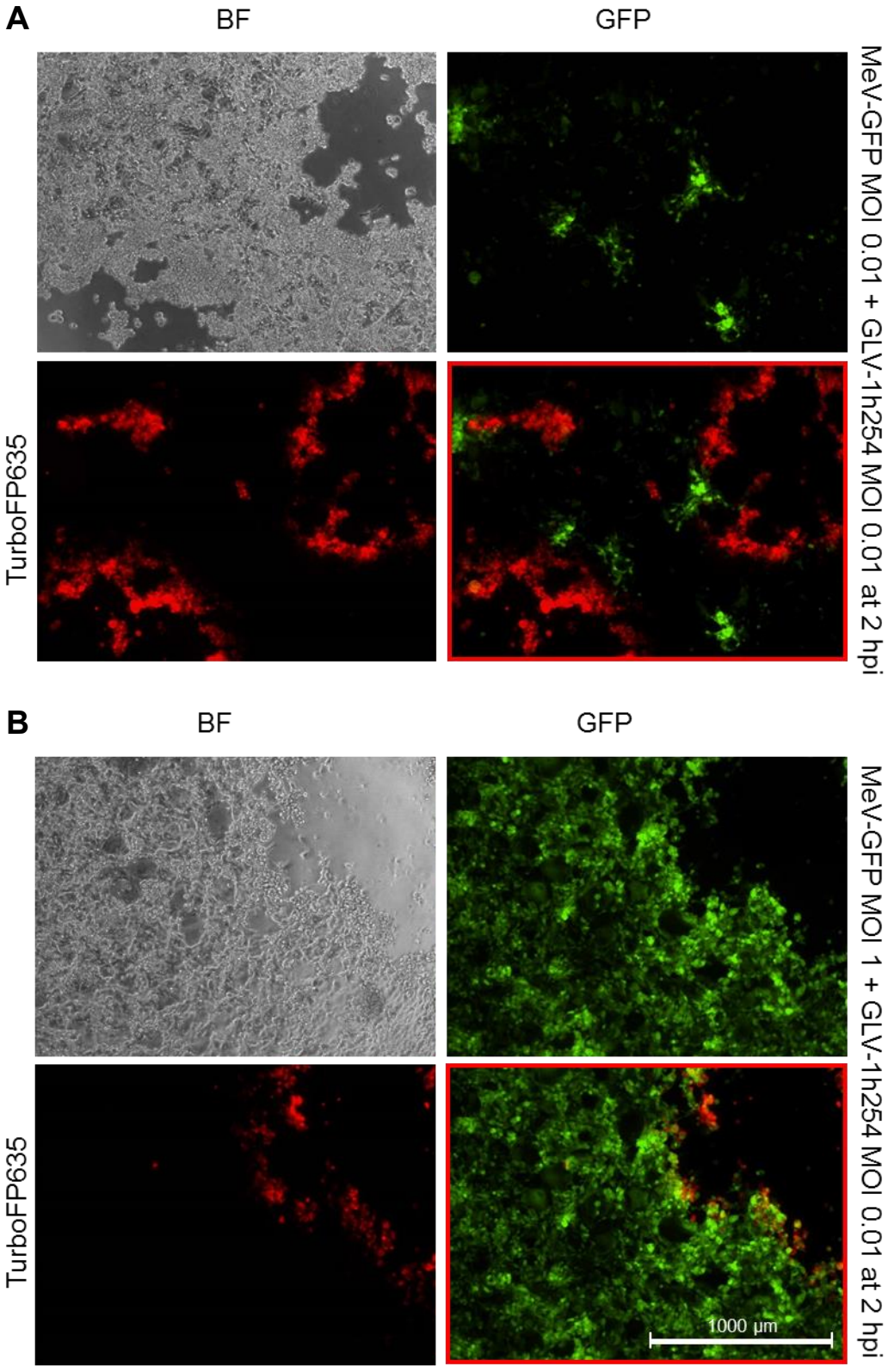

Figure 24. Fluorescence and bright-field pictures from combinatorial infected ACHN cells, MeV-GFP prior to VACV GLV-1h254 at 2 hpi. Selection of Figure 25

ACHN cells were seeded in 24-well plates and either infected by MeV-GFP at MOI 0.01 (**A**) or MOI 1 (**B**), respectively. At 2 hpi, cells were additionally inoculated with VACV GLV-1h254 at

MOI 0.01. At 4 dpi, fluorescence (TurboFP635, GFP) and bright-field (BF) pictures were taken using Olympus IX50 fluorescence microscope. The image in the bottom right corner shows the overlay of both fluorescence pictures. Infected cells showed TurboFP635 and GFP expression as marker for VACV and MeV-GFP viral gene expression. Scale bar in the right lower corner applies to all panels.

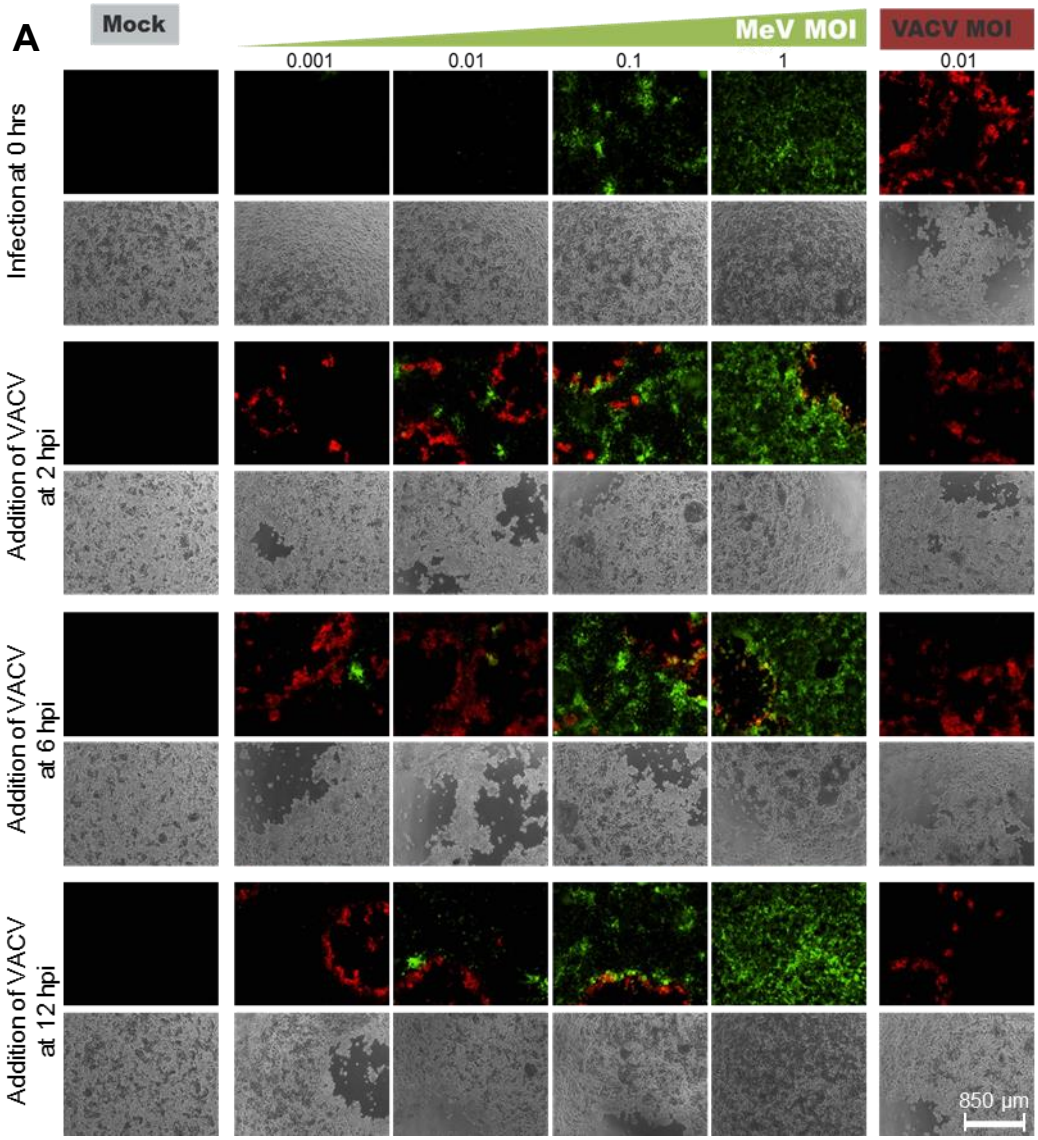

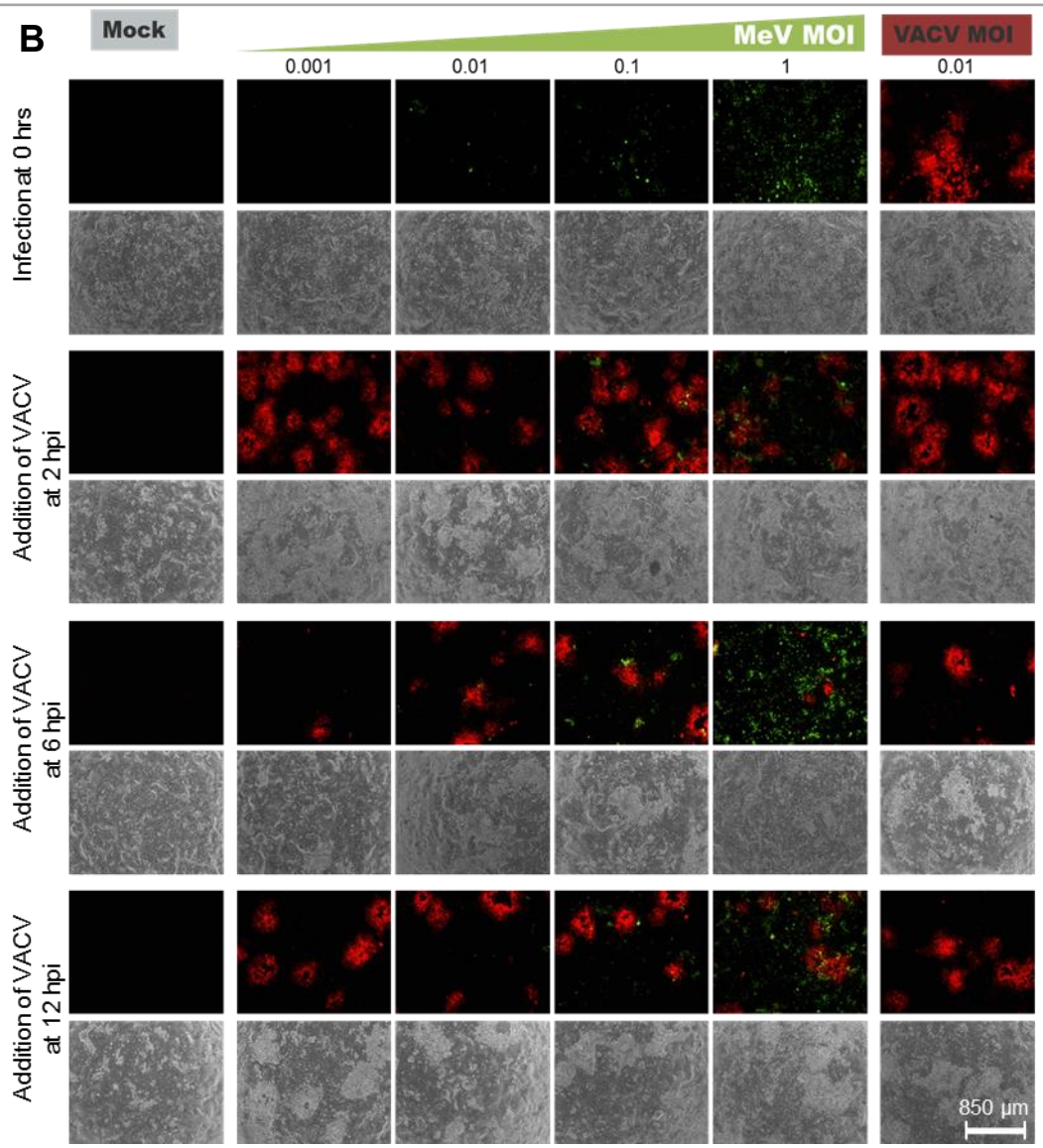
B
Mock
MeV MOI
VACV MOI
0.001
0.01
0.1
1
0.01
Infection at 0 hrs
Addition of VACV at 2 hpi
Addition of VACV at 6 hpi
Addition of VACV at 12 hpi
850 µm

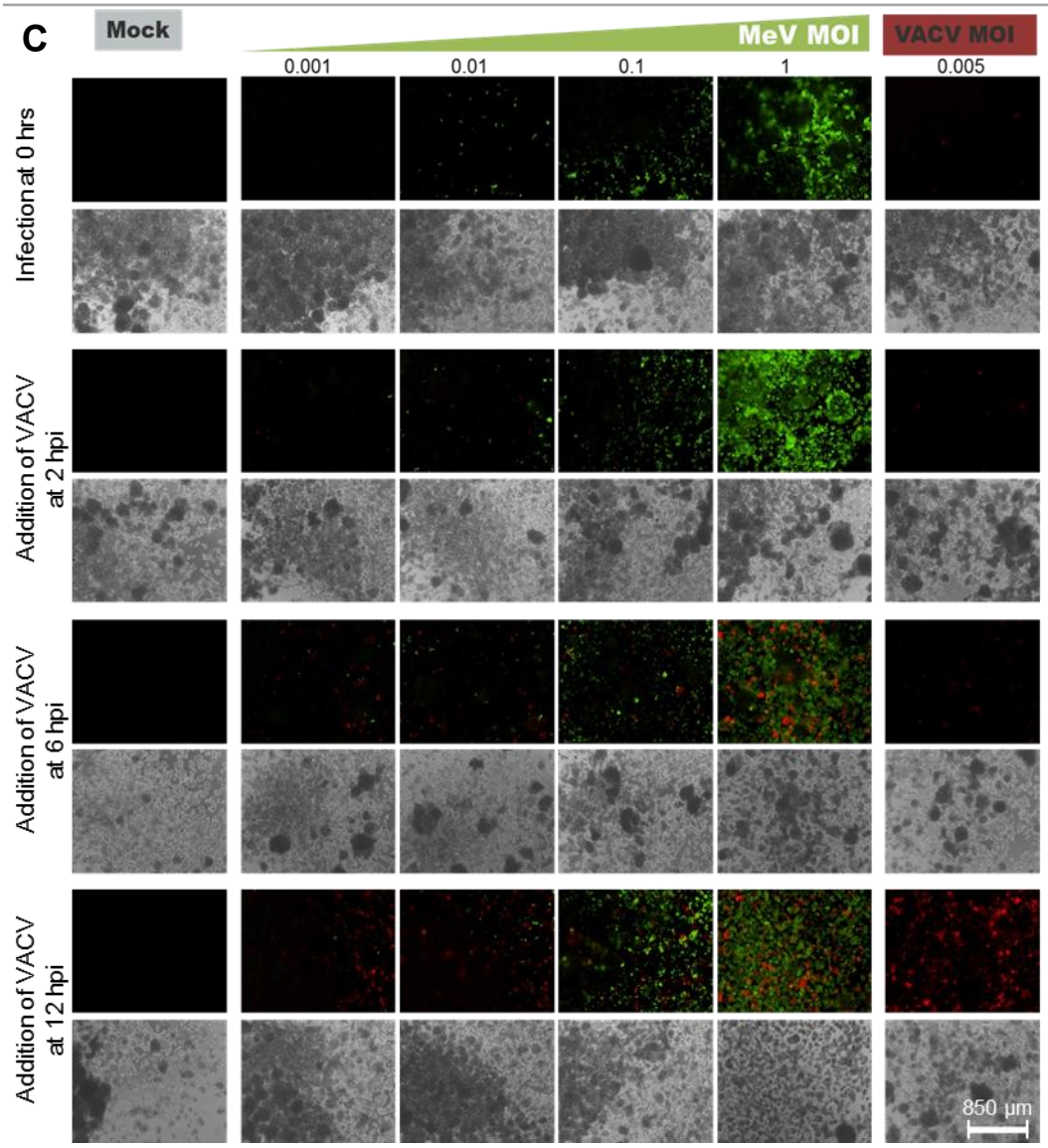

Figure 25. Overlays of fluorescence and bright-field pictures from double-infected human tumor cell lines, MeV-GFP prior to VACV GLV-1h254

ACHN (**A**), HCT15 (**B**) and KM12 (**C**) cells were plated in 24-well plates as listed in Table 2. Cells were either infected by MeV-GFP at ascending MOIs from 0.001 to 1, or mock-treated. Secondary virus infection by VACV GLV-1h254 at MOI 0.01 (ACHN, HCT15), respectively MOI 0.005 (KM12), took place at 2, 6 or 12 hpi (row three to eight). Single virus infections as controls were performed with VACV (right column) at each time point (0, 2, 6, 12 hpi), respectively at 0 hrs with MeV-GFP (first and second row). Pictures were taken at 4 dpi prior to SRB assay analysis. Fluorescence pictures are overlays. Infected cells show TurboFP635 and GFP expression as marker for VACV and MeV-GFP viral gene expression, as well as plaque formation (VACV) and syncytia building (MeV-GFP). Scale bar in the right lower corner applies to all panels.

In a next step, the cytopathic effect in this experiment was examined by SRB viability assay (Figure 26). As a result, double-infected ACHN and KM12 tumor cells (columns in yellow) showed improved rates of oncolysis. Particularly, tumor cell masses were reduced below 75 % remaining cell mass when tumor cells were inoculated with MeV-GFP at MOI 1 followed by VACV GLV-1h254 at MOI 0.01 (ACHN), respectively MOI 0.005 (KM12). HCT15 cells, on the contrary, did not benefit from sequential infections.

Except for ACHN and KM12 cells treated with MeV-GFP at the highest MOI (MOI 1), MeV-GFP infected controls (columns in green) showed no oncolytic effect. Controls of VACV infection (columns in red) revealed variations dependent on different time points of secondary virus treatment. Especially, ACHN cells treated at 2 hpi showed a slightly reduced cell mass compared to other controls.

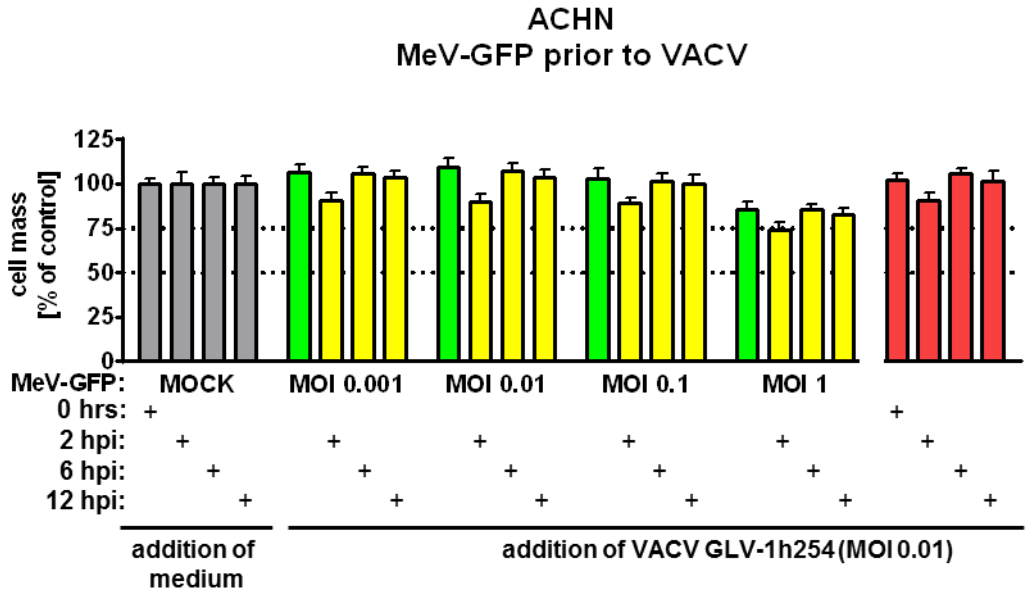

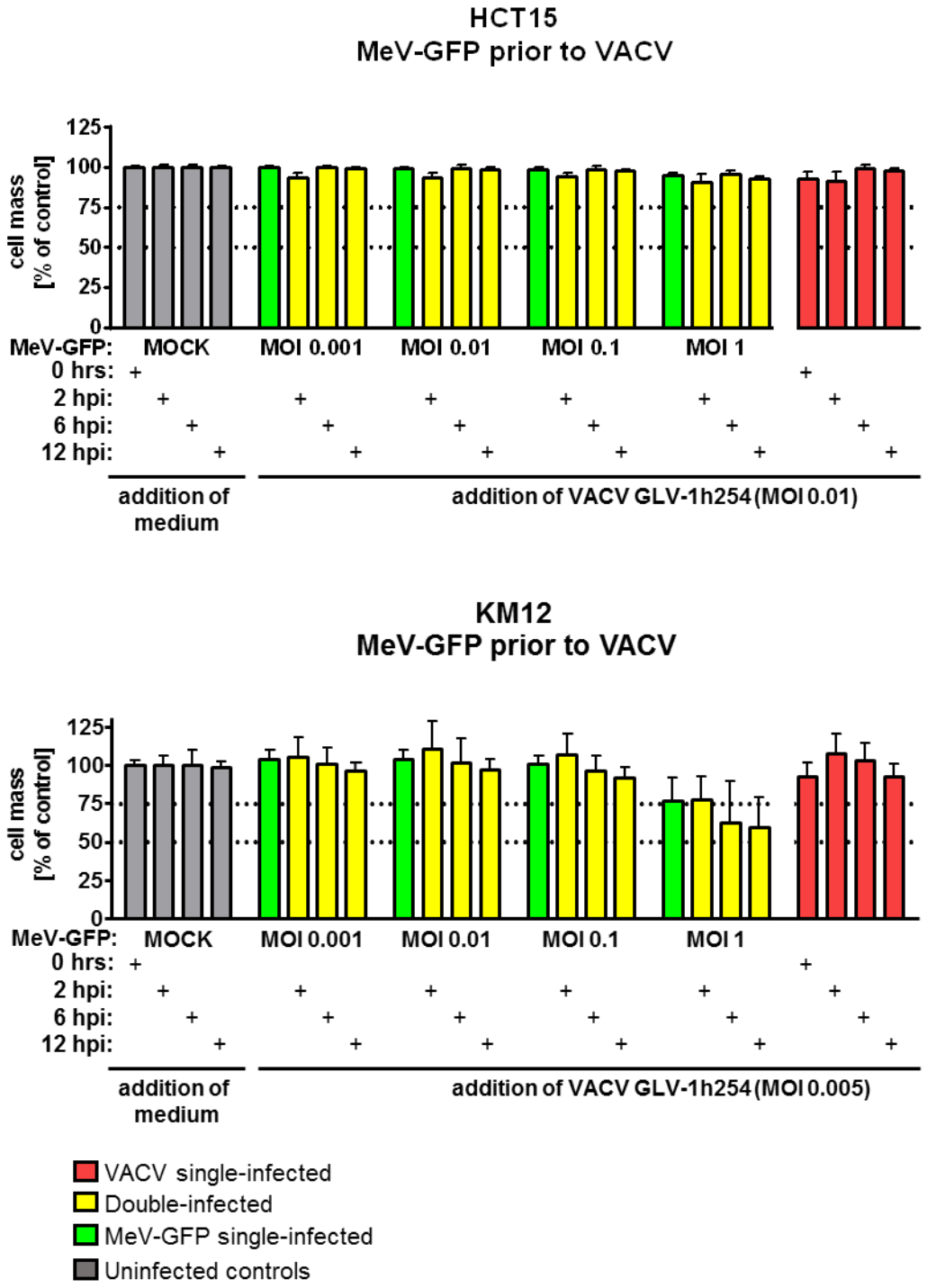

Figure 26. Cytopathic effect of combinatorial treatment with MeV-GFP prior to VACV GLV-1h254

ACHN, HCT15 and KM12 cells were plated in 24-well plates as listed in Table 2. Cells were either inoculated with MeV-GFP at ascending MOIs from 0.001 to 1 or mock-treated.

Single-infected controls were implemented (green columns). Secondary virus infection by VACV GLV-1h254 at MOI 0.01 (ACHN, HCT15), respectively MOI 0.005 (KM12) was performed at 2, 6 or 12 hpi with the first virus (yellow columns). At each time point (2, 6, 12 hpi and additionally at 0 hrs), single virus infections with VACV as controls were executed (red columns). Plates were incubated until 96 hpi with the first virus, the remaining cell mass was measured by SRB assay. Mock-treated controls were set 100 % (grey column 1 to 4 at 0, 2, 6 and 12 hpi). Dotted lines highlight the 50 and 75 % remaining cell mass. Values are means of three independent experiments. Error bars: SD.

When taking the results detailed in section 3.2.1 into account, the following annotations had to be made:

- Oncolysis was best, when VACV was applied prior to MeV.
- Different time points of secondary virus infection (2, 6 or 12 hpi) modified the cytotoxic effect only marginally. Nevertheless, best results were ascertained at 6 hpi.

Resulting, tumor cell lines were double-infected with MeV-GFP as secondary virus at 6 hpi in the following trials.

3.3 **Combinatorial treatment - VACV prior to modified MeV infection**

Next, we wanted to investigate whether an improved cytotoxic effect of the combinatorial treatment regime was due to synergistic or just additive effects.

Thus, cells were infected by VACV at MOI 0.01 (ACHN, HCT15), respectively at MOI 0.005 (KM12) first or mock-treated.

On the assumption that a synergistic effect would already appear at slightly lower MOIs of the second virus, cells were double-infected by MeV-GFP at ascending viral concentrations (MOI 0.1, 0.25, 0.5 and 1) at 6 hpi or medium was added. Virus-encoded fluorescent proteins were observed daily to monitor virus infection and spreading. At 96 hpi with the first virus, plates were analyzed by SRB assay. The application scheme is attached below.

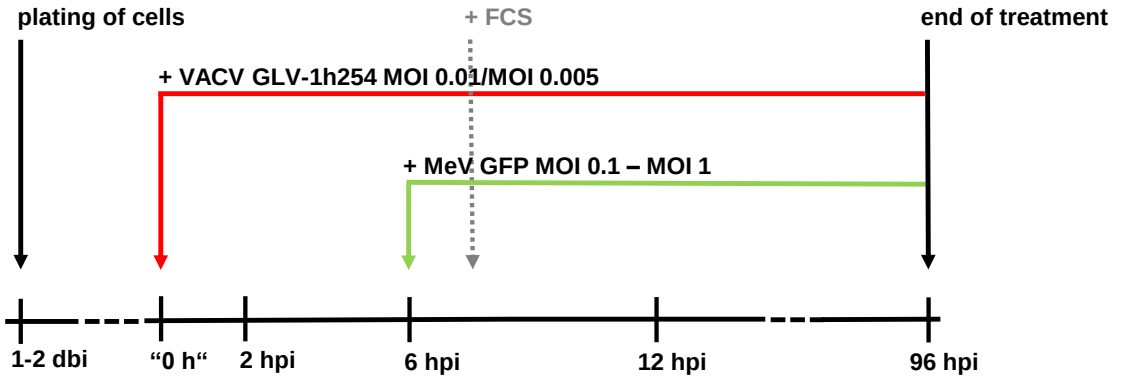

Figure 27. Application scheme for double-infections, VACV GLV-1h254 prior to MeV-GFP at 6 hpi at ascending viral concentrations

Cells were plated in 24-well plates and infected in quadruplicates by VACV GLV-1h254 at MOI 0.01 (ACHN, HCT15), respectively MOI 0.005 (KM12), or mock-treated. At 6 hpi, cells were double-infected by MeV-GFP at ascending viral concentrations (MOI 0.1, 0.25, 0.5 and 1) or medium was added to mock-treated and single-infected wells. Plates were incubated until 96 hpi with the first virus.

Infected cells showed red (VACV) and green (MeV) fluorescence, as well as plaque formation and syncytia building in the corresponding bright-field pictures (Figure 28). At ascending viral concentrations of the second virus, the number of green fluorescence emitting cells increased in all cell lines, except for HCT15 cells.

A

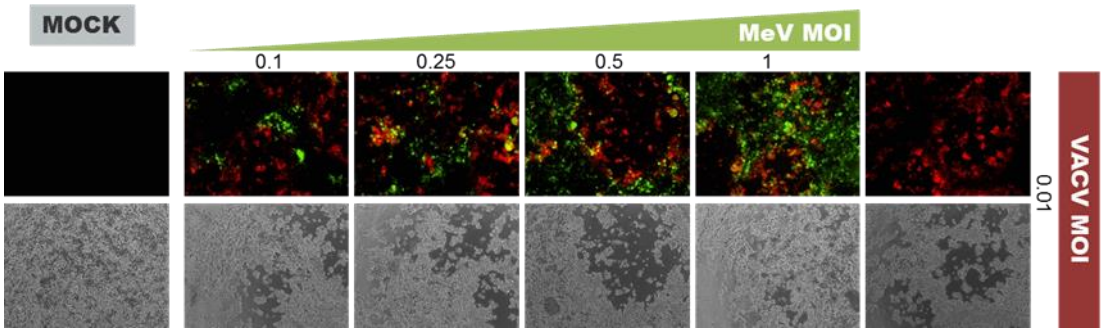

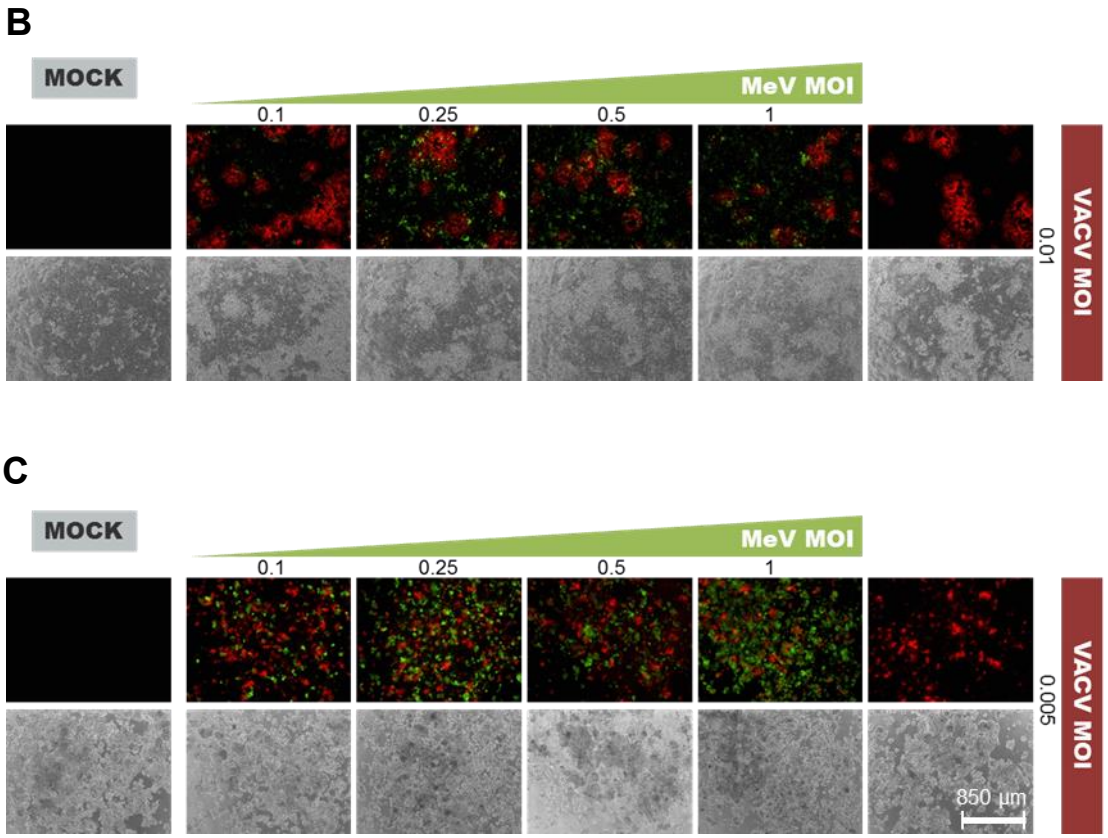

Figure 28. Overlays of fluorescence and bright-field pictures from combinatorial infected human tumor cell lines, VACV GLV-1h254 prior to MeV-GFP at 6 hpi

ACHN (**A**), HCT15 (**B**) and KM12 (**C**) cells were plated in 24-well plates as listed in Table 2. Cells were either infected by VACV at MOI 0.01 (ACHN, HCT15), respectively MOI 0.005 (KM12), or mock-treated. At 6 hpi, MeV-GFP at ascending MOIs from 0.001 to 1 or medium was added to mock-treated and VACV single-infected cells. Pictures were taken at 3 dpi. Fluorescence pictures are overlays. Infected cells show TurboFP635 or GFP expression as marker for VACV or MeV-GFP viral gene expression, as well as plaque formation (VACV) and syncytia building (MeV-GFP). Scale bar in the right lower corner applies to all panels.

Results of a subsequent SRB assay analysis (Figure 29) displayed the following:

- No synergistic effect was found. The plotted cell mass reduction of double-infected cells (columns in yellow) was commensurate to the increased MOIs of MeV-GFP (columns in green).
- Worth mentioning, HCT15 cells were only slightly diminished at ascending viral concentrations and showed less oncolytic efficiency than in previous work performed under equal conditions (see section 3.2.1).

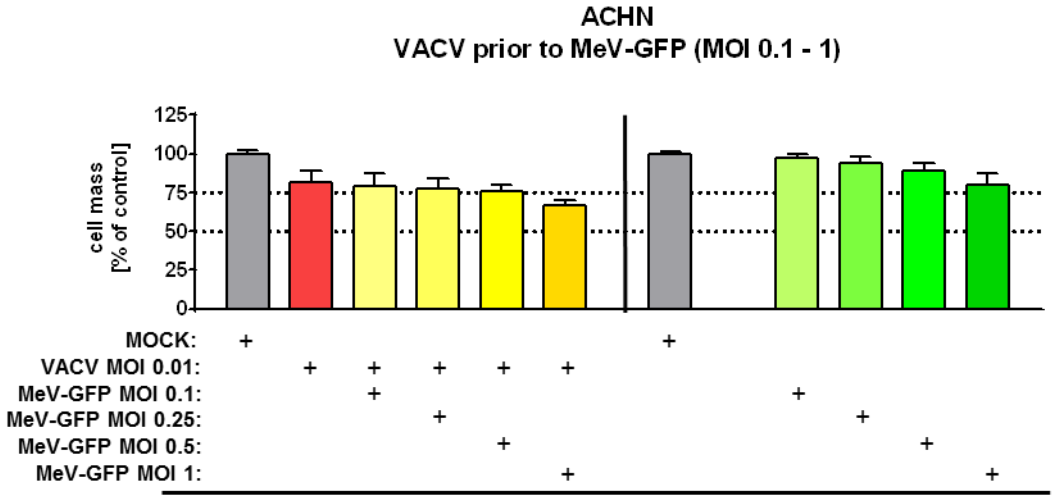
ACHN
VACV prior to MeV-GFP (MOI 0.1 - 1)
cell mass
[% of control]
125
100
75
50
25
0
MOCK:
VACV MOI 0.01:
MeV-GFP MOI 0.1:
MeV-GFP MOI 0.25:
MeV-GFP MOI 0.5:
MeV-GFP MOI 1:

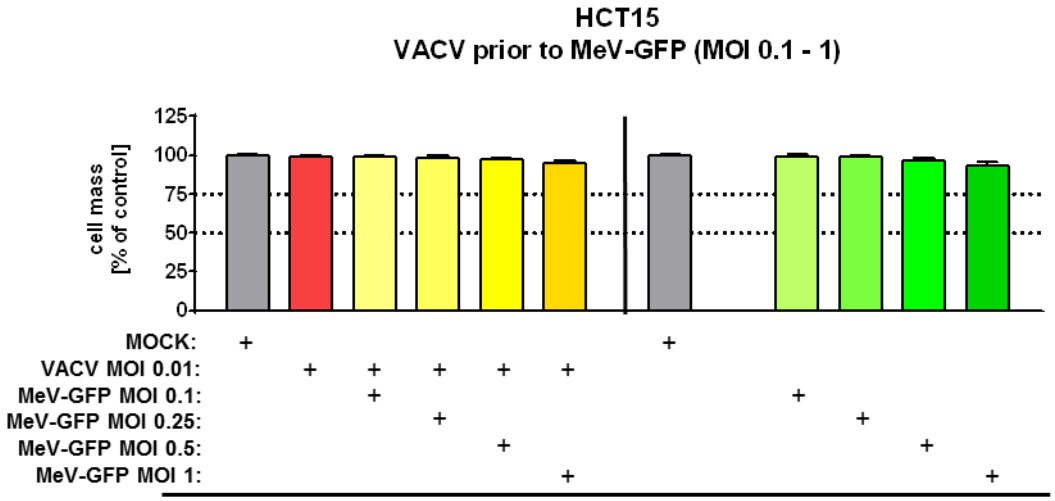
HCT15
VACV prior to MeV-GFP (MOI 0.1 - 1)
cell mass
[% of control]
125
100
75
50
25
0
MOCK:
VACV MOI 0.01:
MeV-GFP MOI 0.1:
MeV-GFP MOI 0.25:
MeV-GFP MOI 0.5:
MeV-GFP MOI 1:

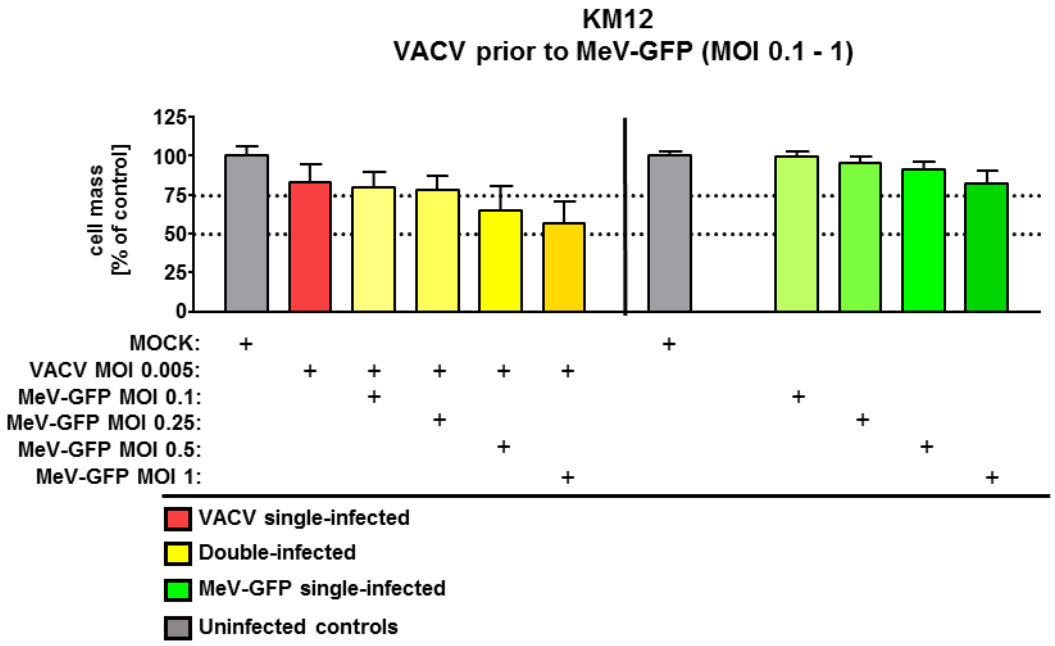

Figure 29. Cytopathic effect of combinatorial treatment with VACV GLV-1h254 prior to MeV-GFP at 6 hpi in SRB assays

ACHN, HCT15 and KM12 cells were plated in 24-well plates as listed in Table 2. Cells were either inoculated in quadruplicates with VACV GLV-1h254 at MOI 0.01, respectively MOI 0.005 (KM12), or mock-treated. MeV-GFP infection followed at 6 hpi at MOI 0.1, 0.25, 0.5 or 1 (yellow columns), or medium was added to mock-treated and VACV single-infected (red column) cells. Single-infections with MeV-GFP as controls are pictured on the right side of the dash (green columns). Plates were incubated until 96 hpi with the first virus, the remaining cell mass was measured by SRB assay. Mock-treated (grey columns) controls were set 100 %. Dotted lines highlight the 50 and 75 % remaining cell mass. Values are means of three (KM12), four (ACHN) and six (HCT15) independent experiments. Error bars: SD.

3.4 Comparison between SRB and MTT assay results

To assure that the measured cell mass reduction, analyzed by SRB assay, actually represented cell death, MTT assay was complementarily performed and results were compared. Since plates were not only fixed and analyzed at 96 hpi, but additionally at 0, 24, 48 and 72 hpi, it was possible to plot changes in cell masses over the course of the entire incubation period. As a proof of principle, the comparison between SRB and MTT assay results was done for ACHN cells only.

Accordingly, ACHN cells were seeded in 24-well plates and infected in quadruplicates by VACV GLV-1h254 at MOI 0.01 or mock-treated. At 6 hpi,

cells were inoculated with MeV-GFP at MOI 1 as second virus or DMEM was added to mock-treated and VACV single-infected cells. One plate was fixed prior to infection (0 hrs) both for the SRB and MTT method. Double-infected plates were incubated for 24, 48, 72 or 96 hpi, fixed with TCA and analyzed by SRB or MTT assay. Values were plotted in relation to “0 hrs” and in relation to mock. Additionally, virus-encoded TurboFP635 and GFP were monitored daily under a fluorescence microscope (Figure 31). The application scheme is attached below.

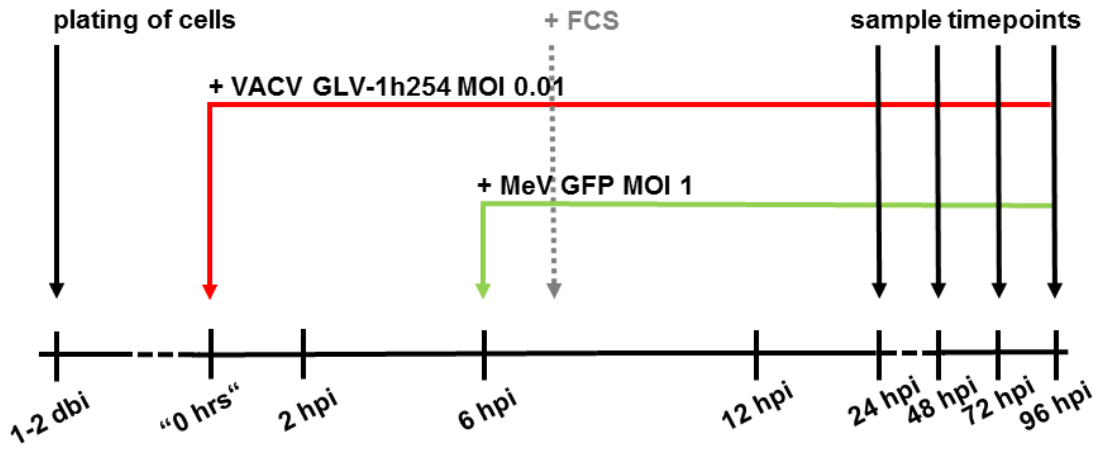

Figure 30. Application scheme for double-infections, VACV GLV-1h254 prior to MeV-GFP, 24-96 hpi

ACHN cells were plated in 24-well plates and infected in quadruplicates the next day. First, VACV was applied at MOI 0.01 or cells were mock-treated. At 6 hpi, infected and uninfected cells were inoculated with MeV-GFP at MOI 1, medium was added to mock-treated and VACV single-infected wells. Plates were incubated 24, 48, 72 or 96 hpi with the first virus. Cell mass was measured by SRB or MTT assay.

As shown in Figure 31, infected cells were examined daily under a fluorescence microscope to supervise the process of infection and spreading in ACHN cells. Whereas at 1 dpi, there was almost no fluorescence detectable, at 4 dpi, infected cells showed high intensities of green and red fluorescence. Mock-treated cells were uninfected and viable at 4 dpi.

In conclusion, the combinatorial treatment with VACV 6 hrs prior to MeV-GFP infection was successfully conducted and equal conditions could be ensured for the following analysis by SRB (**A**) or MTT (**B**) assay.

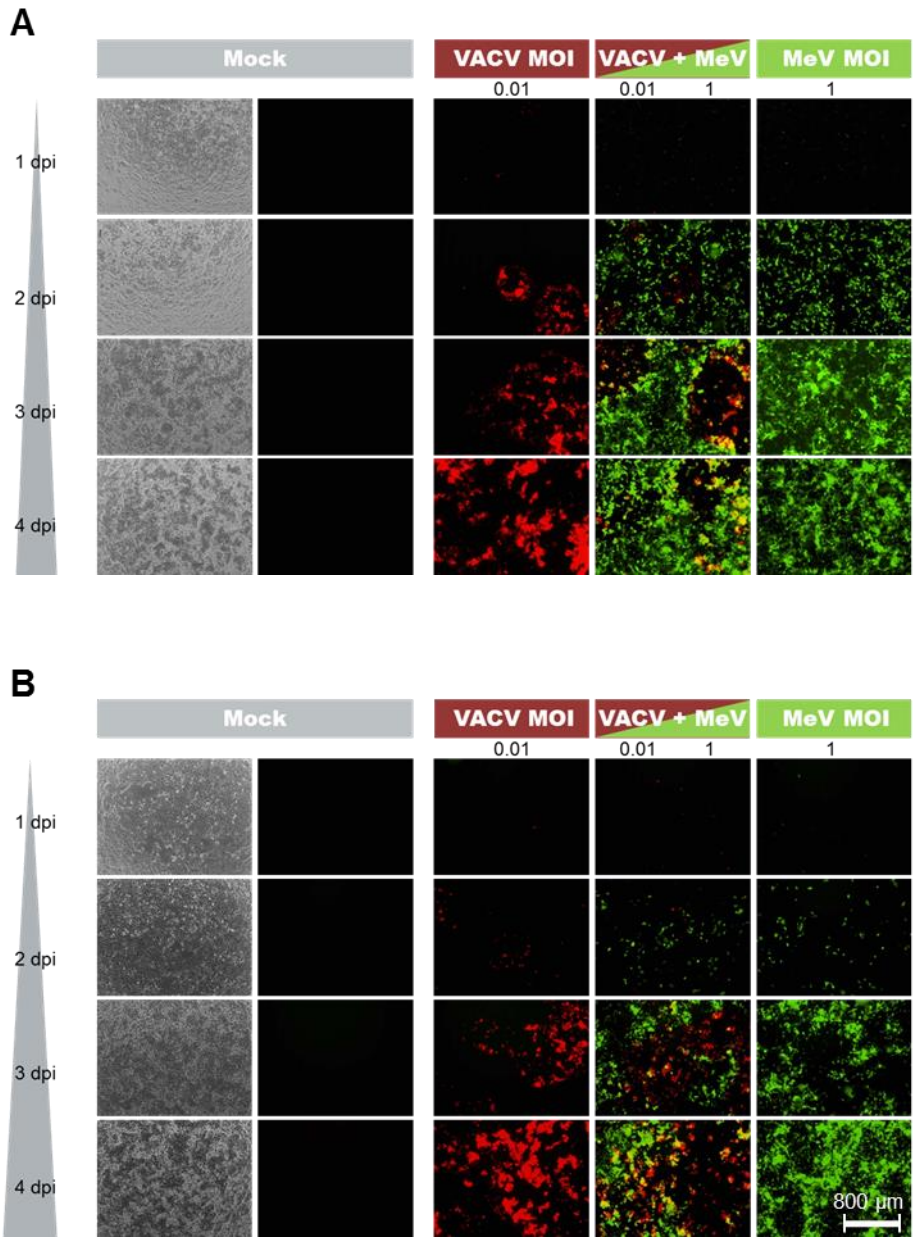

Figure 31. Overlays of fluorescence and bright-field pictures from combinatorial infected ACHN cells, VACV GLV-1h254 prior to MeV-GFP at 6 hpi, 1-4 dpi

ACHN cells were plated in 24-well plates (**A** = SRB), (**B** = MTT) and either infected by VACV at MOI 0.01 or mock-treated. At 6 hpi, MeV-GFP at MOI 1 was added to uninfected (right column) and infected cells (fourth column) or medium was added to mock-treated (first and second column) and VACV single-infected (third column) cells. Cells were observed and pictures were taken daily under a fluorescence microscope. Fluorescence pictures are overlays. Infected cells show TurboFP635 and GFP expression as marker for VACV and MeV-GFP viral gene expression. Scale bar in the right lower corner applies to all panels.

Analysis by SRB and MTT assay are depicted below (Figure 32). Expectedly, the highest cytotoxic effects were reached in combinatorial treated cells (**A**). Uninfected controls, measured by SRB assay, proliferated well until 72 hpi, at 96 hpi, however, cells reached a plateau. In MTT assay, mock-treated cells proliferated until 96 hpi, but means showed larger standard deviations.

In another representation of the data, when values from mock-treated cells were set 100 % and other values were plotted in relation to the corresponding mock, best cell mass reductions were obtained in double-infected cells at 96 hpi, with no discrepancy between SRB or MTT assay (**B**).

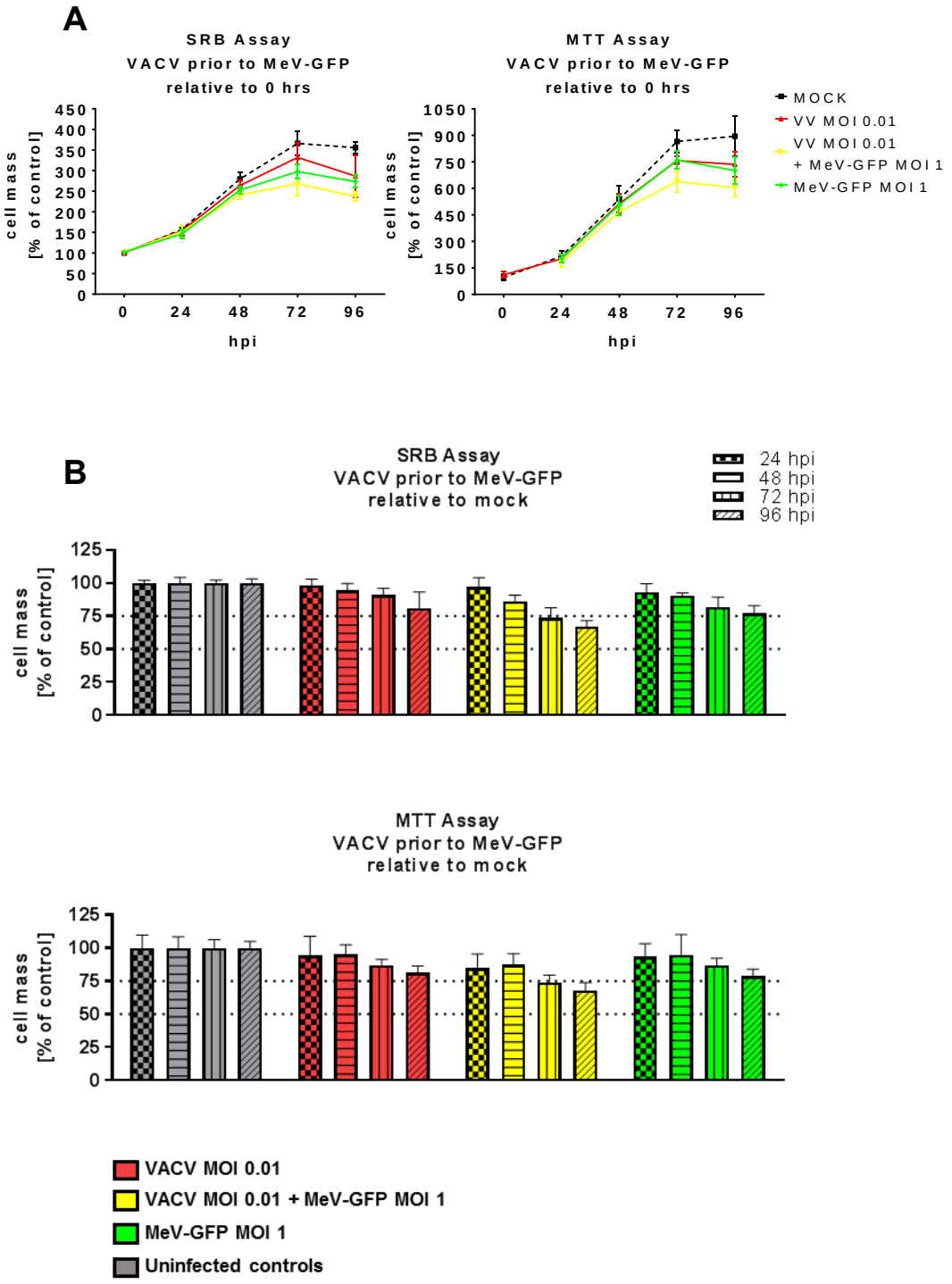

Figure 32. Comparison between SRB and MTT assay results. Cytopathic effect of combinatorial treatment of ACHN cells with VACV GLV-1h254 prior to MeV-GFP at 6 hpi relative to 0 hrs (A), relative to mock (B)

ACHN cells were plated in 24-well plates. The next day, one plate/trial was fixed prior to infection to gain output values ("0 hrs", **A**), other cells were either infected by VACV at MOI 0.01 or mock-treated. At 6 hpi, MeV-GFP MOI 1 was added to VACV-infected or uninfected cells

(MeV single control) or medium was added to mock-treated and VACV single-infected wells. At 24, 48, 72 and 96 hpi with the first virus, cells were fixed and measured by SRB or MTT assay. Values are means of three independent experiments and were either plotted as relative to 0 hrs (**A**) or as relative to mock (**B**) at 24, 48, 72 and 96 hpi. **B:** Grey columns show mock-treated (uninfected) controls, which were set 100 %. Dotted lines highlight the 50 and 75 % remaining cell mass. Red (VACV) and green (MeV) columns represent single-infected controls, yellow columns show combinatorial treated cells. Error bars: SD.

3.5 Monitoring of viral marker gene expression to further investigate the phenomenon of "viral competition"

3.5.1 Fluorescence microscope Olympus IX50 images

In sections 3.2.1 and 3.2.2, fluorescence pictures showed VACV and MeV-GFP infected cells at 4 dpi. At this time point, the cell layer of coinfected cells was already diminished to a great extent. Consequently, one might assume that the impression of "viral competition" was only received because less viable cells remained (after infection with the first agent), which could be infected in the second round, and subsequently express the fluorescent marker protein of the second virus. In order to exclude this assumption, we here present another set of bright-field and fluorescence pictures of sequentially infected ACHN cells taken at 2 dpi. Cells were plated and infected as described in section 3.2.1.

As pictured in Figure 33, the corresponding bright-field images of sequentially infected ACHN cells ascertained vitality at 2 dpi. Nevertheless, infected cells, visualized by VACV-encoded TurboFP635 and measles vaccine virus-encoded GFP expression, exhibited "viral competition".

- The majority of ACHN cells, infected first with GLV-1h254 at MOI 0.01 and second by MeV-GFP at MOI 1, expressed GFP.
- At a tenfold higher MOI of VACV (MOI 0.1), ACHN cells expressed mainly the red fluorescent protein TurboFP635, although the viral concentration of MeV-GFP did not change.

Cells expressed either TurboFP635 or GFP but not both viral marker proteins at the same time. Thus, "viral competition" arose independent of the condition of the cell layer.

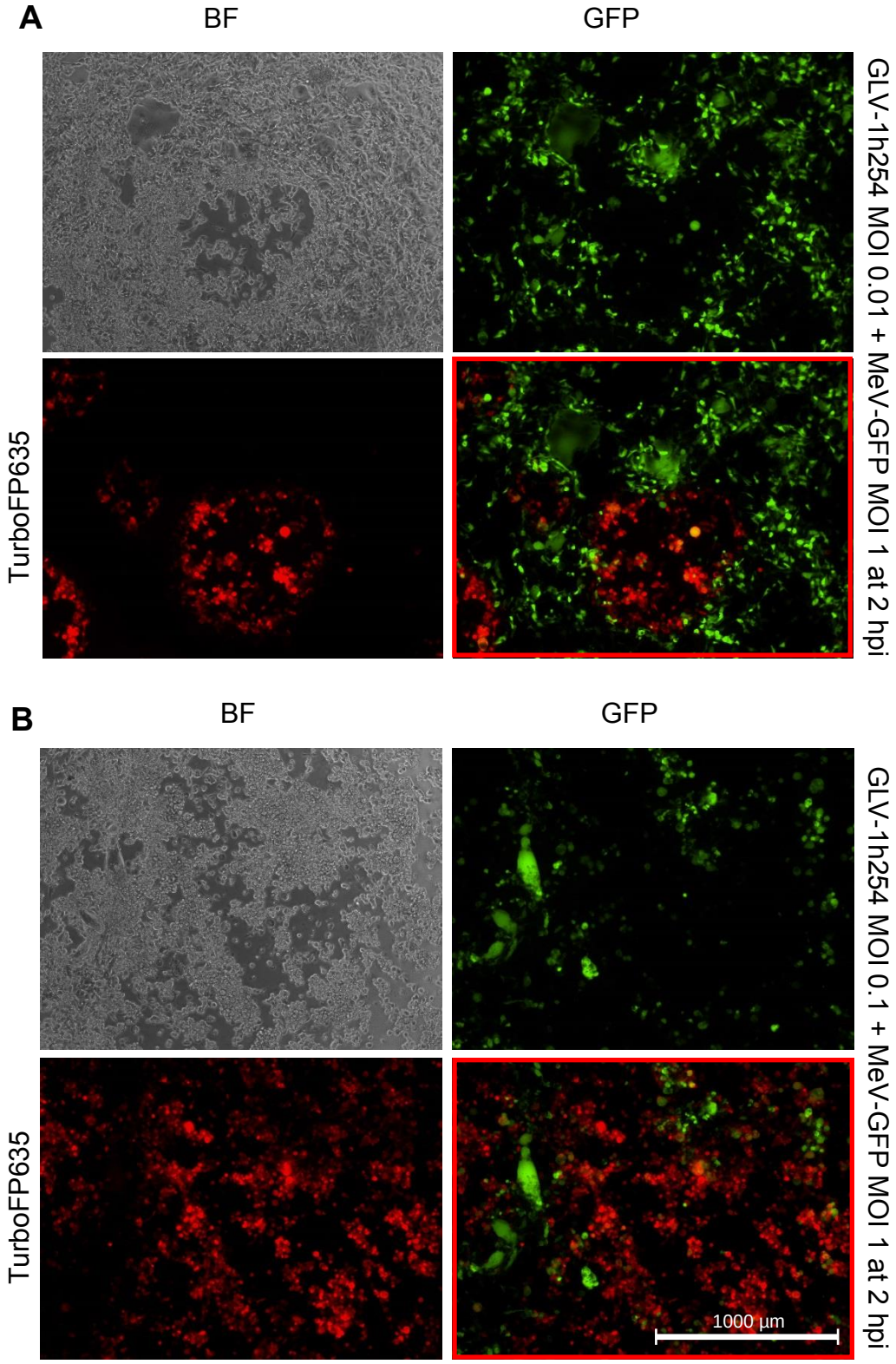

Figure 33. Fluorescence and bright-field pictures from combinatorial infected ACHN cells, VACV GLV-1h254 prior to MeV-GFP at 2 hpi

ACHN cells were seeded in 24-well plates and either infected by VACV at MOI 0.01 (**A**) or MOI 0.1 (**B**), respectively. At 2 hpi, cells were additionally inoculated with MeV-GFP at MOI 1.

At 2 dpi, fluorescence (TurboFP635, GFP) and bright-field (BF) pictures were taken using Olympus IX50 fluorescence microscope. The image in the bottom right corner shows the overlay of both fluorescence pictures. Infected cells showed TurboFP635 and GFP expression as marker for VACV and MeV-GFP viral gene expression. Scale bar in the right lower corner applies to all panels.

3.5.2 All-in-One BZ-9000 fluorescence microscope pictures

In previous sequential infection trials we observed that the majority of cells expressed either red or green fluorescent. Nevertheless, singular cells glowed yellow, which might indicate coinfection of one and the same cell by VACV and MeV-GFP.

To further distinguish between an actual superinfection and overlapping of neighboring, fluorescent-emitting cells, the Keyence microscope was applied. With the All-in-One BZ-9000 fluorescence microscope we were able to follow up viral marker gene expression in a real-time manner and, moreover, to monitor the infection of singular cells by ensured planar cell growth.

For this purpose, ACHN tumor cells were plated at 1.5×10^4 cells/well in an open µ-Slide with 8 wells and incubated with VACV at MOI 0.01 or mock-treated the next day. At 6 hpi, second virus infection with MeV-GFP at MOI 1 was performed. Each well was reviewed for expression of viral marker proteins. Thus, virus-encoded GFP and TurboFP635 expression were observed constantly until 98 hpi using the All-in-One BZ-9000 fluorescence microscope (KEYENCE, Osaka, Japan).

In Figure 34, digital images of sequentially infected cells at 63 hrs (counted from the beginning of the record) are presented. Here, a subconfluent cell layer ensured planar cell growth and therefore monitoring of singular cells.

Using this technique, the following result was obtained:

- Superinfections of one and the same cell arose at a quite low frequency (arrows point to double-infected cells). The majority of ACHN cells revealed sole infection either by VACV or by MeV-GFP.

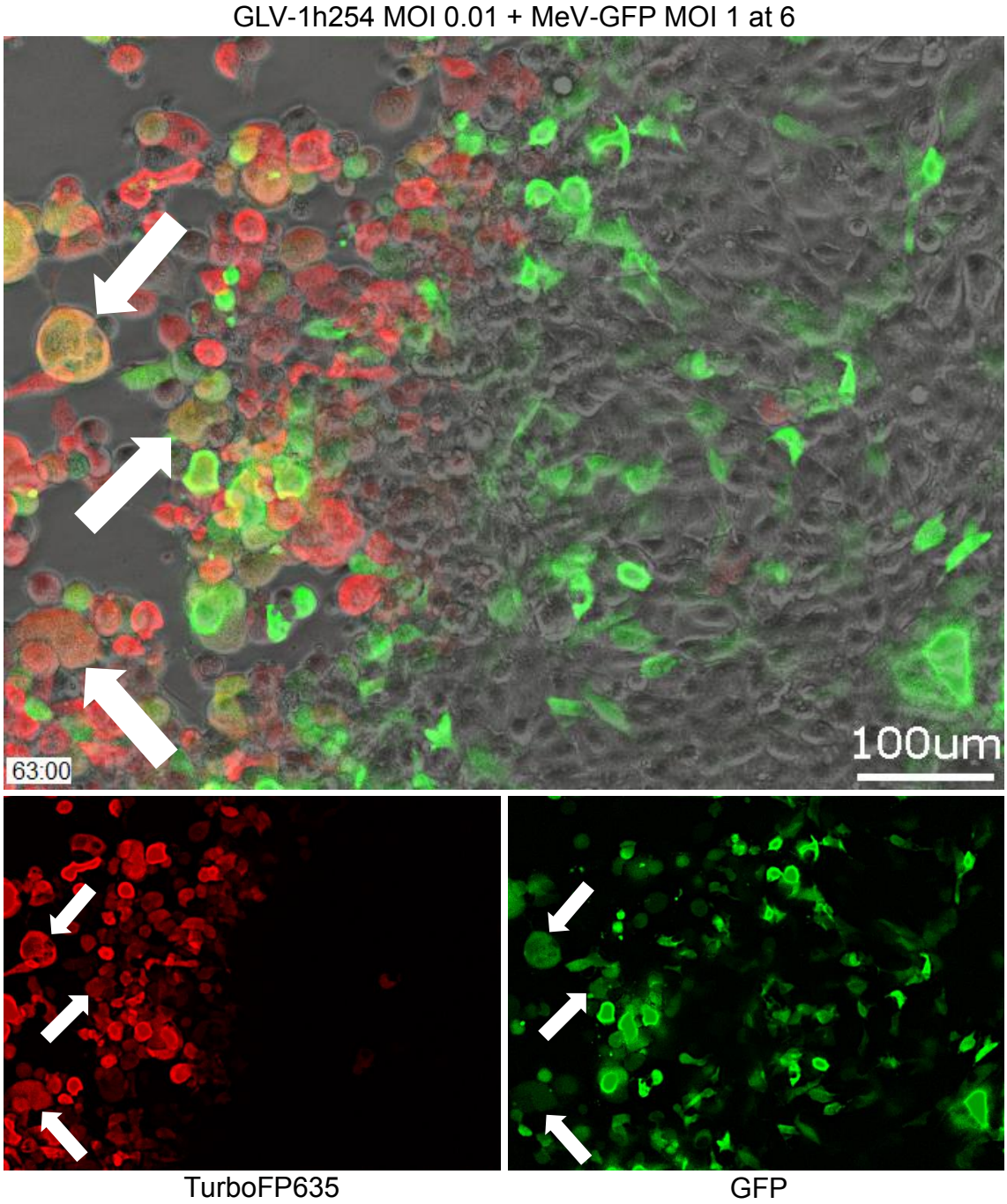

Figure 34. All-in-One BZ-9000 fluorescence microscope pictures of sequentially infected ACHN cells, VACV GLV-1h254 prior to MeV-GFP at 6 hpi

ACHN cells were plated in an open µ-Slide and inoculated first with VACV GLV-1h254 at MOI 0.01, followed by MeV-GFP infection at MOI 1 at 6 hpi. At 63 hrs (counted from the beginning of the record), fluorescence and bright-field pictures were taken using All-in-One BZ-9000 fluorescence microscope. The upper photo shows an overlay of the lower images and the corresponding bright-field picture. VACV infected cells express TurboFP635, MeV infected cells show GFP expression. Arrows point to singular cells, which are double-infected by VACV and MeV-GFP.

3.6 Western blot analysis - viral protein expression in infected ACHN cells

Electrophoresis and western blot were implemented to investigate the expression of virus-specific proteins. In order to monitor changes in cell masses over the course of the entire incubation period and to detect its influence on viral protein expression, we abstained from harmonization of the protein content. Thus, the 8-15 % gradient gel SDS-PAGE was performed without protein quantification and equalization by Bradford assay. Vinculin was chosen as loading control.

ACHN cells were plated at 5×10^4 cells/well in 24-well plates and incubated overnight. The next day, after determination of the current cell count, cells were infected by VACV at MOI 0.01 or mock-treated. At 6 hpi, cells were either additionally infected with MeV-GFP at MOI 1 or medium was added to mock-treated and VACV single-infected wells. At 24, 48, 72 and 96 hpi, cell lysates were prepared for the following analysis by Western blot.

The following results (Figure 35) were ascertained:

- Western blot analysis approved the expression of the viral proteins ß-galactosidase and Vaccinia (antigen A27L) for VACV (**A**), respectively N-protein and GFP for MeV (**B**).
- As expected, Vinculin showed alterations of the protein content over the course of time. Whereas mock-treated cells survived until 96 hpi, VACV single- and double-infected cells exhibited reduced protein contents from 72 hpi on. Contrarily, Vinculin of MeV single-infected cells indicated high remnant cell mass at 72 hpi.
- VACV single- and double-infected cells exhibited increased expression of ß-galactosidase and Vaccinia antigen A27L at 72 hpi. At 96 hpi, however, the expression of both viral proteins decreased (**A**). Furthermore, we monitored a slight difference between the VACV single and double infection group. At 72 and 96 hpi, the expression of Vaccinia antigen A27L in single-infected cells was higher than in double-infected cells. The expression of ß-galactosidase, however, showed no alterations.

- Similarly, Western blot analysis showed enhanced expression of MeV viral proteins (N-protein and GFP) in single- compared to double-infected cells at 72 and 96 hpi (**B**).

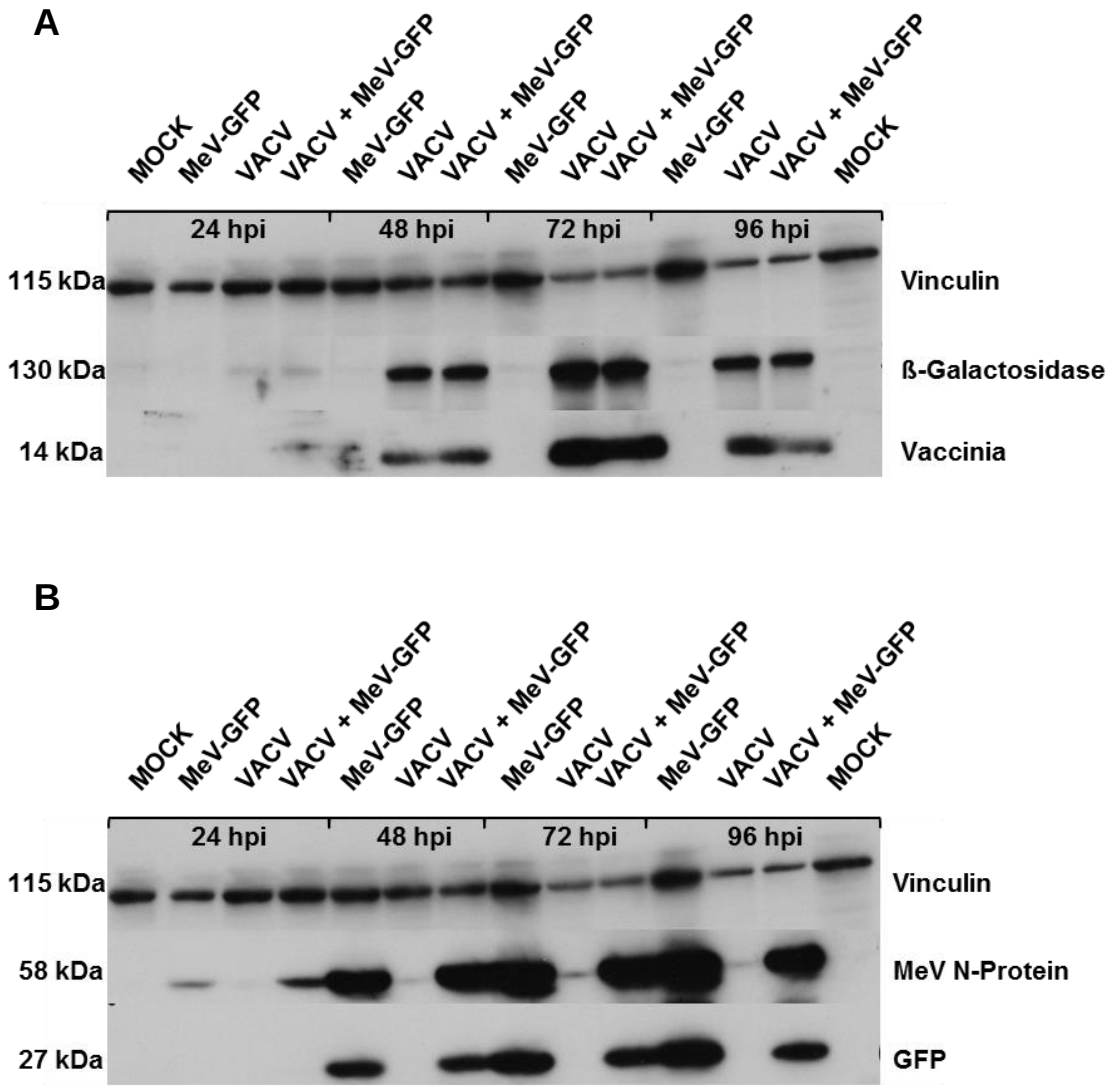

Figure 35. Western blot analysis of viral protein expression in ACHN cells

ACHN cells were plated at 5 x 10^4 cells/well in 24-well plates. The next day, cells were either infected with VACV at MOI 0.01 or mock-treated. At 6 hpi, cells were inoculated with MeV-GFP at MOI 1 or medium was added to single-infected and mock-treated cells. Cells were harvested 24, 48, 72 and 96 hpi. Lysates of mock-treated, single- and double-infected cells were separated by 8-15 % gradient SDS-PAGE and blotted on a PVDF membrane. Antibodies against Vinculin were used for "housekeeping" protein detection as loading control (**A, B**).
Viral protein detection was realized by using antibodies against ß-galactosidase and Vaccinia antigen A27L (VACV) (**A**), and antibodies against MeV N-protein and GFP (MeV-GFP) (**B**). VACV was detected at 14 kDa, GFP at 27 kDa, MeV N-Protein at 58 kDa, Vinculin at 115 kDa and ß-galactosidase at 130 kDa.

4 Discussion

Although the combined application of standard care and novel therapeutics has recorded considerable successes in the treatment of various cancers, a complete, sustainable remission remains rare.

Oncolytic viruses can be designed to complement established treatment modalities, thus, offering a promising attempt to handle metastatic disease. These anticancer agents fight tumors both by direct cell killing and the hereinafter establishment of a specific antitumor immune response (Kaufman *et al*, 2015). Naturally or by genetic engineering, virus constructs are exclusively directed against cancerous cells, while normal tissue is spared (Russell & Peng, 2007; Russell *et al*, 2012).

Remaining obstacles to a successful application of virotherapy have been overcome in some cases, as indicated by the accreditation of adenovirus H101 in 2005 (Garber, 2006; Jiang *et al*, 2006) and herpes simples virus T-VEC in 2015 (Andtbacka *et al*, 2015; Ledford, 2015; Zhang, 2015).

Nevertheless, inherent resistance of cancer cells towards oncolytic virus treatment remains a major issue. Thus, maintained antiviral activity of cancer cells hinders oncolytic viruses to completely eradicate tumor sides (Russell *et al*, 2012).

Besides other approaches, Le Boeuf *et al.* applied the attenuated Western Reserve strain of vaccinia virus together with a vesicular stomatitis virus to circumvent cellular innate immunity of highly resistant tumor cells (Le Boeuf *et al*, 2010). Furthermore, Tysome *et al.* performed sequential infections using the attenuated Lister vaccine strain of vaccinia virus and wildtype adenovirus (Tysome *et al*, 2012). Both research teams were able to demonstrate that a combinatorial treatment regime was superior to single virus infections.

The susceptibility to cellular innate antiviral immune response is traded as a central issue to a successful application of oncolytic viruses. Le Boeuf *et al.* revealed that some high resistant tumor cell lines derived from the NCI-60 panel are equipped with partial responsiveness to IFN (Le Boeuf *et al*, 2010).

Subsequently, the researchers applied a double-deleted vaccinia virus to complement a recombinant VSV version, which replication and spreading is most effectively hindered by IFN (Le Boeuf *et al*, 2010). The authors confirmed that a combined application of both virus constructs did not only support infection and spreading of VSV; moreover, it established the basis for synergistic interaction (Le Boeuf *et al*, 2010).

Here, in this wok, we set out to investigate whether these findings are reproducible when now applying the virotherapeutic vector GLV-1h254 (being derived from the attenuated Lister strain of vaccinia virus) together with oncolytic measles vaccine virus MeV-GFP.

The application of immunological distinct viruses may not only increase chances for multiple virus infections, but improve tumor cell destruction by collaboration of both viral agents in multiple ways (Le Boeuf *et al*, 2010; Tysome *et al*, 2012).

Three out of five tumor cell lines investigated in this thesis, i.e., ACHN, HCT15 and KM12, have been defined resistant to VACV infection by Ascierto *et al.* (Ascierto *et al*, 2011). The treated cell lines exhibited a most heterogeneous susceptibility to GLV-1h68, a close relative to GLV-1h254. Thus, resistance was not only found to be independent of tumor cell origin, it was also found to be independent of the chosen vaccinia virus strain in further investigations (Ascierto *et al*, 2011). When results were confirmed by the application of a VSV, Ascierto *et al.* were convinced that common virotherapy resistance patterns must exist (Ascierto *et al*, 2011). Additionally, ACHN, HCT15 and KM12 cells were declared highly resistant to MeV-SCD infection (Noll *et al*, 2013). Noll *et al.* suspected the incomplete blockage of the innate cellular immune defense of these tumor cell lines as crux of the matter (Noll *et al*, 2013). Thus, a functional IFN release upon MeV-SCD infection is traded as key mechanism to a reduced susceptibility to virus infection (Noll *et al*, 2013).

Recombinant vaccinia virus GLV-1h68 has been assigned for the treatment of human sarcomas as well (He *et al*, 2012). He *et al.* detected oncolytic activity against fibrosarcoma, osteosarcoma, fibrohistiocytoma and rhabdomyosarcoma cell lines *in vitro* and *in vivo*. Notably, the chosen MOI for infection of sarcoma

cells appeared quite high (MOI 5) and supports the presumption that responsiveness to oncolytic virotherapy was weaker than intended. Although SRH and CCS cells, two sarcoma cell lines investigated in this thesis, were not evaluated by this research group, cell lines were found to be resistant to MeV-SCD infection by Berchtold *et al.* (Berchtold *et al*, 2013). Although CD46 expression and primary infection were guaranteed for both cell lines, SRH and CCS cells presented either a transient or “slow and weak” virus production in viral growth curve analysis (Berchtold *et al*, 2013). Berchtold *et al.* attributed these findings to differential patterns of innate immune defense. Thus, MeV-SCD infection resulted in a strong induction of RIG-I and IFIT1 in SRH cells (Berchtold *et al*, 2013).

4.1 **Tumor cell resistance against oncolytic virotherapy is relative and can be diminished by ascending viral concentrations.**

First, it was necessary to define threshold MOIs for each viral vector in single infection approaches to satisfy the criterion of resistance, defined as cell mass reduction of less than 25 % compared to uninfected controls 96 hpi. As demonstrated repeatedly by applying VACV and MeV at ascending viral concentrations, tumor cell resistance is relative and can be partially overcome by increased virus titers. Evidence of this observation has also been provided by other members of our group (Berchtold *et al*, 2013; Lange *et al*, 2013; Noll *et al*, 2013; Yurttas *et al*, 2014).

Now, one might assume that the hurdle of resistance could be overtaken by simply employing elevated virus titers; however, this approach cannot be traded as a serious solution. At first, the production of high titer lysates has already become a challenge since most viruses are propagated in laborious tissue cultures (Kaufman *et al*, 2015). Secondly, even if a high titer production is feasible, premature viral clearance, neutralization of virus particles and limited virus delivery may represent further obstacles *in vivo*.

Moreover, as demonstrated in this thesis, resistant tumor cell lines are not completely erased, but “only” diminished at ascending viral concentrations. As a

consequence, surviving tumor cells, for example non-cycling cells, may prepare the breeding ground for new tumor growth soon afterwards (Kaufman *et al*, 2015). Resulting, we here established a treatment regime applying two different virus constructs in order to fight cancer by interlocking mechanisms.

4.2 **Determination of threshold MOIs depends on cellular confluence.**

As suggested by previous work from C. Raff (unpublished data) and M. Noll (Noll *et al*, 2013), who had screened the commonly applied NCI-60 panel for its susceptibility either to VACV- or MeV-based virotherapeutics, we initially plated all tumor cell lines equally (section 3.1.1). For reasons of practicability, we additionally seeded the sarcoma cell lines SRH and CCS uniformly. Whereas ACHN and HCT15 cells grew well and were considered to be ready to VACV-infection already the next day, KM12, CCS and SRH cells revealed insufficient confluence 1 dpi.

The following analysis by SRB viability assay provided corresponding results: While values of ACHN and HCT15 cells showed small standard deviations, those of KM12, SRH and CCS differed enormously. Moreover, even though the experimental setting was comparable, our SRB assay results diverged from the results previously obtained by C. Raff. Based on this finding, we decided to have a closer look at the chosen initial cell counts, resulting confluence and growth inhibition, and its influence on virus spreading.

Thus, so called “confluence trials” were performed to optimize the density of cell layers right before virus infection, as well as to guarantee survival of mock-infected controls until the end of the experiment. We noticed that (i) pro-longation of the time that HCT15, KM12, SRH and CCS cells were plated before any subsequent infection, as well as (ii) increased initial cell counts (CCS and KM12) led to enhanced cell density and therefore confluence.

Encouraged by Niepel *et al.*, who recommended to take diverging cell division times into account, we then determined individual incubation periods and plating densities for each cell line (Table 1) (Niepel *et al*, 2017).

However, we have to admit that the survival of mock-infected cells was not guaranteed by these "confluence trials". Since monitoring of cell density was performed with the naked eye, analysis was most vulnerable to error. A clear differentiation between a confluent and an overgrown well was not practicable, especially with cell lines such as CCS and KM12 that agglomerated quickly (independent of their initial cell count) but never reached total confluence.

In accordance, Skehan *et al.* have reported problems concerning fixation of cells growing as floating aggregates (Skehan *et al*, 1990). Moreover, Niepel *et al.* emphasized the underestimated relevance of interfering factors to drug sensitivity assays like SRB (Niepel *et al*, 2017). The authors underlined that the condition of the applied cell culture at the time point of seeding, initial cell counts and cell division time "are (...) variables with a substantial impact on cell proliferation" (Niepel *et al*, 2017). Since evidence grows that high cell numbers support drug resistance (Chauffert *et al*, 1998; Dimanche-Boitrel *et al*, 1993; Fang *et al*, 2007; Garrido *et al*, 1995; Hafner *et al*, 2016; Niepel *et al*, 2017), Niepel *et al.* suggest to perform experimental trials in the time frame of steady state growth (Niepel *et al*, 2017).

VACV infected "optimized-plated" SRH and CCS cells (section 3.1.3) showed reduced cell masses, when compared to non-optimized plated cells (section 3.1.1). Improved virus spreading due to tighter cell-to-cell contacts may offer an explanation. Worth mentioning, washing steps of the applied SRB assay were accidentally modified: after staining with SRB dye, plates were washed once with tap water instead of using 1 % acetic acid for washing exclusively. As this aminoxanthene dye dissociates under basic conditions, the remained cell mass may have been underestimated (Skehan *et al*, 1990; Vichai & Kirtikara, 2006). On the contrary, since this mistake affected all treated cell lines and not only SRH and CCS cells, the interference might be negligible. Surprisingly, although fluorescence pictures of infected HCT15 and KM12 cells (section 3.1.3) showed large plaque forming units (HCT15) and a high proportion of TurboFP635 expression at higher MOIs, cell masses were even less reduced than before (see section 3.1.1). We presume that suitable initial cell counts might have led to a more sufficient cell attachment and reduced cell loss during procedure

steps of the SRB assay (Vichai & Kirtikara, 2006). Additionally, lower standard deviations of KM12 cells supported this conclusion.

In MeV single infection trial (section 3.1.4), virus infection was successfully conducted, demonstrated by virus-encoded GFP expression and syncytia formation in all cell lines, except for SRH. Although analysis of SRB data represented reduced cell masses at MOI 1 and 10, SRH cells seemed only marginally infected on the belonging overlay pictures. A closer examination of these photographs exhibited a subconfluent cell layer of SRH cells at 96 hpi. Poor cell-to-cell contract might have led to reduced virus spreading, and, consequently, limited virus marker gene expression. In accordance, Berchtold *et al.* declared SRH and CCS cells as resistant to MeV-SCD infection (Berchtold *et al*, 2013). For HCT15 cells, overlays of fluorescence and bright-field pictures revealed marginal signs of infection, and remnants were inappreciably reduced at 96 hpi in SRB assay analysis. Consistent with our findings, Noll *et al.* defined ACHN, HCT15 and KM12 cells highly resistant to MeV-SCD infection at MOI 1 (Noll *et al*, 2013). Whereas, ACHN and KM12 cells exhibited a primary infection rate > 20 % by MeV-GFP at MOI 1, less than 3 % of HCT15 cells expressed GFP (Noll *et al*, 2013). Moreover, viral growth curves exhibited only transient viral replication in HCT15 cells, and western blot analysis confirmed decreased expression of MeV-encoded proteins at 72 and 96 hpi (Noll *et al*, 2013). The researchers argued that a strong interferon response by intense expression of IFIT1 might be responsible for the mentioned differences between HCT15 and other highly resistant cell lines (Noll *et al*, 2013).

To confirm findings regarding confluence, its impact on virus spreading and survival of uninfected controls, an xCELLigence trial was performed. By registration of differences in electrical impedance, cell viability and proliferation is evaluated in real-time (Ke *et al*, 2011). Contingent upon selected cell numbers, mock-treated ACHN cells either proliferated until 96 hpi (1000 cells/well, respectively 2000 cells/well), hit a plateau (4000 cells/well) or levelled off (8000 cells/well). This finding indicated that high plating densities cause growth inhibition or cell death of uninfected controls. Furthermore, the disparity of the normalized cell index between mock-treated and VACV MOI 0.1

infected cells increased dependent on higher plating densities. Accordingly, we assumed that the efficiency of virus spreading and oncolysis correlates with the initial cell counts of infected cells and therefore with confluence. The higher the cell-seeding density, the better the virus spreading - as long as cells range in the exponential increase phase. Niepel *et al.* considered the xCELLigence platform as a reliable tool to assess confluence in real-time, nevertheless they emphasized its limitations, since its application is restricted to monolayers (Niepel *et al*, 2017).

Both observations of the xCELLigence trial were affirmed by another single-infection approach using VACV (section 3.1.5). To survey the survival of mock-treated and infected cells reliant on initial cell counts, cells were assessed daily by fluorescence microscopy and SRB assay. For KM12 cells, which were plated at several densities, agglomeration of cells was registered independent on the initial cell count, but at 2 x 10^5 cells/well, KM12 cells overgrew and levelled off when analyzed by SRB assay. Accordingly, we admit that KM12 cells were plated far too high in previous trials. Although bright-field pictures revealed dense cell layers of ACHN and HCT15 cells already 1dpi, we maintained initial cell counts because the SRB assay result ensured proliferation until 96 hpi. Retrospectively, uninfected controls of ACHN and HCT15 cells indicated cell growth after log phase at this time point. As a consequence, plating numbers should have been determined by daily performance of the SRB method in the first place.

In accordance with findings of the xCELLigence trial, KM12 cells were erased more efficiently when plated at the higher cell-seeding density. Although values of 2 x 10^5 cells/well must be interpreted with caution (since the corresponding mock declined at 96 hpi), cell remnants of the MOI 0.01 treatment group were diminished to a greater extent. Thus, we demonstrated once again that virus spreading is reliant of confluence. Surprisingly, at 1 x 10^5 cells/well, infected cell remnants were less reduced than at 5 x 10^4 cells/well. Improved cell attachment of 1 x 10^5 cells/well might have had influence.

Finally, when results of section 3.1.5 were compared to those generated in section 3.1.1 and 3.1.3, respectively, we noticed differences regarding cell indices of remnants. In section 3.1.5, infected ACHN and HCT15 cells were reduced to a greater extent, although plating conditions and initial cell counts did not change. However, from section 3.1.5 on, we variegated the mode of infection: at 1.5 hpi, the virus-containing inoculum was no longer removed, but 22 % FBS-supplemented DMEM was added to the wells. Thus, the incubation period of vaccinia virus particles was greatly prolonged and SRB assay results may display enhanced oncolysis.

4.3 **Combinatorial virus infections are superior to single infections.**

As detailed above, the extensive determination of reliable threshold MOIs for each viral vector was necessary in the run. Thereafter, oncolytic vaccinia and measles vaccine virus were examined in several application schemes in double-infection approaches with ACHN, HCT15 and KM12 cells. Thus, different orders of viruses and time points of secondary virus infection were tested to identify the most promising design.

In section 3.2.1, ACHN, HCT15 and KM12 cells were infected with VACV at various MOIs prior to MeV at MOI 1 at 2, 6 or 12 hpi. As reflected by fluorescence pictures, VACV marker protein expression was dependent on ascending viral concentrations. Moreover, we observed a phenomenon called “viral competition”, which is discussed in detail in section 4.6.

As analyzed by the SRB assay, remnant cell masses of all three cell lines were found to be reduced more effectively when double-infected. At threshold MOIs, cell indices of combinatorial treated ACHN and KM12 cells were reduced below the critical value of 75 % remaining cell mass, independent of the time point of secondary virus infection. Double-treated HCT15 cells, however, reached the borderline only when infected with MeV at 6 hpi.

In section 3.2.2, cells were infected vice versa (ACHN, HCT15 and KM12 cells were infected with MeV at various MOIs prior to “fixed-dosage (MOI)” infection with VACV). A dose-dependent MeV marker protein expression was

documented in all cell lines by fluorescence pictures. In the SRB assay analysis, double-infected ACHN and KM12 cells showed an improved oncolytic effect in the 2 hpi- (ACHN), respectively 6 hpi- and 12 hpi-treatment group (KM12). Of note, remnant HCT15 cells did not benefit from sequential infections. Consequently, all three highly resistant tumor cell lines were combatted best when inoculated first with VACV. Moreover, at threshold MOIs cell indices of double-infected cells did no longer comply with the criterion of high-grade resistance.

Time points for secondary virus infection were aligned to vaccinia virus life cycle. Since early viral mRNAs are known to suppress the emerging cellular immune response (Moore & Smith, 1992; Schramm & Locker, 2005; Thorne *et al*, 2005), 2 hpi appeared to be an appropriate time period for the following measles virus infection. Whereas differences between MeV-second-infected remnants at 2, 6 and 12 hpi (section 3.2.1) were found to be negligible and without correlation to the belonging controls, variations in VACV-second-treated cells (section 3.2.2) corresponded to up- and downturns of the single-infected controls. Fittingly, the belonging fluorescence pictures highlighted unequal TurboFP635 expression in HCT15 and KM12 cells. Thus, we reasoned, fluctuations were most likely explainable by execution errors than by real differences. Nevertheless, for reasons of feasibility, we decided to further on perform all double-infections at 6 hpi with VACV.

Le Boeuf *et al.* established a double-deleted vaccinia virus (VVDD) prior to recombinant VSVΔ51 to sensitize a resistant monolayer to VSV-derived oncolysis (Le Boeuf *et al*, 2010). This combination was most successful because of its rational design. Since Le Boeuf *et al.* handled partial responsiveness to IFN as prime suspect of a reduced susceptibility to oncolytic virotherapy, they applied a VACV version with a soluble IFN-receptor to suppress remaining antiviral immune response (Le Boeuf *et al*, 2010). Furthermore, even a synergistic effect was established by applying a VSV version that additionally expressed a protein, which improved the spreading of VACV.

Here, in this work, we were challenged by the fact that ACHN, HCT15 and KM12 tumor cells were resistant both to oncolytic vaccinia and measles virus treatment. Nevertheless, since double-infections with VACV prior to MeV-GFP ("VACV first, MeV second", section 3.2.1) proved to be superior both to single- and the "alternative round" double-infection regime ("MeV first, VACV second", section 3.2.2), we reasoned that a vaccinia-mediated IFN blockage might have turned the scales.

B*18*R, the soluble type I IFN-receptor Le Boeuf reported on, is expressed ubiquitously as ascertained by comparison of genome sequences of various vaccinia virus strains (Qin *et al*, 2015). Among others, Lister strain VACV107 encodes B*18*R, respectively open reading frame number 194 (Qin *et al*, 2015). Accordingly, we assumed that VACV GLV-1h254 might encode this soluble IFN receptor as well.

Moreover, Smith *et al.* reviewed that poxviruses apply a multitude of strategies to inhibit host antiviral responses (Smith *et al*, 2013). In addition to B*18*R, VACV establishes lots of immune-modulatory proteins to block complement factors, cyto- and chemokine production, and counteracts host cell signaling pathways to inhibit apoptosis and viral clearance (Smith *et al*, 2013).

In another study, Tysome *et al.* proved that three Syrian hamster tumor cell lines supported viral gene expression after oncolytic adenovirus and vaccinia virus treatment (Tysome *et al*, 2012). *In vitro*, HPD-1NR, HPD-2NR and HaK cells were either infected with Ad5 or VVLister but not combined. *In vivo*, the combined application of Ad5 and VVLister erased established tumors in an immunocompetent Syrian hamster model. Although the study design was not directly comparable to our setting, the advantage of a sequential treatment regime was demonstrated convincingly.

4.4 **No hint of synergism - the superiority of sequential infections is explained by additive effects.**

In general, the combined application of drugs - in our case of two genetically distinct oncolytic agents (i.e., a DNA type (VACV) and an RNA type (MeV)

virus) - leads to three different types of interaction. Besides the most wanted synergism, both addition and antagonism are alternative mechanisms. While synergistic interaction improves outcomes, addition fulfills and antagonism falls behind the expectation gained from the singular activity of each component (Bukowska *et al*, 2015).

In this context, Le Boeuf *et al.* were able to induce synergism between VSV and VACV, both *in vitro* and *in vivo* (Le Boeuf *et al*, 2010). Beyond that, also Tysome *et al.* demonstrated synergistic interaction *in vivo* since they were able to halve the applied doses of Ad5 and VVLister in the combinatorial setting (Tysome *et al*, 2012). In contrast to Le Boeuf *et al.*, who constructed their OVs most carefully, we hypothesized that our “unmodified” virotherapeutic agents might complement each other naturally. In this line, we were convinced that VACV-encoded immune-modulatory proteins support the infection and spreading of a second virus that is most dependent on IFN signaling. Moreover, we assumed that syncytia formation emerging upon MeV-GFP infection, would lead to a ping-pong effect in terms of virus infection and spreading of both counterparts.

To further investigate whether there are synergistic or only additive effects, ACHN, HCT15 and KM12 cells were infected with VACV at defined threshold MOIs followed by an infection with MeV at slightly deviating viral concentrations 6 hpi. Fluorescence pictures of HCT15 cells showed barely signs of MeV infection. Fittingly, cell indices of infected HCT15 cells were reduced inappreciably. As expected, in double-infected ACHN and KM12 cells, GFP expression and syncytia formation were dependent on the virus concentration applied, and corresponding cell masses were reduced in accordance. What is more, cell mass reduction of each double-infected cohort was reflected by its belonging single-infection treatment group. Thus, we did not receive any hints of synergism, but of additive effects here.

4.5 **Both viabilitiy assays, SRB and MTT, exhibit comparable results.**

SRB and MTT viability assays are widely applied colorimetric assays to determine cell counts after a wide variety of cytotoxic treatments. Both methods convince with cost-efficiency, time saving and practicability.

Because the SRB dye binds to cellular proteins, the amount of subsequent dissolved dye is directly proportional to the cell number stained (Skehan *et al*, 1990). Although this assay detects cytotoxic effects most accurately, it is not able to differentiate between viable and dead cells (Vichai & Kirtikara, 2006).

The MTT assay, however, detects metabolic active, viable cells by enzymatic conversion of a tetrazolium salt into a dark-colored formazan dye (Mosmann, 1983). Thus, the MTT assay is a great tool to review results obtained with the SRB method.

In order to evaluate whether the results of the SRB assay were comparable to those of the MTT assay, and, moreover, to investigate, if reduction of cell mass actually indicated cell death, a comparative trail was performed (section 3.4).

For this purpose, sequential infection with VACV followed by MeV was performed. Then, infected and uninfected ACHN cells were analyzed at 0, 24, 48, 72 and 96 hpi with the SRB or MTT assay, respectively. Fluorescence and bright-field pictures ensured equal cell-seeding and comparable rates of infection.

When values from mock-treated cells were set 100 % and other values were plotted in relation to the corresponding mock, there were no differences between SRB and MTT assay results detectable. Thus, we reasoned, cell mass reductions analyzed by SRB assay actually indicated cell death.

Analogically, other groups have demonstrated that results of both assays are highly comparable (Haselsberger *et al*, 1996; Perez *et al*, 1993; Rubinstein *et al*, 1990). However, the generated signal of the MTT assay is dependent on the overall cell count, but in addition, it is reliant on the metabolic activity of each and every cell (Riss *et al*, 2004). Riss *et al.* explicated that different factors, e.g. growth inhibition, altered pH and depletion of nutrients, reduce the amount of

produced formazan, which deregulates the “linearity between absorbance and cell number” (Riss *et al*, 2004). Consequently, the SRB and MTT method need to be performed at logarithmic cell phase growth (van Meerloo *et al*, 2011; Vichai & Kirtikara, 2006). In our experiment, cell growth of uninfected controls plateaued in the SRB assay analysis at 96 hpi. Although mock-treated cells proliferated until the end of the trial in the MTT assay, growth curves indicated that cells were measured after log phase.

4.6 **The majority of sequentially infected cells exhibits sole infection by “only” one virus.**

Many viruses have evolved mechanisms to prevent superinfection of an already “occupied”, i.e. primarily infected cell.

For this phenomenon, downregulation of viral entry receptors, blockage of secondary virus RNA translation and genome replication, as well as activation of IFN signaling pathway are held responsible (Schaller *et al*, 2007).

Prohibition of superinfection has been demonstrated for a wide variety of distinct viruses, such as hepatitis C virus (HCV) (Schaller *et al*, 2007; Tscherne *et al*, 2007), human immunodeficiency virus type 1 (Wildum *et al*, 2006), Old and New World arenaviruses (Huang *et al*, 2012; Huang *et al*, 2015), NDV (Li *et al*, 2012), rubella virus (Claus *et al*, 2007) and West Nile virus (Zou *et al*, 2009).

Among other poxviruses, VACV is known to circumvent superinfection both by blockage of the “membrane fusion step” (Laliberte & Moss, 2014) and expression of virally encoded proteins like haemagglutinin (A56) and K2 (Turner & Moyer, 2008; Wagenaar & Moss, 2009), A33 and A36 (Doceul *et al*, 2010).

In the majority of cases reviewed, superinfection exclusion was observed upon secondary virus infection with progeny of the same virus construct. In addition, researchers also reported of “heterologous superinfection exclusion” upon secondary virus infection with related or even distinct viruses (Eaton, 1979; Huang *et al*, 2015; Karpf *et al*, 1997; Nasar *et al*, 2015; Parkman *et al*, 1964; Tscherne *et al*, 2007).

As illustrated by fluorescence pictures, Le Boeuf *et al.* observed that DsRed and GFP expression did mainly not occur in the same cell after coinfection with VACV and VSV (Le Boeuf *et al*, 2010). However, the oncolytic potential of this combinatorial approach was undoubted. Consequently, the researchers presumed that a “sensitization of neighboring cells” upon VACV infection must have led to enhanced susceptibility to the following application of VSV (Le Boeuf *et al*, 2010).

Here, in our work, we noticed that the majority of sequentially infected cells were either infected by VACV or by MeV but not by both viral agents simultaneously (sections 3.2.1, 3.2.2 and 3.5.1). Furthermore, successful secondary virus infections, here monitored by viral marker gene expression, were demonstrated to be dependent on viral concentrations of the first agent: (i) at low MOIs of the first virus, cells were infected to a greater extent by the second virus; (ii) at higher MOIs of the first virus, it was the other way round and cells were already occupied by the first agent. We called this phenomenon “viral competition” and considered a kind of superinfection exclusion as responsible reason.

By performing our Keyence trial (section 3.5.2), i.e., applying real-time All-in-One BZ-9000 fluorescence microscope, it was possible to monitor planar cell growth and, more important, real-time infection of singular cells. Although the majority of sequentially infected cells illuminated either red or green, some cells were double-infected by VACV and GFP, visualized by a yellow glow. To our knowledge, this is the first report of “viral competition” concerning heterologous superinfection exclusion in regards to VACV and MeV.

However, since analysis of SRB assays (sections 3.2.1 and 3.2.2) revealed that remnant cells were reduced more effectively when being infected sequentially, “viral competition” did not hinder the oncolytic potential of these coinfection trials.

4.7 **Western blot analysis verifies the observed phenomenon of "viral competition": Viral protein expression is altered in double-infected cells.**

Western blot analysis was performed to confirm the expression of viral proteins upon combinatorial treatment with VACV and MeV, as well as to further investigate the observed phenomenon of "viral competition".

In order to study changes of cell mass over the course of the entire incubation period, we abstained from equalization of the protein content by Bradford assay.

As demonstrated in section 3.6, both single- and double-infected ACHN cells expressed VACV and MeV proteins. From 24 to 96 hpi, alterations of the protein content of infected cells suggested proceeding cell loss due to virus infection and following oncolysis. Especially VACV-infected cells exhibited reduced cell masses at advanced time points. Thus, a prior finding of the SRB assay was confirmed: cell death of double-infected cells is most contingent upon VACV infection.

In accordance to our findings, Le Boeuf *et al.* indicated that tumor cell infection by both candidates was mainly triggered by VACV (Le Boeuf *et al*, 2010). At 96 hpi, ß-galactosidase and Vaccinia protein expression decreased relative to levels reached at 72 hpi. Since viral proteins were extracted from cell lysates, this observation was no surprise: at 72 and even more at 96 hpi, cell masses were erased almost completely; consequently, the breeding ground for production of new virions was diminished. Nevertheless, N-protein and GFP were highly expressed until 96 hpi. Thus, ACHN cells survived MeV sole infection until the end of the experiment. In accordance with this finding, N. Mayer demonstrated survival of MeV single-infected sarcoma cells until 144 hpi (Mayer, 2014).

Concerning the phenomenon of "viral competition", we observed that viral proteins were expressed higher in single- than in double-infected cells at 72 and 96 hpi. At these advanced time points, cells were almost completely infected by both viral agents, which might have triggered "viral competition" regarding uninfected cells. We suppose that the described phenomenon of heterologous

superinfection exclusion contributed to this finding. Although other groups barely applied western blot analysis to follow up superinfection exclusion, Tscherne *et al.* indicated reduced protein levels upon secondary virus infection with HCV (Tscherne *et al*, 2007).

5 Perspectives

VACV- and MeV-based virotherapeutics have already proved to be safe and effective weapons in the fight against various cancer entities. In this thesis we investigated whether a combined application of VACV GLV-1h254 and MeV-GFP *in vitro* would overcome limiting barriers to a successful treatment of highly resistant human tumor cell lines.

In the course of the work we encountered methodical difficulties referring to cell viability assays. With respect to our elaborated findings, we recommend to determine suitable initial cell counts for each *in vitro* experiment by SRB assay. This suggestion was also made by Vichai and Kirtikara, who explain the procedure in detail (Vichai & Kirtikara, 2006). Thus, logarithmic cell growth of controls will be guaranteed until the end of the experiment, while monolayers are allowed to grow subconfluent. Although Skehan *et al.* reported about possible modifications of the SRB assay to fix cell aggregates, we suggest to apply this method only to firmly adhered cells (Skehan *et al*, 1990).

Furthermore, we emphasize the importance of comparative trials. Thus, results are confirmed and, moreover, become accessible for further interpretation, demonstrated in this thesis by comparison of the SRB and MTT data. In 1992, Sasaki *et al.* introduced another cytotoxicity assay that measures the activity of a cytosolic enzyme, the lactate dehydrogenase (LDH), which is released upon cell death (Sasaki *et al*, 1992). While the SRB and MTT assay mirror the reduction of cell mass and metabolic activity, respectively, the LDH method actually indicates cytolysis. Accordingly, we propose to supplement the LDH assay in further studies.

Another exciting side show of this thesis is the described phenomenon of “viral competition”. As explicated before, the majority of sequentially infected cells exhibited sole infection, nevertheless, singular cells were coinfected by both virus constructs. In 1964, Parkman *et al.* indicated that rubella virus interfered with heterologous virus constructs like enteroviruses, mumps, influenza, para-influenza and rubeola (Parkman *et al*, 1964). Nevertheless, research primarily focuses on homologous superinfection exclusion. Further studies should pursue

the here described phenomenon and its underlying mechanism applying additional methods as well as other oncolytic virus platforms.

Moreover, the survival of MeV single-infected ACHN cells until 96 hpi (section 3.6) attracted our interest. In a previous paragraph, we argued that the experimental settings of cytotoxicity assays must be kept consistent to obtain reliable results. Consequently, we do not advise to simply stretch time frames of such assays, but apply another method to detect potential delayed oncolytic effects.

Primary resistance phenomenon of human tumor cell lines towards oncolytic virotherapy remains a major hurdle to a successful application of this novel approach. In this thesis, we ascertained that sequential infections with VACV GLV-1h254 and MeV-GFP were superior to single infections. Best results were achieved, when VACV was applied first, while differences between time points of secondary virus infection were negligible. Admittedly, we did not receive any hint of synergistic interaction between the applied oncolytic viruses, and additive effects were only marginal. Nevertheless, it might be of some interest to further explore the molecular mechanisms of the described viral interactions and their impact on IFN signaling.

In addition, studies should investigate the potential capacity of other “oncolytic tag-teams” by sequential infection of a wide range of tumor entities (Le Boeuf & Bell, 2010). To increase the occurrence of synergistic interaction, team partners must be matched thoroughly. Careful evaluation of each other´s benefits and malfunctions will be indispensable in order to develop well-fitting counterparts.

Regarding the complex interactions between the host immune response and oncolytic viruses, Tysome *et al.* highlighted the importance to apply immunocompetent tumor models (Tysome *et al*, 2012).

6 Summary

Oncolytic viruses such as VACV and MeV are live, self-replicating biological anticancer agents, which have supplemented established therapies for quite a while (Bell, 2007). While sparing normal tissue, OVs destroy cancer cells by direct tumor cell lysis and the establishment of a host antitumor immune response (Kaufman *et al*, 2015). Nevertheless, primary resistance phenomenon to this novel approach hinders its widespread application.

In 2010, Le Boeuf *et al.* published a promising attempt by demonstrating synergistic interaction between a VACV and a VSV strain (Le Boeuf *et al*, 2010). MeV and VACV proved to be safe, and moreover, convinced in some cases with outstanding oncolytic efficacy. On the basis of highly resistant tumor cells, we here investigated *in vitro* whether Le Boeuf´s findings were reproducible for VACV GLV-1h254 and vaccine-based measles construct MeV-GFP. In accordance with the researchers, we supposed that partial responsiveness to IFN could have led to a reduced susceptibility of resistant tumor cells to oncolytic virotherapy (Le Boeuf *et al*, 2010). With GLV-1h254, however, we aimed to suppress the upcoming host antivirus immune reaction.

Prior to double infection trials, it was necessary to determined suitable virus concentrations of both vectors for each cell line. We noticed that every cell line required different plating densities to reach confluence and, moreover, that cell density influenced survival of uninfected controls as well as virus spreading.

After determination of threshold MOIs, we examined different orders of virus treatment and time points for secondary virus infection in double infection trials. SRB assay analysis ensured the superiority of the combinatorial treatment regime. Thus, sequential infections applying VACV prior to MeV-GFP achieved best results, while differences between time points of secondary virus infection had only minor impact. Admittedly, synergistic interaction was not observed and additive effects were limited.

Naturally, our *in vitro* setting is unable to reflect the complex interactions between oncolytic agents and the host immune response. Thus, we recommend to pursue the here described findings in an immunocompetent tumor model.

This procedure albeit is hindered by the highly restricted host range of measles viruses, which only allows replicative infections in primates and humans.

Sequential infections illustrated a phenomenon called “viral competition”. The majority of double-infected cells was either infected by one or the other, but not by both virus constructs simultaneously. The Keyence microscope was applied to examine this finding in detail. Although most sequentially infected cells exhibited sole infection, some of them glowed yellow, which indicated coinfection by VACV and MeV-GFP. Further trials applying SRB assay and western blot ensured that “viral competition” did not limit the oncolytic potential of the combinatorial treatment regime. However, further studies should focus on the underlying mechanism of the here described phenomenon and its occurrence with other oncolytic virus platforms.

7 Zusammenfassung

Onkolytische Viren wie beispielsweise Vaccinia- und Masernimpfviren sind lebende, sich selbst replizierende biologische Krebsmedikamente, die schon seit einigen Jahren zusammen mit etablierten Therapien eingesetzt werden (Bell, 2007). Während normales Gewerbe geschont wird, zerstören onkolytische Viren Krebszellen zielgerichtet durch Tumorlyse sowie durch die Etablierung einer wirtseigenen, gerichteten Immunreaktion gegen die malignen Zellen (Kaufman *et al*, 2015). Primäre Resistenzphänomene hochresistenter Tumorzellen verhindern zurzeit einen flächendeckenden Einsatz dieser neuen Therapeutika.

Im Jahr 2010 präsentierten Le Boeuf *et al.* einen vielversprechenden Ansatz (Le Boeuf *et al*, 2010). Durch den kombinierten Einsatz von Vaccinia und Vesicular stomatitis Viren konnte ein Synergismus erreicht, und dadurch primäre Resistenzen überwunden werden (Le Boeuf *et al*, 2010). Masern- und Vacciniaviren haben bewiesen, dass sie nicht nur sicher sind, sondern in einigen Fällen auch äußerst effizient Tumorzellen bekämpfen.

Auf der Grundlage hochresistenter menschlicher Tumorzellen haben wir in dieser Arbeit untersucht, ob Le Boeufs Erkenntnisse auf das Vacciniavirus GLV-1h254 und das Masernimpfvirus MeV-GFP übertragbar sind. In Übereinstimmung mit den Forschern vermuteten wir, dass eine noch in Teilen bestehende Interferonantwort der Tumorzellen für das Auftreten primärer Virotherapie-Resistenzen verantwortlich sein könnte (Le Boeuf *et al*, 2010). Mit dem Einsatz des Vacciniavirus GLV-1h254 versuchten wir nun die gegen beide Viren gerichtete Immunreaktion zu unterbinden.

Bevor mit den Doppelinfektionen begonnen werden konnte, war es nötig die für jede Tumorzelllinie passende Konzentration beider Viruskonstrukte zu bestimmen. Dabei fiel auf, dass jede Zelllinie unterschiedliche Auslegezellzahlen benötigte um Konfluenz zu erreichen, und mehr noch, dass dies sowohl das Überleben nicht infizierter Kontrollen als auch die Virusausbreitung beeinflusste.

Nachdem die passenden Virusmengen bestimmt worden waren, untersuchten wir in Doppelinfektionsversuchen unterschiedliche Reihenfolgen und Zeitpunkte der Applikation der beiden Viruskonstrukte.

Mit Hilfe des SRB Assays konnten wir die Überlegenheit eines kombinierten Verfahrens gegenüber Einzelinfektionen herausstellen. Doppelinfektionen mit Vaccinia als erstem Virus erzielten dabei die besten Ergebnisse, während der Zeitpunkt der Zweitinfektion die Resultate nur unwesentlich beeinflusste. Synergismus konnte dennoch nicht bestätigt werden, und auch die beobachteten additiven Effekte fielen nur gering aus.

Naturgegeben ist unser *in vitro*-Setting nicht ausreichend um die komplexen Zusammenhänge zwischen onkolytischer Virotherapie und wirtseigener Immunreaktion zu bewerten. Wir empfehlen daher die hier erzielten Ergebnisse in einem immunkompetentem Tiermodel nachzuvollziehen. Zugegebenermaßen wird dieser Ansatz dadurch erschwert werden, dass Masernviren ausschließlich Primaten- und menschliche Zellen infizieren und sich in ihnen vermehren können.

Während der Doppelinfektionsversuche beobachteten wir ein Phänomen, das wir „viralen Wettkampf“ tauften. Die Mehrzahl der doppelinfizierten Zellen war entweder vom ersten oder zweiten Viruskonstrukt infiziert, nicht jedoch von beiden gleichzeitig. Das Keyence Mikroskop half diese Beobachtung weiter zu verfolgen. Obwohl sich die meisten Zellen als einzelinfiziert zeigten, leuchteten einige wenige gelb auf und wurden somit als koinfiziert bewertet. Nachfolgende Analysen unter Verwendung des SRB Assays und Western Blot stellten sicher, dass der „virale Wettkampf“ nicht zu einer eingeschränkten Effektivität der Doppelinfektionen führte. Zukünftige Forschung sollte sich auf die zugrundeliegenden Mechanismen des hier beschriebenen Phänomens und ihr mögliches Auftreten bei weiteren onkolytischen Viren konzentrieren.

8 References

Adelfinger M, Bessler S, Frentzen A, Cecil A, Langbein-Laugwitz J, Gentschev I, Szalay AA (2015) Preclinical Testing Oncolytic Vaccinia Virus Strain GLV-5b451 Expressing an Anti-VEGF Single-Chain Antibody for Canine Cancer Therapy. *Viruses* **7**(7)**:** 4075-92

Alemany R (2013) Viruses in cancer treatment. *Clinical & translational oncology : official publication of the Federation of Spanish Oncology Societies and of the National Cancer Institute of Mexico* **15**(3)**:** 182-8

Anderson BD, Nakamura T, Russell SJ, Peng KW (2004) High CD46 receptor density determines preferential killing of tumor cells by oncolytic measles virus. *Cancer research* **64**(14)**:** 4919-26

Andtbacka RH, Kaufman HL, Collichio F, Amatruda T, Senzer N, Chesney J, Delman KA, Spitler LE, Puzanov I, Agarwala SS, Milhem M, Cranmer L, Curti B, Lewis K, Ross M, Guthrie T, Linette GP, Daniels GA, Harrington K, Middleton MR, Miller WH, Jr., Zager JS, Ye Y, Yao B, Li A, Doleman S, VanderWalde A, Gansert J, Coffin RS (2015) Talimogene Laherparepvec Improves Durable Response Rate in Patients With Advanced Melanoma. *Journal of clinical oncology : official journal of the American Society of Clinical Oncology* **33**(25)**:** 2780-8

Appleyard G, Hapel AJ, Boulter EA (1971) An antigenic difference between intracellular and extracellular rabbitpox virus. *The Journal of general virology* **13**(1)**:** 9-17

Asada T (1974) Treatment of human cancer with mumps virus. *Cancer* **34**(6)**:** 1907-28

Ascierto ML, Worschech A, Yu Z, Adams S, Reinboth J, Chen NG, Pos Z, Roychoudhuri R, Di Pasquale G, Bedognetti D, Uccellini L, Rossano F, Ascierto PA, Stroncek DF, Restifo NP, Wang E, Szalay AA, Marincola FM (2011) Permissivity of the NCI-60 cancer cell lines to oncolytic Vaccinia Virus GLV-1h68. *BMC cancer* **11:** 451

Baer A, Kehn-Hall K (2014) Viral concentration determination through plaque assays: using traditional and novel overlay systems. *Journal of visualized experiments : JoVE*(93)**:** e52065

Bell JC (2007) Oncolytic viruses: what's next? *Current cancer drug targets* **7**(2)**:** 127-31

Berchtold S, Lampe J, Weiland T, Smirnow I, Schleicher S, Handgretinger R, Kopp HG, Reiser J, Stubenrauch F, Mayer N, Malek NP, Bitzer M, Lauer UM (2013) Innate immune defense defines susceptibility of sarcoma cells to measles vaccine virus-based oncolysis. *Journal of virology* **87**(6)**:** 3484-501

Bierman HR, Crile DM, Dod KS, Kelly KH, Petrakis NI, White LP, Shimkin MB (1953) Remissions in leukemia of childhood following acute infectious disease. Staphylococcus and streptococcus, varicella, and feline panleukopenias. *Cancer* **6**(3)**:** 591-605

Blechacz B, Splinter PL, Greiner S, Myers R, Peng KW, Federspiel MJ, Russell SJ, LaRusso NF (2006) Engineered measles virus as a novel oncolytic viral therapy system for hepatocellular carcinoma. *Hepatology (Baltimore, Md)* **44**(6)**:** 1465-77

Bluming A, Ziegler J (1971) Originally published as Volume 2, Issue 7715 REGRESSION OF BURKITT'S LYMPHOMA IN ASSOCIATION WITH MEASLES INFECTION. *The Lancet* **298**(7715)**:** 105-106

Boone C, Blackman K, Brandchaft P (1971) Tumour immunity induced in mice with cell-free homogenates of influenza virus-infected tumour cells. *Nature* **231**(5300)**:** 265-6

Bosset JF, Collette L, Calais G, Mineur L, Maingon P, Radosevic-Jelic L, Daban A, Bardet E, Beny A, Ollier JC (2006) Chemotherapy with preoperative radiotherapy in rectal cancer. *The New England journal of medicine* **355**(11)**:** 1114-23

Bukowska B, Gajek A, Marczak A (2015) Two drugs are better than one. A short history of combined therapy of ovarian cancer. *Contemporary oncology (Poznan, Poland)* **19**(5)**:** 350-3

Buller RM, Smith GL, Cremer K, Notkins AL, Moss B (1985) Decreased virulence of recombinant vaccinia virus expression vectors is associated with a thymidine kinase-negative phenotype. *Nature* **317**(6040)**:** 813-5

Buller RML, Chakrabarti S, Moss B, Fredricksont T (1988) Cell proliferative response to vaccinia virus is mediated by VGF. *Virology* **164**(1)**:** 182-192

Burnette WN (1981) "Western blotting": electrophoretic transfer of proteins from sodium dodecyl sulfate--polyacrylamide gels to unmodified nitrocellulose and radiographic detection with antibody and radioiodinated protein A. *Analytical biochemistry* **112**(2)**:** 195-203

Capitanio U, Montorsi F (2016) Renal cancer. *Lancet (London, England)* **387**(10021)**:** 894-906

Cassel WA, Murray DR (1992) A ten-year follow-up on stage II malignant melanoma patients treated postsurgically with Newcastle disease virus oncolysate. *Medical oncology and tumor pharmacotherapy* **9**(4)**:** 169-71

Cattaneo R, Miest T, Shashkova EV, Barry MA (2008) Reprogrammed viruses as cancer therapeutics: targeted, armed and shielded. *Nature reviews Microbiology* **6**(7)**:** 529-40

Chauffert B, Dimanche-Boitrel MT, Garrido C, Ivarsson M, Martin M, Martin F, Solary E (1998) New insights into the kinetic resistance to anticancer agents. *Cytotechnology* **27**(1-3)**:** 225-35

Chen NG, Yu YA, Zhang Q, Szalay AA (2011) Replication efficiency of oncolytic vaccinia virus in cell cultures prognosticates the virulence and antitumor efficacy in mice. *Journal of translational medicine* **9:** 164

Chiocca EA, Rabkin SD (2014) Oncolytic viruses and their application to cancer immunotherapy. *Cancer immunology research* **2**(4)**:** 295-300

Claus C, Tzeng WP, Liebert UG, Frey TK (2007) Rubella virus-induced superinfection exclusion studied in cells with persisting replicons. *The Journal of general virology* **88**(Pt 10)**:** 2769-73

Colamonici OR, Domanski P, Sweitzer SM, Larner A, Buller RM (1995) Vaccinia virus B18R gene encodes a type I interferon-binding protein that blocks interferon alpha transmembrane signaling. *The Journal of biological chemistry* **270**(27)**:** 15974-8

Cunningham D, Atkin W, Lenz HJ, Lynch HT, Minsky B, Nordlinger B, Starling N (2010) Colorectal cancer. *Lancet (London, England)* **375**(9719)**:** 1030-47

Dengina N, Tsimafeyeu I, Mitin T (2017) Current Role of Radiotherapy for Renal-Cell Carcinoma: Review. *Clinical genitourinary cancer* **15**(2)**:** 183-187

DePace N (1912) Rabies virus treatment of cervical cancer. *Ginecologia* **9:** 82

Dimanche-Boitrel MT, Garrido C, Chauffert B (1993) Kinetic resistance to anticancer agents. *Cytotechnology* **12**(1-3)**:** 347-56

Doceul V, Hollinshead M, van der Linden L, Smith GL (2010) Repulsion of superinfecting virions: a mechanism for rapid virus spread. *Science (New York, NY)* **327**(5967)**:** 873-876

Dock G (1904) THE INFLUENCE OF COMPLICATING DISEASES UPON LEUKAEMIA.*. *The American Journal of the Medical Sciences* **127**(4)**:** 563-592

Dorig RE, Marcil A, Chopra A, Richardson CD (1993) The human CD46 molecule is a receptor for measles virus (Edmonston strain). *Cell* **75**(2)**:** 295-305

Downie A (1939) The immunological relationship of the virus of spontaneous cowpox to vaccinia virus. *British journal of experimental pathology* **20**(2)**:** 158

Downs-Canner S, Guo ZS, Ravindranathan R, Breitbach CJ, O'Malley ME, Jones HL, Moon A, McCart JA, Shuai Y, Zeh HJ, Bartlett DL (2016) Phase 1 Study of Intravenous Oncolytic Poxvirus (vvDD) in Patients With Advanced Solid Cancers. *Molecular therapy : the journal of the American Society of Gene Therapy* **24**(8)**:** 1492-501

Eaton BT (1979) Heterologous interference in Aedes albopictus cells infected with alphaviruses. *Journal of virology* **30**(1)**:** 45-55

Elde NC, Child SJ, Geballe AP, Malik HS (2009) Protein kinase R reveals an evolutionary model for defeating viral mimicry. *Nature* **457**(7228)**:** 485-9

Enders JF, Peebles TC (1954) Propagation in tissue cultures of cytopathogenic agents from patients with measles. *Proceedings of the Society for Experimental Biology and Medicine Society for Experimental Biology and Medicine (New York, NY)* **86**(2)**:** 277-86

Fakih MG (2015) Metastatic colorectal cancer: current state and future directions. *Journal of clinical oncology : official journal of the American Society of Clinical Oncology* **33**(16)**:** 1809-24

Fang Y, Sullivan R, Graham CH (2007) Confluence-dependent resistance to doxorubicin in human MDA-MB-231 breast carcinoma cells requires hypoxia-inducible factor-1 activity. *Experimental cell research* **313**(5)**:** 867-77

Fenner F (1993) Smallpox: emergence, global spread, and eradication. *History and philosophy of the life sciences***:** 397-420

Ferlay J, Soerjomataram I, Dikshit R, Eser S, Mathers C, Rebelo M, Parkin DM, Forman D, Bray F (2015) Cancer incidence and mortality worldwide: sources, methods and major patterns in GLOBOCAN 2012. *International journal of cancer* **136**(5)**:** E359-86

Ferlay J, Soerjomataram I, Ervik M, Dikshit R, Eser S, Mathers C, Rebelo M, Parkin DM, Forman D, Bray F (2013) GLOBOCAN 2012 v 1.0, Cancer Incidence and Mortality Worldwide: IARC CancerBase No. 11 [Internet]. Lyon, France: International Agency for Research on Cancer. Available from: http://globocan.iarc.fr, accessed on 14/09/2017.

Fishelson Z, Donin N, Zell S, Schultz S, Kirschfink M (2003) Obstacles to cancer immunotherapy: expression of membrane complement regulatory proteins (mCRPs) in tumors. *Molecular immunology* **40**(2-4)**:** 109-23

Fontana JM, Bankamp B, Rota PA (2008) Inhibition of interferon induction and signaling by paramyxoviruses. *Immunological reviews* **225:** 46-67

Frezza AM, Stacchiotti S, Gronchi A (2017) Systemic treatment in advanced soft tissue sarcoma: what is standard, what is new. *BMC medicine* **15**(1)**:** 109

Galanis E, Atherton PJ, Maurer MJ, Knutson KL, Dowdy SC, Cliby WA, Haluska P, Jr., Long HJ, Oberg A, Aderca I, Block MS, Bakkum-Gamez J, Federspiel MJ, Russell SJ, Kalli KR, Keeney G, Peng KW, Hartmann LC (2015) Oncolytic measles virus expressing the sodium iodide symporter to treat drug-resistant ovarian cancer. *Cancer research* **75**(1)**:** 22-30

Galanis E, Hartmann LC, Cliby WA, Long HJ, Peethambaram PP, Barrette BA, Kaur JS, Haluska PJ, Jr., Aderca I, Zollman PJ, Sloan JA, Keeney G, Atherton PJ, Podratz KC, Dowdy SC, Stanhope CR, Wilson TO, Federspiel MJ, Peng KW, Russell SJ (2010) Phase I trial of intraperitoneal administration of an oncolytic measles virus strain engineered to express carcinoembryonic antigen for recurrent ovarian cancer. *Cancer research* **70**(3)**:** 875-82

Garber K (2006) China approves world's first oncolytic virus therapy for cancer treatment. *Journal of the National Cancer Institute* **98**(5)**:** 298-300

Garrido C, Chauffert B, Pinard D, Tibaut F, Genne P, Assem M, Dimanche-Boitrel MT (1995) Circumvention of confluence-dependent resistance in a human multi-drug-resistant colon-cancer cell line. *International journal of cancer* **61**(6)**:** 873-9

Gomella LG, Mastrangelo MJ, McCue PA, Maguire HJ, Mulholland SG, Lattime EC (2001) Phase i study of intravesical vaccinia virus as a vector for gene therapy of bladder cancer. *The Journal of urology* **166**(4)**:** 1291-5

Griffin D (2001) Measles Virus. In *Fields Virology*, 4th edn, Chapter 44, pp 1401 – 1428. Philadelphia, PA: Lippincott Williams & Wilkins

Griffin DE, Pan CH, Moss WJ (2008) Measles vaccines. *Frontiers in bioscience : a journal and virtual library* **13:** 1352-70

Grote D, Russell SJ, Cornu TI, Cattaneo R, Vile R, Poland GA, Fielding AK (2001) Live attenuated measles virus induces regression of human lymphoma xenografts in immunodeficient mice. *Blood* **97**(12)**:** 3746-54

Guo ZS, Naik A, O'Malley ME, Popovic P, Demarco R, Hu Y, Yin X, Yang S, Zeh HJ, Moss B, Lotze MT, Bartlett DL (2005) The enhanced tumor selectivity of an oncolytic vaccinia lacking the host range and antiapoptosis genes SPI-1 and SPI-2. *Cancer research* **65**(21)**:** 9991-8

Hafner M, Niepel M, Chung M, Sorger PK (2016) Growth rate inhibition metrics correct for confounders in measuring sensitivity to cancer drugs. *Nature methods* **13**(6)**:** 521-7

Hanahan D, Weinberg RA (2011) Hallmarks of cancer: the next generation. *Cell* **144**(5)**:** 646-74

Harrison SC, Alberts B, Ehrenfeld E, Enquist L, Fineberg H, McKnight SL, Moss B, O'Donnell M, Ploegh H, Schmid SL, Walter KP, Theriot J (2004) Discovery of antivirals against smallpox. *Proceedings of the National Academy of Sciences of the United States of America* **101**(31)**:** 11178-92

Haselsberger K, Peterson DC, Thomas DG, Darling JL (1996) Assay of anticancer drugs in tissue culture: comparison of a tetrazolium-based assay and a protein binding dye assay in short-term cultures derived from human malignant glioma. *Anti-cancer drugs* **7**(3)**:** 331-8

Hastie E, Grdzelishvili VZ (2012) Vesicular stomatitis virus as a flexible platform for oncolytic virotherapy against cancer. *The Journal of general virology* **93**(Pt 12)**:** 2529-45

He S, Li P, Chen CH, Bakst RL, Chernichenko N, Yu YA, Chen N, Szalay AA, Yu Z, Fong Y, Wong RJ (2012) Effective oncolytic vaccinia therapy for human sarcomas. *The Journal of surgical research* **175**(2)**:** e53-60

Heinzerling L, Kunzi V, Oberholzer PA, Kundig T, Naim H, Dummer R (2005) Oncolytic measles virus in cutaneous T-cell lymphomas mounts antitumor immune responses in vivo and targets interferon-resistant tumor cells. *Blood* **106**(7)**:** 2287-94

Heo J, Reid T, Ruo L, Breitbach CJ, Rose S, Bloomston M, Cho M, Lim HY, Chung HC, Kim CW, Burke J, Lencioni R, Hickman T, Moon A, Lee YS, Kim MK, Daneshmand M, Dubois K, Longpre L, Ngo M, Rooney C, Bell JC, Rhee BG, Patt R, Hwang TH, Kirn DH (2013) Randomized dose-finding clinical trial of oncolytic immunotherapeutic vaccinia JX-594 in liver cancer. *Nature medicine* **19**(3)**:** 329-36

Hoster HA, Zanes RP, Jr., Von Haam E (1949) Studies in Hodgkin's syndrome; the association of viral hepatitis and Hodgkin's disease; a preliminary report. *Cancer research* **9**(8)**:** 473-80

Huang C, Kolokoltsova OA, Yun NE, Seregin AV, Poussard AL, Walker AG, Brasier AR, Zhao Y, Tian B, de la Torre JC, Paessler S (2012) Junin virus infection activates the type I interferon pathway in a RIG-I-dependent manner. *PLoS neglected tropical diseases* **6**(5)**:** e1659

Huang C, Kolokoltsova OA, Yun NE, Seregin AV, Ronca S, Koma T, Paessler S (2015) Highly Pathogenic New World and Old World Human Arenaviruses Induce Distinct Interferon Responses in Human Cells. *Journal of virology* **89**(14)**:** 7079-88

Jager E, Karbach J, Gnjatic S, Neumann A, Bender A, Valmori D, Ayyoub M, Ritter E, Ritter G, Jager D, Panicali D, Hoffman E, Pan L, Oettgen H, Old LJ, Knuth A (2006) Recombinant vaccinia/fowlpox NY-ESO-1 vaccines induce both humoral and cellular NY-ESO-1-specific immune responses in cancer patients. *Proceedings of the National Academy of Sciences of the United States of America* **103**(39)**:** 14453-8

Jenner E (1800) *An inquiry into the causes and effects of the variolae vaccinae: a disease discovered in some of the western counties of England, particularly Gloucestershire, and known by the name of the cow pox*: printed, for the author, by Sampson Low...; and sold by Law... and Murray and Hihghley

Jiang H, McCormick F, Lang FF, Gomez-Manzano C, Fueyo J (2006) Oncolytic adenoviruses as antiglioma agents. *Expert review of anticancer therapy* **6**(5)**:** 697-708

Jones RP, Hamann S, Malik HZ, Fenwick SW, Poston GJ, Folprecht G (2014) Defined criteria for resectability improves rates of secondary resection after systemic therapy for liver limited metastatic colorectal cancer. *European journal of cancer (Oxford, England : 1990)* **50**(9)**:** 1590-601

Kaji H, Sendo F, Shirai T, Saito H, Kodama T (1969) [Immunological therapy of rat tumors by the tumor cells infected by Friend virus]. *Saishin igaku Modern medicine* **24**(6)**:** 1329-33

Kanesa-thasan N, Smucny JJ, Hoke CH, Marks DH, Konishi E, Kurane I, Tang DB, Vaughn DW, Mason PW, Shope RE (2000) Safety and immunogenicity of NYVAC-JEV and ALVAC-JEV attenuated recombinant Japanese encephalitis virus--poxvirus vaccines in vaccinia-nonimmune and vaccinia-immune humans. *Vaccine* **19**(4-5)**:** 483-91

Kärber G (1931) Beitrag zur kollektiven Behandlung pharmakologischer Reihenversuche. *Naunyn-Schmiedebergs Archiv für experimentelle pathologie und pharmakologie* **162**(4)**:** 480-483

Karpf AR, Lenches E, Strauss EG, Strauss JH, Brown DT (1997) Superinfection exclusion of alphaviruses in three mosquito cell lines persistently infected with Sindbis virus. *Journal of virology* **71**(9)**:** 7119-23

Kasi PM, Hubbard JM, Grothey A (2015) Selection of biologics for patients with metastatic colorectal cancer: the role of predictive markers. *Expert review of gastroenterology & hepatology* **9**(3)**:** 273-6

Kaufman HL, Kohlhapp FJ, Zloza A (2015) Oncolytic viruses: a new class of immunotherapy drugs. *Nature reviews Drug discovery* **14**(9)**:** 642-62

Ke N, Wang X, Xu X, Abassi YA (2011) The xCELLigence system for real-time and label-free monitoring of cell viability. *Methods in molecular biology (Clifton, NJ)* **740:** 33-43

Kelly E, Russell SJ (2007) History of oncolytic viruses: genesis to genetic engineering. *Molecular therapy : the journal of the American Society of Gene Therapy* **15**(4)**:** 651-9

Kim JH, Oh JY, Park BH, Lee DE, Kim JS, Park HE, Roh MS, Je JE, Yoon JH, Thorne SH, Kirn D, Hwang TH (2006) Systemic armed oncolytic and immunologic therapy for cancer with JX-594, a targeted poxvirus expressing GM-CSF. *Molecular therapy : the journal of the American Society of Gene Therapy* **14**(3)**:** 361-70

Kirn DH, Thorne SH (2009) Targeted and armed oncolytic poxviruses: a novel multi-mechanistic therapeutic class for cancer. *Nature reviews Cancer* **9**(1)**:** 64-71

Kirn DH, Wang Y, Le Boeuf F, Bell J, Thorne SH (2007) Targeting of interferon-beta to produce a specific, multi-mechanistic oncolytic vaccinia virus. *PLoS medicine* **4**(12)**:** e353

Kumagai T, Shimizu T, Ikeda S, Matumoto M (1961) A new in vitro method (END) for detection and measurement of hog cholera virus and its antibody by means of effect of HC virus on Newcastle disease virus in swine tissue culture. I. Establishment of standard procedure. *Journal of immunology (Baltimore, Md : 1950)* **87:** 245-56

Laemmli UK (1970) Cleavage of structural proteins during the assembly of the head of bacteriophage T4. *Nature* **227**(5259)**:** 680-5

Laliberte JP, Moss B (2014) A novel mode of poxvirus superinfection exclusion that prevents fusion of the lipid bilayers of viral and cellular membranes. *Journal of virology* **88**(17)**:** 9751-68

Lamb RA, Kolakofsky D (2001) Paramyxoviridae: The viruses and their replication. In *Fields Virology*, 4th edn, Chapter 41, pp 1305 – 1340. Philadelphia, PA: Lippincott Williams & Wilkins

Lane JM, Ruben FL, Neff JM, Millar JD (1969) Complications of smallpox vaccination, 1968. *The New England journal of medicine* **281**(22)**:** 1201-8

Lange S, Lampe J, Bossow S, Zimmermann M, Neubert W, Bitzer M, Lauer UM (2013) A novel armed oncolytic measles vaccine virus for the treatment of cholangiocarcinoma. *Human gene therapy* **24**(5)**:** 554-64

Le Boeuf F, Bell JC (2010) United virus: the oncolytic tag-team against cancer! *Cytokine & growth factor reviews* **21**(2-3)**:** 205-11

Le Boeuf F, Diallo JS, McCart JA, Thorne S, Falls T, Stanford M, Kanji F, Auer R, Brown CW, Lichty BD, Parato K, Atkins H, Kirn D, Bell JC (2010) Synergistic interaction between oncolytic viruses augments tumor killing. *Molecular therapy : the journal of the American Society of Gene Therapy* **18**(5)**:** 888-95

Ledford H (2015) Cancer-fighting viruses win approval. *Nature* **526**(7575)**:** 622-3

Li J, Hu H, Yu Q, Diel DG, Li DS, Miller PJ (2012) Generation and characterization of a recombinant Newcastle disease virus expressing the red fluorescent protein for use in co-infection studies. *Virology journal* **9:** 227

Lindenmann J, Klein PA (1967) Viral oncolysis: increased immunogenicity of host cell antigen associated with influenza virus. *The Journal of experimental medicine* **126**(1)**:** 93-108

Liu S, Ruban L, Wang Y, Zhou Y, Nesbeth DN (2017) Establishing elements of a synthetic biology platform for Vaccinia virus production: BioBrick design, serum-free virus production and microcarrier-based cultivation of CV-1 cells. *Heliyon* **3**(2)**:** e00238

Lopez MV, Viale DL, Cafferata EG, Bravo AI, Carbone C, Gould D, Chernajovsky Y, Podhajcer OL (2009) Tumor associated stromal cells play a critical role on the outcome of the oncolytic efficacy of conditionally replicative adenoviruses. *PloS one* **4**(4)**:** e5119

Magge D, Guo ZS, O'Malley ME, Francis L, Ravindranathan R, Bartlett DL (2013) Inhibitors of C5 complement enhance vaccinia virus oncolysis. *Cancer gene therapy* **20**(6)**:** 342-50

Mahmood T, Yang PC (2012) Western blot: technique, theory, and trouble shooting. *North American journal of medical sciences* **4**(9)**:** 429-34

Malkin AJ, McPherson A, Gershon PD (2003) Structure of intracellular mature vaccinia virus visualized by in situ atomic force microscopy. *Journal of virology* **77**(11)**:** 6332-40

Martuza RL, Malick A, Markert JM, Ruffner KL, Coen DM (1991) Experimental therapy of human glioma by means of a genetically engineered virus mutant. *Science (New York, NY)* **252**(5007)**:** 854-6

Mastrangelo MJ, Maguire HC, Jr., Eisenlohr LC, Laughlin CE, Monken CE, McCue PA, Kovatich AJ, Lattime EC (1999) Intratumoral recombinant GM-CSF-encoding virus as gene therapy in patients with cutaneous melanoma. *Cancer gene therapy* **6**(5)**:** 409-22

Mayer N (2014) Difficult to treat cancer entities such as sarcomas and

peritoneal carcinosis challenged by suicide genearmed virotherapeutic vector systems MeV and VACV. In *Tübingen. Univ., Diss., 2014* p 134

McCart JA, Ward JM, Lee J, Hu Y, Alexander HR, Libutti SK, Moss B, Bartlett DL (2001) Systemic cancer therapy with a tumor-selective vaccinia virus mutant lacking thymidine kinase and vaccinia growth factor genes. *Cancer research* **61**(24)**:** 8751-7

McDonald CJ, Erlichman C, Ingle JN, Rosales GA, Allen C, Greiner SM, Harvey ME, Zollman PJ, Russell SJ, Galanis E (2006) A measles virus vaccine strain derivative as a novel oncolytic agent against breast cancer. *Breast cancer research and treatment* **99**(2)**:** 177-84

Melcher A, Parato K, Rooney CM, Bell JC (2011) Thunder and lightning: immunotherapy and oncolytic viruses collide. *Molecular therapy : the journal of the American Society of Gene Therapy* **19**(6)**:** 1008-16

Mell LK, Brumund KT, Daniels GA, Advani SJ, Zakeri K, Wright ME, Onyeama SJ, Weisman RA, Sanghvi PR, Martin PJ, Szalay AA (2017) PHASE I TRIAL OF INTRAVENOUS ONCOLYTIC VACCINIA VIRUS (GL-ONC1) WITH CISPLATIN AND RADIOTHERAPY IN PATIENTS WITH LOCOREGIONALLY ADVANCED HEAD AND NECK CARCINOMA. *Clinical cancer research : an official journal of the American Association for Cancer Research*

Miller JD, van der Most RG, Akondy RS, Glidewell JT, Albott S, Masopust D, Murali-Krishna K, Mahar PL, Edupuganti S, Lalor S, Germon S, Del Rio C, Mulligan MJ, Staprans SI, Altman JD, Feinberg MB, Ahmed R (2008) Human effector and memory CD8+ T cell responses to smallpox and yellow fever vaccines. *Immunity* **28**(5)**:** 710-22

Moore AE (1952) Viruses with oncolytic properties and their adaptation to tumors. *Annals of the New York Academy of Sciences* **54**(6)**:** 945-52

Moore AE (1954) Effects of viruses on tumors. *Annual Reviews in Microbiology* **8**(1)**:** 393-410

Moore JB, Smith GL (1992) Steroid hormone synthesis by a vaccinia enzyme: a new type of virus virulence factor. *The EMBO journal* **11**(5)**:** 1973-80

Mosmann T (1983) Rapid colorimetric assay for cellular growth and survival: application to proliferation and cytotoxicity assays. *Journal of immunological methods* **65**(1-2)**:** 55-63

Moss B (2007) Poxviridae: the viruses and their replication. In *Fields Virology*, 5th edn, pp 2905–2946. Philadelphia, PA: Lippincott Williams & Wilkins

Moss B, Earl PL (2001) Overview of the vaccinia virus expression system. *Current protocols in protein science* **Chapter 5:** Unit5.11

Myers R, Harvey M, Kaufmann TJ, Greiner SM, Krempski JW, Raffel C, Shelton SE, Soeffker D, Zollman P, Federspiel MJ, Blanco M, Galanis E (2008) Toxicology study of repeat intracerebral administration of a measles virus derivative producing carcinoembryonic antigen in rhesus macaques in support of a phase I/II clinical trial for patients with recurrent gliomas. *Human gene therapy* **19**(7)**:** 690-8

Nakatsu Y, Ma X, Seki F, Suzuki T, Iwasaki M, Yanagi Y, Komase K, Takeda M (2013) Intracellular transport of the measles virus ribonucleoprotein complex is mediated by Rab11A-positive recycling endosomes and drives virus release from the apical membrane of polarized epithelial cells. *Journal of virology* **87**(8)**:** 4683-93

Naniche D, Varior-Krishnan G, Cervoni F, Wild TF, Rossi B, Rabourdin-Combe C, Gerlier D (1993) Human membrane cofactor protein (CD46) acts as a cellular receptor for measles virus. *Journal of virology* **67**(10)**:** 6025-32

Nasar F, Erasmus JH, Haddow AD, Tesh RB, Weaver SC (2015) Eilat virus induces both homologous and heterologous interference. *Virology* **484:** 51-8

Niepel M, Hafner M, Chung M, Sorger PK (2017) Measuring Cancer Drug Sensitivity and Resistance in Cultured Cells. *Current protocols in chemical biology* **9**(2)**:** 55-74

Noll M, Berchtold S, Lampe J, Malek NP, Bitzer M, Lauer UM (2013) Primary resistance phenomena to oncolytic measles vaccine viruses. *International journal of oncology* **43**(1)**:** 103-12

Norman KL, Lee PW (2000) Reovirus as a novel oncolytic agent. *The Journal of clinical investigation* **105**(8)**:** 1035-8

Noyce RS, Bondre DG, Ha MN, Lin L-T, Sisson G, Tsao M-S, Richardson CD (2011) Tumor cell marker PVRL4 (nectin 4) is an epithelial cell receptor for measles virus. *PLoS pathogens* **7**(8)**:** e1002240

Ohno S, Ono N, Takeda M, Takeuchi K, Yanagi Y (2004) Dissection of measles virus V protein in relation to its ability to block alpha/beta interferon signal transduction. *The Journal of general virology* **85**(Pt 10)**:** 2991-9

Ottolino-Perry K, Diallo JS, Lichty BD, Bell JC, McCart JA (2010) Intelligent design: combination therapy with oncolytic viruses. *Molecular therapy : the journal of the American Society of Gene Therapy* **18**(2)**:** 251-63

Parato KA, Breitbach CJ, Le Boeuf F, Wang J, Storbeck C, Ilkow C, Diallo JS, Falls T, Burns J, Garcia V, Kanji F, Evgin L, Hu K, Paradis F, Knowles S,

Hwang TH, Vanderhyden BC, Auer R, Kirn DH, Bell JC (2012) The oncolytic poxvirus JX-594 selectively replicates in and destroys cancer cells driven by genetic pathways commonly activated in cancers. *Molecular therapy : the journal of the American Society of Gene Therapy* **20**(4)**:** 749-58

Park BH, Hwang T, Liu TC, Sze DY, Kim JS, Kwon HC, Oh SY, Han SY, Yoon JH, Hong SH, Moon A, Speth K, Park C, Ahn YJ, Daneshmand M, Rhee BG, Pinedo HM, Bell JC, Kirn DH (2008) Use of a targeted oncolytic poxvirus, JX-594, in patients with refractory primary or metastatic liver cancer: a phase I trial. *The Lancet Oncology* **9**(6)**:** 533-42

Parkman PD, Buescher EL, Artenstein MS, McCown JM, Mundon FK, Druzd AD (1964) STUDIES OF RUBELLA. I. PROPERTIES OF THE VIRUS. *Journal of immunology (Baltimore, Md : 1950)* **93:** 595-607

Pasquinucci G (1971) Possible effect of measles on leukaemia. *Lancet (London, England)* **1**(7690)**:** 136

Peng KW, Ahmann GJ, Pham L, Greipp PR, Cattaneo R, Russell SJ (2001) Systemic therapy of myeloma xenografts by an attenuated measles virus. *Blood* **98**(7)**:** 2002-7

Perez RP, Godwin AK, Handel LM, Hamilton TC (1993) A comparison of clonogenic, microtetrazolium and sulforhodamine B assays for determination of cisplatin cytotoxicity in human ovarian carcinoma cell lines. *European journal of cancer (Oxford, England : 1990)* **29a**(3)**:** 395-9

Phuong LK, Allen C, Peng KW, Giannini C, Greiner S, TenEyck CJ, Mishra PK, Macura SI, Russell SJ, Galanis EC (2003) Use of a vaccine strain of measles virus genetically engineered to produce carcinoembryonic antigen as a novel therapeutic agent against glioblastoma multiforme. *Cancer research* **63**(10)**:** 2462-9

Putz MM, Midgley CM, Law M, Smith GL (2006) Quantification of antibody responses against multiple antigens of the two infectious forms of Vaccinia virus provides a benchmark for smallpox vaccination. *Nature medicine* **12**(11)**:** 1310-5

Qin L, Favis N, Famulski J, Evans DH (2015) Evolution of and evolutionary relationships between extant vaccinia virus strains. *Journal of virology* **89**(3)**:** 1809-24

Quirke P, Steele R, Monson J, Grieve R, Khanna S, Couture J, O'Callaghan C, Myint AS, Bessell E, Thompson LC, Parmar M, Stephens RJ, Sebag-Montefiore D (2009) Effect of the plane of surgery achieved on local recurrence in patients with operable rectal cancer: a prospective study using data from the MRC CR07 and NCIC-CTG CO16 randomised clinical trial. *Lancet (London, England)* **373**(9666)**:** 821-8

Rabenau HF, Schwebke I, Blumel J, Eggers M, Glebe D, Rapp I, Sauerbrei A, Steinmann E, Steinmann J, Willkommen H, Wutzler P (2015) [In Process Citation]. *Bundesgesundheitsblatt, Gesundheitsforschung, Gesundheitsschutz* **58**(4-5)**:** 493-504

Riss TL, Moravec RA, Niles AL, Duellman S, Benink HA, Worzella TJ, Minor L (2004) Cell Viability Assays. In *Assay Guidance Manual*, Sittampalam GS, Coussens NP, Brimacombe K, Grossman A, Arkin M, Auld D, Austin C, Baell J, Bejcek B, Chung TDY, Dahlin JL, Devanaryan V, Foley TL, Glicksman M, Hall MD, Hass JV, Inglese J, Iversen PW, Kahl SD, Kales SC, Lal-Nag M, Li Z, McGee J, McManus O, Riss T, Trask OJ, Jr., Weidner JR, Xia M, Xu X (eds). Bethesda (MD): Eli Lilly & Company and the National Center for Advancing Translational Sciences

Rochlitz C, Figlin R, Squiban P, Salzberg M, Pless M, Herrmann R, Tartour E, Zhao Y, Bizouarne N, Baudin M, Acres B (2003) Phase I immunotherapy with a modified vaccinia virus (MVA) expressing human MUC1 as antigen-specific immunotherapy in patients with MUC1-positive advanced cancer. *The journal of gene medicine* **5**(8)**:** 690-9

Rodriguez JF, Paez E, Esteban M (1987) A 14,000-Mr envelope protein of vaccinia virus is involved in cell fusion and forms covalently linked trimers. *Journal of virology* **61**(2)**:** 395-404

Rubinstein LV, Shoemaker RH, Paull KD, Simon RM, Tosini S, Skehan P, Scudiero DA, Monks A, Boyd MR (1990) Comparison of in vitro anticancer-drug-screening data generated with a tetrazolium assay versus a protein assay against a diverse panel of human tumor cell lines. *Journal of the National Cancer Institute* **82**(13)**:** 1113-8

Rudin CM, Poirier JT, Senzer NN, Stephenson J, Jr., Loesch D, Burroughs KD, Reddy PS, Hann CL, Hallenbeck PL (2011) Phase I clinical study of Seneca Valley Virus (SVV-001), a replication-competent picornavirus, in advanced solid tumors with neuroendocrine features. *Clinical cancer research : an official journal of the American Association for Cancer Research* **17**(4)**:** 888-95

Russell SJ, Peng KW (2007) Viruses as anticancer drugs. *Trends in pharmacological sciences* **28**(7)**:** 326-33

Russell SJ, Peng KW (2009) Measles virus for cancer therapy. *Current topics in microbiology and immunology* **330:** 213-41

Russell SJ, Peng KW, Bell JC (2012) Oncolytic virotherapy. *Nature biotechnology* **30**(7)**:** 658-70

Sasaki T, Kawai K, Saijo-Kurita K, Ohno T (1992) Detergent cytotoxicity: simplified assay of cytolysis by measuring LDH activity. *Toxicology in vitro : an international journal published in association with BIBRA* **6**(5)**:** 451-7

Schaller T, Appel N, Koutsoudakis G, Kallis S, Lohmann V, Pietschmann T, Bartenschlager R (2007) Analysis of hepatitis C virus superinfection exclusion by using novel fluorochrome gene-tagged viral genomes. *Journal of virology* **81**(9)**:** 4591-603

Schmidt FI, Bleck CK, Mercer J (2012) Poxvirus host cell entry. *Current opinion in virology* **2**(1)**:** 20-7

Schneider-Schaulies S, ter Meulen V (2002) Measles virus and immunomodulation: molecular bases and perspectives. *Expert reviews in molecular medicine* **4**(13)**:** 1-18

Schramm B, Locker JK (2005) Cytoplasmic organization of POXvirus DNA replication. *Traffic (Copenhagen, Denmark)* **6**(10)**:** 839-46

Shoemaker RH (2006) The NCI60 human tumour cell line anticancer drug screen. *Nature reviews Cancer* **6**(10)**:** 813-23

Siegel RL, Miller KD, Fedewa SA, Ahnen DJ, Meester RGS, Barzi A, Jemal A (2017) Colorectal cancer statistics, 2017. *CA: a cancer journal for clinicians* **67**(3)**:** 177-193

Siegel RL, Miller KD, Jemal A (2016) Cancer statistics, 2016. *CA: a cancer journal for clinicians* **66**(1)**:** 7-30

Skafida E, Kokkali S, Nikolaou M, Digklia A (2017) Metastatic soft tissue sarcoma: current treatment landscape and future perspectives. *Expert review of anticancer therapy* **17**(6)**:** 537-543

Skehan P, Storeng R, Scudiero D, Monks A, McMahon J, Vistica D, Warren JT, Bokesch H, Kenney S, Boyd MR (1990) New colorimetric cytotoxicity assay for anticancer-drug screening. *Journal of the National Cancer Institute* **82**(13)**:** 1107-12

Smith GL, Benfield CT, Maluquer de Motes C, Mazzon M, Ember SW, Ferguson BJ, Sumner RP (2013) Vaccinia virus immune evasion: mechanisms, virulence and immunogenicity. *The Journal of general virology* **94**(Pt 11)**:** 2367-92

Smith GL, Moss B (1983) Infectious poxvirus vectors have capacity for at least 25 000 base pairs of foreign DNA. *Gene* **25**(1)**:** 21-8

Smith GL, Vanderplasschen A, Law M (2002) The formation and function of extracellular enveloped vaccinia virus. *The Journal of general virology* **83**(Pt 12)**:** 2915-31

Southam CM, Moore AE (1952) Clinical studies of viruses as antineoplastic agents, with particular reference to Egypt 101 virus. *Cancer* **5**(5)**:** 1025-1034

Spearman C (1908) The method of 'right and wrong cases'('constant stimuli') without Gauss's formulae. *British Journal of Psychology, 1904-1920* **2**(3)**:** 227-242

Sugimoto M, Yamanouchi K (1994) Characteristics of an attenuated vaccinia virus strain, LC16m0, and its recombinant virus vaccines. *Vaccine* **12**(8)**:** 675-81

Sun M, Abdollah F, Bianchi M, Trinh QD, Jeldres C, Thuret R, Tian Z, Shariat SF, Montorsi F, Perrotte P, Karakiewicz PI (2012) Treatment management of small renal masses in the 21st century: a paradigm shift. *Annals of surgical oncology* **19**(7)**:** 2380-7

Symons JA, Alcami A, Smith GL (1995) Vaccinia virus encodes a soluble type I interferon receptor of novel structure and broad species specificity. *Cell* **81**(4)**:** 551-60

Takaki H, Watanabe Y, Shingai M, Oshiumi H, Matsumoto M, Seya T (2011) Strain-to-strain difference of V protein of measles virus affects MDA5-mediated IFN-beta-inducing potential. *Molecular immunology* **48**(4)**:** 497-504

Taqi AM, Abdurrahman MB, Yakubu AM, Fleming AF (1981) Regression of Hodgkin's disease after measles. *Lancet (London, England)* **1**(8229)**:** 1112

Tesfay MZ, Ammayappan A, Federspiel MJ, Barber GN, Stojdl D, Peng KW, Russell SJ (2014) Vesiculovirus neutralization by natural IgM and complement. *Journal of virology* **88**(11)**:** 6148-57

Thorne SH, Bartlett DL, Kirn DH (2005) The use of oncolytic vaccinia viruses in the treatment of cancer: a new role for an old ally? *Current gene therapy* **5**(4)**:** 429-43

Thorne SH, Hwang TH, O'Gorman WE, Bartlett DL, Sei S, Kanji F, Brown C, Werier J, Cho JH, Lee DE, Wang Y, Bell J, Kirn DH (2007) Rational strain selection and engineering creates a broad-spectrum, systemically effective oncolytic poxvirus, JX-963. *The Journal of clinical investigation* **117**(11)**:** 3350-8

Tolonen N, Doglio L, Schleich S, Krijnse Locker J (2001) Vaccinia virus DNA replication occurs in endoplasmic reticulum-enclosed cytoplasmic mini-nuclei. *Molecular biology of the cell* **12**(7)**:** 2031-46

Torre LA, Bray F, Siegel RL, Ferlay J, Lortet-Tieulent J, Jemal A (2015) Global cancer statistics, 2012. *CA: a cancer journal for clinicians* **65**(2)**:** 87-108

Towbin H, Staehelin T, Gordon J (1992) Electrophoretic transfer of proteins from polyacrylamide gels to nitrocellulose sheets: procedure and some applications. 1979. *Biotechnology (Reading, Mass)* **24:** 145-9

Tscherne DM, Evans MJ, von Hahn T, Jones CT, Stamataki Z, McKeating JA, Lindenbach BD, Rice CM (2007) Superinfection exclusion in cells infected with hepatitis C virus. *Journal of virology* **81**(8)**:** 3693-703

Tsuchiya Y, Tagaya I (1970) Enhanced or inhibited plaque formation of superinfecting viruses in Yaba virus-infected cells. *The Journal of general virology* **7**(1)**:** 71-3

Tsuchiya Y, Tagaya I (1972a) General characteristics of enhanced plague formation by poliovirus in poxvirus-infected cells. *The Journal of general virology* **14**(3)**:** 229-35

Tsuchiya Y, Tagaya I (1972b) Mechanism of enhanced plaque formation by poliovirus in poxvirus-infected cells. *The Journal of general virology* **14**(3)**:** 237-42

Turner GS, Squires EJ (1971) Inactivated smallpox vaccine: immunogenicity of inactivated intracellular and extracellular vaccinia virus. *The Journal of general virology* **13**(1)**:** 19-25

Turner PC, Moyer RW (2008) The vaccinia virus fusion inhibitor proteins SPI-3 (K2) and HA (A56) expressed by infected cells reduce the entry of superinfecting virus. *Virology* **380**(2)**:** 226-33

Tysome JR, Li X, Wang S, Wang P, Gao D, Du P, Chen D, Gangeswaran R, Chard LS, Yuan M, Alusi G, Lemoine NR, Wang Y (2012) A novel therapeutic regimen to eradicate established solid tumors with an effective induction of tumor-specific immunity. *Clinical cancer research : an official journal of the American Association for Cancer Research* **18**(24)**:** 6679-89

van Meerloo J, Kaspers GJ, Cloos J (2011) Cell sensitivity assays: the MTT assay. *Methods in molecular biology (Clifton, NJ)* **731:** 237-45

Vichai V, Kirtikara K (2006) Sulforhodamine B colorimetric assay for cytotoxicity screening. *Nature protocols* **1**(3)**:** 1112-6

von Karsa L, Patnick J, Segnan N, Atkin W, Halloran S, Lansdorp-Vogelaar I, Malila N, Minozzi S, Moss S, Quirke P, Steele RJ, Vieth M, Aabakken L, Altenhofen L, Ancelle-Park R, Antoljak N, Anttila A, Armaroli P, Arrossi S, Austoker J, Banzi R, Bellisario C, Blom J, Brenner H, Bretthauer M, Camargo Cancela M, Costamagna G, Cuzick J, Dai M, Daniel J, Dekker E, Delicata N, Ducarroz S, Erfkamp H, Espinas JA, Faivre J, Faulds Wood L, Flugelman A, Frkovic-Grazio S, Geller B, Giordano L, Grazzini G, Green J, Hamashima C, Herrmann C, Hewitson P, Hoff G, Holten I, Jover R, Kaminski MF, Kuipers EJ,

Kurtinaitis J, Lambert R, Launoy G, Lee W, Leicester R, Leja M, Lieberman D, Lignini T, Lucas E, Lynge E, Madai S, Marinho J, Maucec Zakotnik J, Minoli G, Monk C, Morais A, Muwonge R, Nadel M, Neamtiu L, Peris Tuser M, Pignone M, Pox C, Primic-Zakelj M, Psaila J, Rabeneck L, Ransohoff D, Rasmussen M, Regula J, Ren J, Rennert G, Rey J, Riddell RH, Risio M, Rodrigues V, Saito H, Sauvaget C, Scharpantgen A, Schmiegel W, Senore C, Siddiqi M, Sighoko D, Smith R, Smith S, Suchanek S, Suonio E, Tong W, Tornberg S, Van Cutsem E, Vignatelli L, Villain P, Voti L, Watanabe H, Watson J, Winawer S, Young G, Zaksas V, Zappa M, Valori R (2013) European guidelines for quality assurance in colorectal cancer screening and diagnosis: overview and introduction to the full supplement publication. *Endoscopy* **45**(1)**:** 51-9

von Mehren M, Randall RL, Benjamin RS, Boles S, Bui MM, Conrad EU, 3rd, Ganjoo KN, George S, Gonzalez RJ, Heslin MJ, Kane JM, 3rd, Koon H, Mayerson J, McCarter M, McGarry SV, Meyer C, O'Donnell RJ, Pappo AS, Paz IB, Petersen IA, Pfeifer JD, Riedel RF, Schuetze S, Schupak KD, Schwartz HS, Tap WD, Wayne JD, Bergman MA, Scavone J (2016) Soft Tissue Sarcoma, Version 2.2016, NCCN Clinical Practice Guidelines in Oncology. *Journal of the National Comprehensive Cancer Network : JNCCN* **14**(6)**:** 758-86

Wagenaar TR, Moss B (2009) Expression of the A56 and K2 proteins is sufficient to inhibit vaccinia virus entry and cell fusion. *Journal of virology* **83**(4)**:** 1546-54

Walsh SR, Dolin R (2011) Vaccinia viruses: vaccines against smallpox and vectors against infectious diseases and tumors. *Expert review of vaccines* **10**(8)**:** 1221-40

Wang H, Chen NG, Minev BR, Zimmermann M, Aguilar RJ, Zhang Q, Sturm JB, Fend F, Yu YA, Cappello J, Lauer UM, Szalay AA (2013) Optical Detection and Virotherapy of Live Metastatic Tumor Cells in Body Fluids with Vaccinia Strains. *PloS one* **8**(9)**:** e71105

Wildum S, Schindler M, Munch J, Kirchhoff F (2006) Contribution of Vpu, Env, and Nef to CD4 down-modulation and resistance of human immunodeficiency virus type 1-infected T cells to superinfection. *Journal of virology* **80**(16)**:** 8047-59

Wilkinson MJ, Smith HG, Pencavel TD, Mansfield DC, Kyula-Currie J, Khan AA, McEntee G, Roulstone V, Hayes AJ, Harrington KJ (2016) Isolated limb perfusion with biochemotherapy and oncolytic virotherapy combines with radiotherapy and surgery to overcome treatment resistance in an animal model of extremity soft tissue sarcoma. *International journal of cancer* **139**(6)**:** 1414-22

Yanagi Y, Takeda M, Ohno S, Seki F (2006) Measles virus receptors and tropism. *Japanese journal of infectious diseases* **59**(1)**:** 1-5

Yla-Pelto J, Tripathi L, Susi P (2016) Therapeutic Use of Native and Recombinant Enteroviruses. *Viruses* **8**(3)**:** 57

Yurttas C, Berchtold S, Malek NP, Bitzer M, Lauer UM (2014) Pulsed versus continuous application of the prodrug 5-fluorocytosine to enhance the oncolytic effectiveness of a measles vaccine virus armed with a suicide gene. *Human gene therapy Clinical development* **25**(2)**:** 85-96

Zamarin D, Holmgaard RB, Subudhi SK, Park JS, Mansour M, Palese P, Merghoub T, Wolchok JD, Allison JP (2014) Localized oncolytic virotherapy overcomes systemic tumor resistance to immune checkpoint blockade immunotherapy. *Science translational medicine* **6**(226)**:** 226ra32

Zeh HJ, Downs-Canner S, McCart JA, Guo ZS, Rao UN, Ramalingam L, Thorne SH, Jones HL, Kalinski P, Wieckowski E, O'Malley ME, Daneshmand M, Hu K, Bell JC, Hwang TH, Moon A, Breitbach CJ, Kirn DH, Bartlett DL (2015) First-in-man study of western reserve strain oncolytic vaccinia virus: safety, systemic spread, and antitumor activity. *Molecular therapy : the journal of the American Society of Gene Therapy* **23**(1)**:** 202-14

Zhang Q, Yu YA, Wang E, Chen N, Danner RL, Munson PJ, Marincola FM, Szalay AA (2007) Eradication of solid human breast tumors in nude mice with an intravenously injected light-emitting oncolytic vaccinia virus. *Cancer research* **67**(20)**:** 10038-46

Zhang SX (2015) Turning killer into cure -- the story of oncolytic herpes simplex viruses. *Discovery medicine* **20**(111)**:** 303-9

Zou G, Zhang B, Lim PY, Yuan Z, Bernard KA, Shi PY (2009) Exclusion of West Nile virus superinfection through RNA replication. *Journal of virology* **83**(22)**:** 11765-76

Zuniga A, Wang Z, Liniger M, Hangartner L, Caballero M, Pavlovic J, Wild P, Viret JF, Glueck R, Billeter MA, Naim HY (2007) Attenuated measles virus as a vaccine vector. *Vaccine* **25**(16)**:** 2974-83

Zygiert Z (1971) Hodgkin's disease: remissions after measles. *Lancet (London, England)* **1**(7699)**:** 593

9 Erklärungen zum Eigenanteil

Die Arbeit wurde in der Abteilung Innere Medizin VIII der Medizinischen Universitätsklinik Tübingen unter Betreuung von Herrn Professor Dr. med. Ulrich M. Lauer durchgeführt.
Die Konzeption der Studie erfolgte in Zusammenarbeit mit Herrn Professor Dr. med. Ulrich M. Lauer (Leiter der Forschungsgruppe “Virotherapie”), Frau Dr. rer. nat. Martina Schell (ehem. wissenschaftliche Mitarbeiterin) und Frau Dr. rer. nat. Julia Beil (wissenschaftliche Mitarbeiterin). Frau Dr. rer. nat. Martina Schell und Frau Dr. rer. nat. Julia Beil haben die Arbeit betreut. Sämtliche Versuche, bis auf die unten aufgeführten Vorarbeiten und Versuchsunterstützungen, wurden von mir eigenständig nach Einarbeitung durch die Labormitarbeiterinnen Frau Irina Smirnow, Frau Andrea Schenk, Frau Christine Geisler, Frau Dr. med. Susanne Berchtold, Frau Dr. rer. nat. Julia Beil und Frau Dr. rer. nat. Martina Schell durchgeführt.

Frau Dr. rer. nat. Julia Beil und Frau Dr. rer. nat. Martina Schell unterstützten mich bei der Titration des Vacciniavirus GLV-1h254 (Abschnitt 2.2.4.4.1). Frau Dr. rer. nat. Martina Schell hat die Titration des Masernimpfvirus MeV-GFP durchgeführt (Abschnitt 2.2.4.4.2). Frau Irina Smirnow hat mich bei der Vermehrung des Masernimpfvirus MeV-GFP (Abschnitt 2.2.4.2) sowie bei der Gelelektrophorese und Western Blot (Abschnitt 3.6) unterstützt. Herr Dr. med. Dr. rer. nat. Sascha Venturelli, Herr Dipl. Biochem. Christian Leischner und Frau Dr. rer. nat. Martina Schell habe mich im xCELLigence-Versuch unterstützt (Abschnitt 3.1.2.2).

Ich versichere, das Manuskript selbständig verfasst zu haben und keine weiteren als die von mir angegebenen Quellen verwendet zu haben. Frau Dr. rer. nat. Julia Beil hat das Manuskript korrigiert.

Tübingen, den 27.05.2018

Milena Meinhardt

10 Acknowledgement

Ich möchte mich hiermit sehr herzlich bei meinem Doktorvater Prof. Dr. med. Ulrich M. Lauer für die umfassende Betreuung und das stetige Interesse an meiner Arbeit bedanken. Ob bei der Bewerbung auf mein Promotionsstipendium des Sonderforschungsbereichs 773, in den fast wöchentlichen Ergebnisbesprechungen oder der Vorbereitung meines Beitrages für die DGVS 2013, Herr Prof. Dr. Lauer hat mich jederzeit unterstützt, gefördert und gefordert. Wie so viele vor mir kann auch ich mir keinen besseren Doktorvater wünschen. Ihm gilt mein Dank für die uneingeschränkte Bereitstellung sämtlicher Labormaterialen und Geräte und auch dafür, dass er mir mit seiner Arbeitsgruppe ein Team zu Seite gestellt hat ohne das diese Arbeit schlicht nicht möglich gewesen wäre.

Ich danke der gesamten AG Lauer für die freundliche und hilfsbereite Einführung in die mir bis dahin fremde Laborarbeit, für viele aufbauende Kaffeepausen und diskussionsfreudige Laborseminare. Mein besonderer Dank gilt Frau Irina Smirnow, die mir nicht nur das Pipettieren beibrachte, sondern die darüber hinaus über viele Jahre meine allzeit fröhliche und kompetente Ansprechpartnerin für so ziemlich jede Laborproblematik war.

Ich danke von Herzen Frau Dr. Martina Schell und Frau Dr. Julia Beil für die beispiellose Betreuung. Liebe Martina, ich danke dir für die geduldige Einarbeitung in die komplexen Grundlagen der Virotherapie, für viele Stunden der gemeinsamen Datenbesprechung, deine klugen Einwände und dein herzliches Wesen. Du hast es mir von Anfang an leicht gemacht, mich bei euch wohl zu fühlen und erste eigene wissenschaftliche Schritte zu tun. Liebe Julia, ich verdanke dir mehr als ich aufzählen kann. Danke für deinen unermüdlichen Glauben daran, dass ich diese Arbeit doch noch abschließen werde. Danke, für deine tatkräftige Unterstützung im Labor und für deine aufwendige und kritische Durchsicht dieser Dissertation. Vor allem aber, danke für deine Freundschaft.

Frau Dr. Susanne Berchtold danke ich für ihr beruhigendes „Omm“ in hektischen Situationen und viele Tipps, nicht nur zur richtigen Handhabung der

Sarkomzelllinien. Herrn Dr. Dr. Sascha Venturelli danke ich für seine wertvollen Überlegungen zu den in den Laborseminaren präsentierten Daten, für seine intensive Unterstützung des xCELLigence-Versuchs und seine sorgsame Durchsicht des zugehörigen Kapitels dieser Arbeit. Ich danke an dieser Stelle auch Herrn Christian Leischner sehr herzlich für seine Unterstützung beim xCELLigence-Versuch.

Ich danke Herrn Prof. Dr. R. Handgretinger und Frau Sabine Schleicher aus der Universitäts-Kinderklinik Tübingen für die zur Verfügung gestellten primären Sarkomzelllinien SRH und CCS.

Ein großes Dankeschön geht an Philipp Günthör, der mich seit vielen Jahren und in allen Lebensbereichen unterstützt und begleitet. Danke für deine tatkräftige Unterstützung bei der Literaturrecherche, bei Problemen mit Endnote oder Word und dafür, dass du nach dieser anstrengenden und aufwühlenden Zeit noch immer neben mir stehst.

Abschließend danke ich meinen Eltern, Schwestern und Freunden, die nicht nur während der Doktorarbeit, sondern auch sonst immer für mich da waren und es weiterhin sind. Danke für einen Ansporn zu rechten Zeit und eine mitfühlende Schulter zu einer anderen.